

University of Massachusetts Medical School

eScholarship@UMMS

GSBS Dissertations and Theses

Graduate School of Biomedical Sciences

2020-05-06


Genetic Identification of Novel Mycobacterium tuberculosis Susceptibility and Survival Mechanisms During Antibiotic Treatment

Michelle M. Bellerose

University of Massachusetts Medical School

Let us know how access to this document benefits you.

Follow this and additional works at: https://escholarship.umassmed.edu/gsbs_diss

 Part of the [Bacteriology Commons](#), [Molecular Genetics Commons](#), and the [Pathogenic Microbiology Commons](#)

Repository Citation

Bellerose MM. (2020). Genetic Identification of Novel Mycobacterium tuberculosis Susceptibility and Survival Mechanisms During Antibiotic Treatment. GSBS Dissertations and Theses. <https://doi.org/10.13028/kz6e-z069>. Retrieved from https://escholarship.umassmed.edu/gsbs_diss/1081

Creative Commons License



This work is licensed under a [Creative Commons Attribution-NonCommercial 4.0 License](#)

This material is brought to you by eScholarship@UMMS. It has been accepted for inclusion in GSBS Dissertations and Theses by an authorized administrator of eScholarship@UMMS. For more information, please contact Lisa.Palmer@umassmed.edu.

**GENETIC IDENTIFICATION OF NOVEL *MYCOBACTERIUM*
TUBERCULOSIS SUSCEPTIBILITY AND SURVIVAL
MECHANISMS DURING ANTIBIOTIC TREATMENT**

A Dissertation Presented

By

MICHELLE M. BELLEROSE

Submitted to the Faculty of the
University of Massachusetts Graduate School of Biomedical Sciences, Worcester
in partial fulfillment of the requirements for the degree of

DOCTOR OF PHILOSOPHY

May 6th, 2020

MOLECULAR GENETICS AND MICROBIOLOGY

**GENETIC IDENTIFICATION OF NOVEL *MYCOBACTERIUM TUBERCULOSIS*
SUSCEPTIBILITY AND SURVIVAL MECHANISMS DURING ANTIBIOTIC
TREATMENT**

A Dissertation Presented

By

MICHELLE M. BELLEROSE

This work was undertaken in the Graduate School of Biomedical Sciences
Molecular Genetics and Microbiology Program

Under the mentorship of

Christopher M. Sassetti, Ph.D., Thesis Advisor

Richard E. Baker, Ph.D., Member of Committee

Samuel M. Behar, M.D., Ph.D., Member of Committee

Sanjay Ram, M.D., Member of Committee

Scarlet S. Shell, Ph.D., External Member of Committee

Jon Goguen, Ph.D., Chair of Committee

Mary Ellen Lane, Ph.D.,

Dean of the Graduate School of Biomedical Sciences

May 6th, 2020

For my Family

Thank you for your unconditional love and support.

ACKNOWLEDGMENTS

I have had the pleasure to be surrounded by brilliant and supportive individuals throughout my graduate career. This work could not have been accomplished without the help and guidance of so many of you. Thank you.

Chris Sasseti, I am so grateful for your mentorship these past years. Thank you for your open door and for always being willing to listen to every hurdle and question, no matter how big or small. Thank you for encouraging me to step out of my comfort zone, no matter how much I protested against presenting. I have learned so much from you these past years, both professionally and personally. Thank you for making graduate school challenging, rewarding, and fun.

To the members of my thesis research advisory committee, thank you for your scientific guidance. Jon Goguen, thank you for being the chair of my committee, for always asking rigorous questions, and always answering my simple ones. Richard Baker, thank you for your expertise in all things analytical and for helping me find new, exciting ways to view my data. Samuel Behar, thank you for reminding me to think past the bacterium and teaching me about immunology. Sanjay Ram and Scarlet Shell, thank you for agreeing to be a part of my dissertation committee, I greatly appreciate your time and effort in evaluating this work. This thesis is possible because of all of you.

To the members of the Sasseti lab, both past and present, thank you for the years of support, all of the shared knowledge, and for always asking the hard

questions. To Ed Long, thank you for taking me under your wing and teaching me the “TNseq ropes”. To Megan Proulx, you were my very first teacher during my very first rotation, thank you for answering my never ending questions. To my microbiologists, thank you for sharing your depth and range of knowledge on both TB and all “bugs”. To my immunologists, thanks for teaching me skills which I could have very easily never known or understood. This entire team makes our science better, and I am a better scientist because of this team.

My deepest thanks to my “village”. To Christina Baer, thank you for being a source of knowledge and support both in science and in life. Your mentorship and friendship has meant so much to me, I am forever grateful. To Milka Koupenova, thank you for your support and for all of the laughs, I will miss our coffee meetings. To Clare Smith, thank you for always sharing your science, knowledge, and your mouse expertise. To my fellow MaPS graduate students, we support each other and that support is necessary and invaluable. To Samantha Palace and Caitlin Moss, thank you for always being there and for making me feel truly unsinkable.

Finally, these acknowledgments would not be complete without thanking my larger communities. UMass Medical School has been a wonderful place to grow as a scientist. The MaPS department has been a pillar of support, I wish I could thank you all individually. The greater TB community in this area is one in a million, they are generous in both their knowledge and their support. Thank you all for welcoming me.

ABSTRACT

Effective treatment of tuberculosis requires at least six months of combination therapy involving four antibiotics. Alterations in the physiological state of *Mycobacterium tuberculosis* during infection may reduce drug efficacy and prolong treatment, but these adaptations are incompletely defined. To investigate the mechanisms limiting antibiotic efficacy, I performed a comprehensive genetic study to identify *M. tuberculosis* genes and pathways important for bacterial survival during antibiotic treatment *in vivo*. First, I identified mutants in the glycerol kinase enzyme, GlpK, that promote survival under combination therapy. Similar glycerol catabolic mutants are enriched in extensively drug-resistant clinical isolates, indicating that these mutations may promote survival and the development of resistance in humans. A majority of these mutations are frameshifts within a homopolymeric region of the *glpK* gene, leading to the hypothesis that *M. tuberculosis* may reversibly produce drug-tolerant phenotypes through genetic variation introduced at homopolymer sites as a strategy for survival during antibiotic treatment. Second, I identified bacterial mutants with altered susceptibility to individual first-line anti-mycobacterial drugs. Many of these mutations did not have obvious effects *in vitro*, demonstrating that a wide variety of natural genetic variants can influence drug efficacy *in vivo* without altering standard drug-susceptibility tests. A number of these genes are enriched in drug-resistant clinical isolates, indicating that these genetic variants influence treatment outcome. Together, these data suggest new targets for

improving therapy, as well as mechanisms of genetic adaptations that can reduce antibiotic efficacy and contribute to the evolution of resistance.

TABLE OF CONTENTS

ACKNOWLEDGEMENTS	iv
ABSTRACT	vi
TABLE OF CONTENTS	viii
LIST OF FIGURES	x
LIST OF TABLES	xii
LIST OF PUBLISHED MATERIALS	xiv
CHAPTER I: Introduction	1
Tuberculosis.....	1
<i>Mycobacterium tuberculosis: the causative agent of tuberculosis</i>	1
<i>Antibiotic treatment</i>	2
Strategies to survive antibiotic treatment.....	6
<i>Inherent properties of Mycobacterium tuberculosis</i>	6
<i>Genetic Resistance</i>	9
<i>Tolerance</i>	12
Thesis objectives	15
CHAPTER II: Common variants in the glycerol kinase gene reduce tuberculosis drug efficacy	17
Preface.....	17
Introduction	18
Results	20
<i>Genetic determinants of drug efficacy in the mouse model</i>	20
<i>Glycerol metabolism increases drug efficacy in vitro and during murine infection</i>	25
<i>Glycerol catabolic defects are associated with extensive drug resistance in Korea</i>	32
<i>GlpK frameshift mutations are common in M. tuberculosis isolates and associated with drug resistance in Peru</i>	36
Discussion.....	39
Acknowledgments.....	42
CHAPTER III: Distinct bacterial pathways influence the efficacy of first-line tuberculosis antibiotics	43

Preface	43
Introduction	44
Results	46
<i>Selection of transposon mutant libraries in antibiotic treated mice</i>	46
<i>Identification of genes necessary for bacterial fitness in untreated animals</i>	49
<i>Identification of mutants with altered susceptibility to antibiotics</i>	52
<i>Validation of mutant phenotypes in an aerosol infection model</i>	56
<i>Mutations produce drug-specific effects</i>	64
<i>Many susceptibility phenotypes are in vivo specific</i>	68
<i>Natural variants in efficacy-altering genes are associated with drug resistance</i>	71
Discussion.....	74
Acknowledgments.....	79
CHAPTER IV: Discussion	80
APPENDIX A1: Materials and Methods	88
Transposon sequencing	88
Projection Resampling.....	90
<i>Mycobacterium tuberculosis</i> strains and culturing.....	91
Δ <i>glpK</i> mutant characterization	92
GR50 determination	94
<i>In vitro</i> antibiotic susceptibility	94
<i>In vivo</i> antibiotic susceptibility	95
Phenotypic and genotypic analysis of Korean strains	98
Phenotypic and genotypic analysis of Peruvian strains	100
APPENDIX A2: Lists of genes with altered susceptibility to HRZE treatment <i>in vivo</i> and strain characteristics of Korean Isolates	102
APPENDIX A3: Lists of genes with altered susceptibility to antibiotic treatment <i>in vivo</i>.....	113
REFERENCES	140

LIST OF FIGURES

Figure 1.1 Mechanisms of first-line TB antibiotics.....	5
Figure 2.1 Antibiotic treatment of <i>M. tuberculosis</i> infected mice.....	21
Figure 2.2 Genetic strategy to define bacterial functions that limit drug efficacy.	23
Figure 2.3 Genes with altered susceptibility to HRZE treatment <i>in vivo</i>	25
Figure 2.4 Glycerol metabolism broadly increases drug efficacy <i>in vitro</i>	26
Figure 2.5 Δ <i>glpK</i> antibiotic susceptibility <i>in vitro</i>	28
Figure 2.6 Loss of glycerol kinase increases survival under PZA treatment <i>in vivo</i>	30
Figure 2.7 Growth of extensively drug-resistant strains on individual carbon sources.	33
Figure 2.8 Glycerol catabolic mutations associated with XDR strains.....	35
Figure 2.9 GlpK mutations associated with drug resistance in clinical isolates from Peru.	38
Figure 3.1 Antibiotic treatment of transposon mutant libraries <i>in vivo</i>	48
Figure 3.2 Genetic strategy to identify mutations that alter susceptibility to antibiotic treatment in mice.....	49
Figure 3.3 Genes required for optimal fitness <i>in vivo</i>	51
Figure 3.4 Complexity of antibiotic treated libraries.	53
Figure 3.5 Mutants with altered susceptibility to antibiotics.	55
Figure 3.6 Transposon insertions pre- and post-treatment in genes with altered susceptibility.	58
Figure 3.7 Antibiotic treatment of mutant and wild-type pooled infections.....	59
Figure 3.8 Validation of mutant phenotypes.	63

Figure 3.9 Mutants with altered susceptibility to treatment are specific to individual treatment regimens.	65
Figure 3.10 Multi-dimensional analysis to identify mutations associated with individual antibiotic treatments.	68
Figure 3.11 Rate of killing of mutants <i>in vitro</i>.	70
Figure 3.12 Comparison between <i>in vivo</i> susceptibility and association with clinical resistance.	73

LIST OF TABLES

Table 3.1 Antibiotic susceptibility of deletion strains <i>in vitro</i>	71
Table 3.2 Genes that alter drug susceptibility in mice and contain resistance-associated SNPs in clinical isolates.....	73
Table A1.1 Deletion strains constructed in this study.....	92
Table A1.2 qTag sequencing primers.....	96
Table A2.1 Significantly underrepresented genes post HRZE treatment compared to pretreatment.....	102
Table A2.2 Significantly overrepresented genes post HRZE treatment compared to pretreatment.....	103
Table A2.3 Significantly underrepresented genes 21 days post infection compared to pretreatment.....	103
Table A2.4 Significantly underrepresented genes post HRZE treatment using three-way analysis.....	104
Table A2.5 Significantly overrepresented genes post HRZE treatment using three-way analysis.....	106
Table A2.6 Phenotypic drug sensitivity of Korean <i>M. tuberculosis</i> isolates determined by LJ Agar Assay.....	107
Table A2.7 Phenotypic drug sensitivity of Korean <i>M. tuberculosis</i> isolates determined by MGIT assay.....	109
Table A2.8 Growth on glycerol and <i>glpK</i> genotype of Korean <i>M. tuberculosis</i> isolates.....	111
Table A3.1 Genes required for optimal fitness <i>in vivo</i>	113
Table A3.2 Significantly underrepresented genes post INH treatment compared to pretreatment.....	128
Table A3.3 Significantly overrepresented genes post INH treatment compared to pretreatment.....	130

Table A3.4 Significantly underrepresented genes post EMB treatment compared to pretreatment.....	131
Table A3.5 Significantly overrepresented genes post EMB treatment compared to pretreatment.....	132
Table A3.6 Significantly underrepresented genes post RIF treatment compared to pretreatment	133
Table A3.7 Significantly overrepresented genes post RIF treatment compared to pretreatment	134
Table A3.8 Significantly underrepresented genes post PZA treatment compared to pretreatment	135
Table A3.9 Significantly overrepresented genes post PZA treatment compared to pretreatment	135
Table A3.10 Genes significantly associated with varimax dimension 1, INH treatment.....	136
Table A3.11 Genes significantly associated with varimax dimension 2, untreated	136
Table A3.12 Genes significantly associated with varimax dimension 3, PZA and HRZE treated.....	137
Table A3.13 Genes significantly associated with varimax dimension 4, RIF treatment	138
Table A3.14 Genes significantly associated with varimax dimensions 5 and 6, EMB treatment.....	139

LIST OF PUBLISHED MATERIALS

Bellerose MM, Baek S-H, Huang C-C, Moss CE, Koh E-I, Proulx MK, Smith CM, Baker RE, Lee JS, Eum S, Shin SJ, Cho S-N, Murray M, Sassetti CM. 2019. Common variants in the glycerol kinase gene reduce tuberculosis drug efficacy. *mBio* 10:e00663-19. <https://doi.org/10.1128/mBio.00663-19>.

Copyright © 2019 Bellerose et al. This is an open-access article distributed under the terms of the Creative Commons Attribution 4.0 International License

CHAPTER I: Introduction

Tuberculosis

Mycobacterium tuberculosis: the causative agent of tuberculosis

Robert Koch identified “tubercle bacillus” as the causative agent of tuberculosis in 1882 (1), leading to over a century of research into the bacterial organism *Mycobacterium tuberculosis*. Genomic sequencing of bacterial isolates indicates that *M. tuberculosis*, an obligate human pathogen, has been infecting humans for 70,000 years and has evolved in parallel to humans (2). Currently there are 7 known lineages of *M. tuberculosis*. Each evolved with human migration, leading to increased adaptation between geographical lineages and regional human populations (2, 3). Co-evolution with humans has resulted in a highly specific human pathogen, reflected in genetic differences between non-pathogenic *Mycobacterium* species and *M. tuberculosis* (4). Most commonly, infection with *M. tuberculosis* manifests as a pulmonary disease. Bacteria are transmitted via the inhalation of droplet nuclei expelled from an infected individual. This mode of transmission is most efficient in dense populations, leading to the hypothesis that increasing density of the human population resulted in widespread tuberculosis infection (2).

Tuberculosis (TB) remains a modern-day global health problem, causing more deaths worldwide than any other infectious agent (5). The World Health Organization estimates that 1.7 billion people are infected with *M. tuberculosis*. Most individuals are latently infected, where the infection is controlled and

asymptomatic. Approximately five to ten percent progress to active disease during their lifetime. Treatment of latent infections decreases the risk of activation (5). In 2018, an estimated ten million people were diagnosed with TB (5). Effective therapy requires antibiotic treatment with multiple drugs administered for at least six months, and has a treatment success rate of 85%. Despite availability of effective treatments, approximately 1.2 million deaths were caused by TB in 2018 (5).

Antibiotic treatment

Treatment of TB requires lengthy regimens of multiple antibiotics. Without treatment, the estimated mortality rate of TB is 70% (6). Streptomycin, the first antibiotic effective against *M. tuberculosis*, was introduced in 1946. Clinical trials showed improvement in mortality as compared to bedrest (7); however, streptomycin resistance was also observed (8). This result led to clinical trials of a combination therapy of streptomycin and *para*-amino-salicylic acid (PAS) in the 1950s, and a decrease in streptomycin resistance during treatment was observed (9). In 1952, clinical trials were performed comparing the efficacy of isoniazid and the current combination therapy (10-12). These trials led to the recommendation of a three-drug regimen for at least twelve months or longer for active TB patients (13).

After a series of clinical trials in the 1980s, a six-month, short-course treatment regimen consisting of four antibiotics was introduced (14) and remains

the current standard of care. Treatment of drug-susceptible TB (DS-TB) requires administration of isoniazid (INH), ethambutol (EMB), rifampin (RIF), and pyrazinamide (PZA) for two months, followed by four months of INH and RIF (15). Each of these antibiotics have distinct mechanisms of action, discussed below, that target multiple essential pathways in *M. tuberculosis* (Figure 1.1).

Isoniazid and rifampin are key components of this regimen, administered for the full 6 months. Isoniazid (INH) targets cell wall synthesis, disrupting the production of mycolic acids (16, 17). INH is a pro-drug activated by the bacterial catalase-peroxidase KatG to form INH-NAD adducts. These INH-NAD adducts target the enzyme InhA (18, 19), the NADH dependent eonyl-ACP reductase involved in the fatty acid synthase type II system (FASII) (20, 21). Inhibition of InhA by INH leads to the accumulation of long-chain fatty acids, prevention of mycolic acid biosynthesis and cell death (17, 22). Rifampin (RIF) is a broad-spectrum transcription inhibitor. RIF binds the β -subunit of the DNA-dependent RNA polymerase and blocks the initiation of transcription (23-26) and has bactericidal effects against *M. tuberculosis*.

Ethambutol and pyrazinamide are important in the first 2 months of treatment to prevent resistance development and enhance early sterilization. Ethambutol (EMB), another cell wall synthesis inhibitor disrupting arabinogalactan production (27), targets the *emb* operon. This operon encodes three arabinosyl-transferases involved in the production of arabinan chains for both arabinogalactan and lipoarabinomannan (LAM) (27-29), resulting in growth

arrest. Pyrazinamide (PZA) is a pro-drug activated by the bacterial pyrazinamidase PncA to form pyrazinoic acid (POA) (30, 31) resulting in strong sterilizing activity against *M. tuberculosis* when combined with INH (32). PZA displays poor *in vitro* potency which has made identification of its mechanism of action difficult, although several have been proposed (33-39). Most recently, it has been observed that POA binds to the aspartate decarboxylase PanD (40-44), which has an essential role in the biosynthesis of coenzyme A (45). Inhibition of PanD by PZA results in reduction of coenzyme A followed by accumulation of fatty acids, affecting central carbon metabolism (42). The diverse targets of these antibiotics result in multiple toxicities for the bacteria and, when used in combination, help decrease the development of resistance.

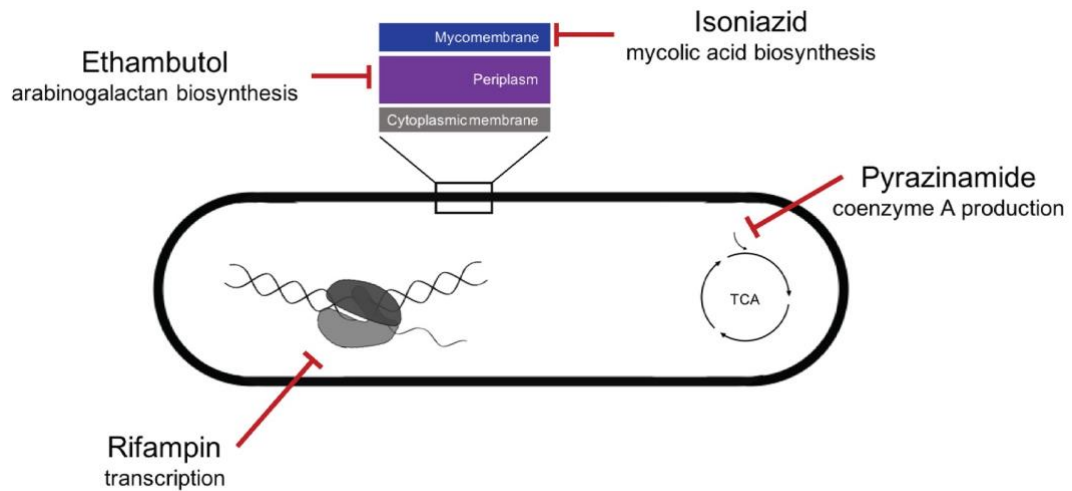


Figure 1.1 | Mechanisms of first-line TB antibiotics.

The current treatment for DS-TB infections, while effective, is not ideal. Six months of treatment with multiple antibiotics is difficult for patients due to significant side effects and the challenge of adhering to the regimen for such an extended time (46-48). Relapse rates are often explained by poor adherence; however, even with directly observed therapy (DOT) or under stringent observation in clinical trials, treatment fails in approximately 10% of cases (49). Insufficient treatment contributes to the overall global burden of TB as well as the development of resistant infections. Understanding how *M. tuberculosis* survives such lengthy treatment regimens is a major goal of the TB field, both to gain insight into the development of resistance and to identify ways to shorten DS-TB treatment.

Strategies to survive antibiotic treatment

Inherent properties of Mycobacterium tuberculosis

Due to the early observation that many compounds have little success in TB treatment, decades of work has been done to investigate the inherent resistance properties of *M. tuberculosis*. The presence of a lipid-rich, thick cell wall, creates a strong barrier that limits antibiotic entry into the cell. Certain antibiotics are pumped out of the cell by transporters or targeted by bacterial enzymes that modify them and prevent activity. Additionally, the host response to infection can negatively impact therapy through the formation of inflammatory lesions that reduce drug penetration. These physiological conditions prevent the use of many common antibiotics and also limit the efficacy of current TB therapies. As the development of genetic resistance renders certain therapies ineffective, an understanding of inherent resistance mechanisms, discussed below, is critical for the development of new antibiotics.

Cell wall permeability. The main components of the cell wall include the cytoplasmic membrane, the periplasm, the mycomembrane, and surface lipids. The high lipid composition of the cell wall presents a barrier to hydrophilic compounds. Early investigation of diffusion of compounds across bacterial membranes observed that mycobacterium membranes are three orders of magnitude less permeable than gram-negative membranes (50). Mycolic acids, the main component of the mycomembrane, make up 34% of the membrane

weight (51), reducing membrane fluidity (52, 53). Overall, this cell wall structure produces a thick, hydrophobic, rigid barrier to many small molecules.

Efflux pumps. Transporters spanning the membrane to efflux small molecules are a method of defense utilized by many bacteria, including *M. tuberculosis*. A large number of efflux pumps are encoded in the *M. tuberculosis* genome in comparison to other organisms (54). Multidrug transporters in *M. tuberculosis* have been studied since the 1990s and are known to efflux multiple distinct classes of antibiotics (55-58). Efflux pump expression can be induced under multiple different conditions such as intracellular growth, environmental stresses, and antibiotic treatment (59-62). A number of these pumps are expressed at elevated levels in clinical isolates (63). Using pump inhibitors as a combination therapy to treat TB is of great interest given the clinical impact of these transporters (64).

Enzymatic inhibition. Shortly after the introduction of penicillins, it was observed that *M. tuberculosis* was unaffected by this class of antibiotics (65). Later work would show that this inherent resistance is due to the expression of a β -lactamase, BlaC, which degrades some β -lactams (66-68). β -lactamase inhibitors in combination with β -lactams can re-sensitize β -lactam-resistant bacteria. This treatment approach has gained interest in treatment of *M. tuberculosis* as antibiotic resistance has increased and new effective regimens are needed (69). Another enzymatic defense used by *M. tuberculosis* is the expression of Erm(37), a methyltransferase which methylates the 23S rRNA

resulting in intrinsic resistance to macrolides (70, 71). Both the modification of antibiotics and of antibiotic targets are successful defense strategies by the bacteria that need to be overcome during the development of new treatment regimens.

Pathology. The host response to infection also complicates TB treatment. Following infection with *M. tuberculosis*, the immune system is activated. Cells are recruited to the site(s) of infection, forming lesions surrounding infected tissue. These lesions, known as granulomas, play a complex role in infection by both working to control bacterial growth by enclosing infected cells and also aiding in transmission upon break-down and release of necrotic tissue (72, 73). Lesions also impact effective antibiotic treatment as antibiotics must penetrate the multiple layers of cell types to reach the bacteria (74). While RIF and PZA are able to efficiently accumulate in lesions at minimum inhibitory concentration (MIC) levels, INH only accumulates in 65 percent of lesions (74). However, RIF and PZA are only administered together for the first two months of therapy. Therefore, during the continuation phase of INH and RIF there may be transient monotherapy in these lesions. Additionally, recent studies have shown that individual antibiotics sterilize lesions variably and at different rates (75). Both decreased concentration of antibiotics and transient monotherapy limit the effectiveness of treatment and potentially increase the development of resistance. Identification of antibiotics which successfully penetrate lesions is crucial in the improvement of TB treatment.

Genetic Resistance

Resistance to the antibiotics used for TB was observed shortly after the introduction of the first treatment regimen (8). In 2018, an estimated half a million new cases of drug-resistant TB were reported globally (5). Treatment of drug-resistant infections requires longer regimens with more toxic antibiotics and has decreased success rates compared to DS-TB (5). Lack of evidence of horizontal gene transfer (HGT) in pathogenic *M. tuberculosis* indicates that all resistance-conferring mutations occur *de novo* during infection. Here, I will discuss the mechanisms of genetic resistance observed for each of the first-line antibiotics used to treat DS-TB.

Isoniazid. Early investigators of INH resistance observed decreased catalase activity in resistant isolates. In the 1990s, genetic experiments identified KatG as the INH-activating catalase-peroxidase and that mutations in the *katG* gene confer INH resistance (76, 77). Shortly after, *katG* mutations were identified in resistant clinical isolates (78-80). Mutations in *katG* are the most common resistance-conferring mutations, specifically the mutation S315T (81). While deficient in the activation of INH, these mutants retain essential catalase-peroxidase activity which may be advantageous *in vivo* (82). Mutations in the target of INH, *inhA*, are also present in resistant isolates. Most commonly, promoter mutations leading to overexpression of *inhA* are found (83). Mutations located in the open reading frame confer resistance via a decrease in affinity for INH-NAD binding (81, 83, 84). Additionally, mutations disrupting formation of

INH-NAD adducts also cause resistance. Observed mutations in *ndh*, encoding the type II NADH dehydrogenase, lead to NADH accumulation and competitive inhibition of InhA binding (83, 85, 86). Additional genes have been identified in INH resistant strains; however, many of these mutations are rare or found only in strains containing more common resistance-conferring mutations (87). Due to resistance-conferring mutations occurring in multiple locations in the genome, INH susceptibility testing is performed phenotypically.

Ethambutol. Resistance to EMB is most commonly caused by mutations within the *emb* operon (88). Multiple mutations in *embA*, *embB*, and *embC* were observed in resistant clinical isolates and transformation of these mutations into susceptible isolates conferred EMB resistance (89, 90). The most frequently observed clinical mutations are in *embB* (88-90). Additionally, EmbB306 mutations have been shown to alter susceptibility to other antibiotics, such as INH and RIF, and are found in strains containing additional resistance-conferring mutations (91, 92), indicating that these mutations potentially provide a stepping stone for progressive resistance development. While a majority of EMB resistant strains contain mutations in the *emb* operon, mutations in other genes and regions have also been identified (88), potentially complicating phenotypic and molecular susceptibility testing for EMB.

Rifampin. High-level RIF resistance is confined to mutations within a region in the β -subunit of the RNA polymerase, known as the rifampin resistance-determining region (RRDR). Mutations in the *M. tuberculosis rpoB* gene,

encoding the β -subunit, was first described in 1993 through PCR-analysis of resistant clinical isolates (93). Due to the specificity of the location of these mutations, PCR-based susceptibility testing was soon introduced (94), and molecular testing for RIF resistance remains the current standard. While RNA polymerase mutations result in fitness costs for the bacteria (3, 95), these deficits can be alleviated by compensatory mutations which have been identified in *rpoA* and *rpoC* in clinical isolates (96). RIF resistance is highly associated with MDR infections. Therefore, due to the speed and efficiency of molecular testing, a majority of RIF-resistant infections are categorized as MDR when choosing treatment regimens.

Pyrazinamide. Loss of pyrazinamidase activity in PZA resistant *M. tuberculosis* strains is a known resistance mechanism (30). The bacterial pyrazinamidase PncA, the activator for PZA, is the most commonly mutated gene in PZA resistant strains (31, 97, 98). PncA is non-essential for bacterial survival and mutations are observed throughout the entire gene; however, three regions associated with the active site are the most commonly mutated (97, 99, 100). Mutations in additional genes outside of *pncA*, including *rpsA* and *panD*, have been observed in rare cases (36, 101-103). Although PZA is a critical component in TB treatment, susceptibility testing is not ideal due to poor *in vitro* efficacy of PZA. Testing requires acidified media and low bacterial density, resulting in inconsistent and false resistance results (104). Despite these challenges,

molecular testing is less sensitive than most phenotypic tests and, therefore, not recommended (105).

M. tuberculosis has evolved genetic resistance for each of the first-line antibiotics used to treat DS-TB which negatively affects patient outcomes and the spread of disease. Additionally, resistance to the second-line and injectable antibiotics used to treat multi-drug resistant (MDR-TB) and extensively-drug resistant (XDR-TB) infections is now common. Treatment of these resistant infections requires longer regimens with more toxic and expensive antibiotics, increasing the global health burden of TB.

Tolerance

Antibiotic tolerance is a bacterial survival strategy. In this case, non-resistant populations have decreased antibiotic sensitivity, resulting in the requirement of prolonged therapy to achieve successful treatment and the prevention of relapse. Experimentally, tolerant populations do not have different minimum inhibitory concentrations (MIC), but alterations in minimum bactericidal concentrations (MBC) and rate of killing (106, 107), as first described in 1970 (108). Early observation of tolerance phenotypes described the clinical implications of the decreased efficacy of cell wall inhibitors against slow and non-growing bacterial populations in multiple organisms (106, 109-111). Antibiotic tolerance can be phenotypically regulated through mechanisms resulting in physiological changes or genetically controlled. A common example of genetic

tolerance is the use of phase and antigenic variation to produce heritable tolerance in bacterial populations, which can occur via multiple mechanisms, such as slip-strand-mispairing (SSM), recombination, and epigenetic regulation (112). Antibiotic tolerance has been described in *M. tuberculosis* populations (113), and is a major contributing factor to the need for lengthy treatment. I will discuss the known mechanisms of antibiotic tolerance in *M. tuberculosis* below.

Slow growth and dormancy. Differences in antibiotic efficacy between growing and non-growing bacteria were observed as early as 1957 (114, 115). *M. tuberculosis* is inherently a slow-growing organism, with a doubling time of approximately 20 hours *in vitro* which greatly slows to approximately 100 hours during infection (116, 117). Growth rate also varies based on asymmetrical cell growth and division, resulting in differential susceptibility to certain antibiotics (118). Additional observations of heterogeneity in daughter cells further implicates cell division as a mechanism of tolerance in *M. tuberculosis* (119). Different environments encountered during infection, such as hypoxia and nutrient deprivation, lead to non-replicating, metabolically active bacterial populations (120-125). Cell wall remodeling is a major adaptation in these environments through mechanisms such as alterations to peptidoglycan cross-linking and cell wall thickening (126, 127). These changes result in reduced drug uptake, leading to drug tolerance (128). Identification of new antibiotics which target both replicating and non-replicating populations remains a major goal in the improvement of TB treatment.

Metabolism alterations. A unique characteristic of *M. tuberculosis* is its ability to co-catabolize multiple different carbon sources feeding into distinct pathways (129). The current knowledge of *M. tuberculosis* central carbon metabolism under different environmental conditions has been gained through a combination of genomics, transcriptomics, metabolomics and systems modeling (129-136). Previous work has shown that, during infection, bacteria utilize fatty acids as a main carbon source (132, 133, 137-140). In response to environmental stresses, such as hypoxia, there is a change in carbon flux and an accumulation of triacylglycerol (TAG) which is used as a fatty acid source (135, 141, 142). TAG accumulation decreases metabolic activity which affects antibiotic activity. *M. tuberculosis* mutants in this pathway are more sensitive to multiple antibiotics, and the enzymes involved can be targeted with small molecules, resulting in killing (143, 144). Targeting the carbon flux of *M. tuberculosis* could reduce antibiotic tolerance, providing a new avenue for drug development.

Genetic tolerance. Genetic tolerance in *M. tuberculosis* has recently been investigated using strains with mutations associated with clinical resistance (145). Transcription factor *prpR* mutants are significantly associated with clinical INH-resistance. Under antibiotic treatment these mutations result in an increase in the minimum duration of killing (MDK) compared to wild-type strains, indicating these strains are antibiotic tolerant (145). Genetic tolerance mediated by phase variation has been observed in certain mycobacterial species (146, 147).

However, phase variation has not been observed in *M. tuberculosis*, and its potential role in antibiotic tolerance is currently unknown. Whole-genome sequencing (WGS) studies of *M. tuberculosis* clinical isolates to identify single nucleotide polymorphisms (SNPs) associated with resistance phenotypes (145, 148-150) could aid in the identification of genetic mutations that prolong survival under treatment.

Thesis objectives

The aim of this work is to better understand how *M. tuberculosis* survives the long and complex treatment regimen. Although antibiotic treatment for TB infections has been used since the 1940s, we still do not fully understand the physiology of the bacteria during treatment, thus limiting the development of new antibiotics and treatment regimens. Significant progress has been made, as discussed above; however, much of this work has been performed under defined conditions. *M. tuberculosis*, an obligate intracellular pathogen, encounters many different environments and stresses throughout infection which are impossible to replicate *in vitro*. To probe mechanisms of survival in complex host environments, I utilized an unbiased, comprehensive genetic approach and the mouse model of TB to identify *M. tuberculosis* mutants with altered susceptibility to antibiotic treatment during infection. Specifically, I aim to:

1. Identify mutants with altered susceptibility to DS-TB combination therapy to gain insight into prolonged survival under complex treatment regimens.
2. Assess mutant fitness under treatment with individual antibiotics to identify both drug-specific and broad mechanisms of antibiotic tolerance in *M. tuberculosis*.

Together these data and analyses will provide insights into *M. tuberculosis* physiological state under antibiotic pressure, contributing to the understanding of antibiotic resistance development and identifying potential new targets for improved treatment.

CHAPTER II: Common Variants in the Glycerol Kinase Gene Reduce Tuberculosis Drug Efficacy

Michelle M. Bellerose,^{a*} Seung-Hun Baek,^{b*} Chuan-Chin Huang,^c Caitlin E. Moss,^a Eun-Ik Koh,^a Megan K. Proulx,^a Clare M. Smith,^a Richard E. Baker,^a Jong Seok Lee,^d Seokyong Eum,^d Sung Jae Shin,^b Sang-Nae Cho,^d Megan Murray,^c Christopher M. Sassetti^a

^aDepartment of Microbiology and Physiological Systems, University of Massachusetts Medical School, Worcester, Massachusetts, USA; ^bDepartment of Microbiology, Institute for Immunology and Immunological Diseases, Yonsei University College of Medicine, Seoul, South Korea; ^cDepartment of Global Health and Social Medicine, Harvard Medical School, Boston, Massachusetts, USA; ^dInternational Tuberculosis Research Center, Changwon, South Korea

*Contributed equally

This chapter was published in 2018 in mBio: <https://doi.org/10.1128/mBio.00663-19>.

MMB, SB, and CMS conceived projects and designed experiments. MMB and CMS prepared the manuscript. REB designed computational analyses for TNseq. EK generated data in figure 2.2A. SB and CEM produced data in Figure 2.4 and REB analyzed WGS data. Data and analyses in figure 2.5 was generated by CH and MM.

Introduction

The currently used multidrug chemotherapy regimen for tuberculosis (TB) was developed in a series of clinical trials in the 1980s (14) and remains the standard of care for this disease (15). Infections with drug-sensitive strains of *Mycobacterium tuberculosis* are treated with a 6-month regimen that includes four drugs, isoniazid (INH), rifampin (RIF), pyrazinamide (PZA), and ethambutol (EMB). While this regimen cures 90% of drug-sensitive cases, the long period over which antibiotics must be administered represents a major limitation. Not only is a complete regimen difficult to deliver, but even in clinical trial settings, incomplete sterilization leads to relapse in a significant fraction of patients (49). The emergence of drug-resistant strains of *M. tuberculosis* further confounds therapy and necessitates even longer regimens with less effective drugs.

The factors that necessitate this extended drug regimen for TB remain difficult to dissect because the *in vitro* efficacy of individual drugs does not predict their effect during infection. For example, PZA is critical for sterilizing an infected host, but it has very modest activity *in vitro*, where it may act via different mechanisms (151). Conversely, both INH and RIF cause relatively rapid cell death *in vitro* but kill bacteria much more slowly during infection. As a result, virtually all TB drug regimens kill bacteria at a lower rate during infection than they do in axenic culture. Two general mechanisms have been proposed to explain the generally drug-tolerant phenotype that is observed during infection. Growth in mammalian tissue triggers changes in mycobacterial gene expression

and metabolism that can reduce drug efficacy (61, 143, 152). In addition, a number of distinct stochastically generated subpopulations have been observed, which arise either via asymmetric cell division (118) or nonheritable regulatory events (119). Some of these subpopulations are relatively insensitive to antibiotics *in vitro* and could prolong the treatment period necessary for sterilization. While none of these mechanisms involve heritable genetic changes, many other bacteria rely on high-frequency reversible genetic variation to produce subpopulations that are tolerant to environmental insults (112). This process of phase variation generally relies on specific DNA sequences, such as homopolymeric regions, that are subject to frequent mutation. While phase variation has been observed in several mycobacterial species (146, 147), it has not been specifically characterized in *M. tuberculosis*, and its potential role in determining drug efficacy is unknown.

To understand the processes that determine drug efficacy during infection, we employed two complementary approaches. A forward genetic study identified bacterial functions that alter drug efficacy in mice. In parallel, whole-genome sequence analysis of *M. tuberculosis* clinical isolates identified genetic variants in candidate genes that are associated with resistance. Together, these approaches defined a variable homopolymeric region in the *glpK* gene that controls glycerol metabolism and drug efficacy. Heritable genetic variation at this site produces a drug-tolerant phenotype that reduces treatment efficacy and is associated with the emergence of resistant clones.

Results

Genetic determinants of drug efficacy in the mouse model

To specifically define bacterial functions that limit efficacy during infection, we used transposon sequencing (TNseq) to identify mutations that alter bacterial killing. Groups of mice were infected with a nearly saturated library of *M. tuberculosis* transposon mutants via the intravenous route. After allowing 2 weeks for bacterial growth and the establishment of adaptive immunity, animals were treated with a regimen based on first-line TB chemotherapy, a mixture of INH, RIF, PZA, and EMB (HRZE) (Figure 2.1A). Each drug in this regimen was shown to be effective individually at the dose given, and the four-drug mixture reduced organ burden by more than 100-fold after 14 days of treatment (Figure 2.1B). To identify mutations with relatively rapid effects on bacterial killing by antibiotics, mutant pools were recovered from the spleen after 1 week of therapy by plating organ homogenates. This analysis was performed in the spleen because this organ contained an adequate bacterial population size to ensure that complexity of the library was maintained throughout the infection. *In vivo*-selected libraries were compared to each other using TNseq, which quantifies the relative abundance of each mutant in a given pool by sequencing all the transposon-chromosome junctions that are present (153).

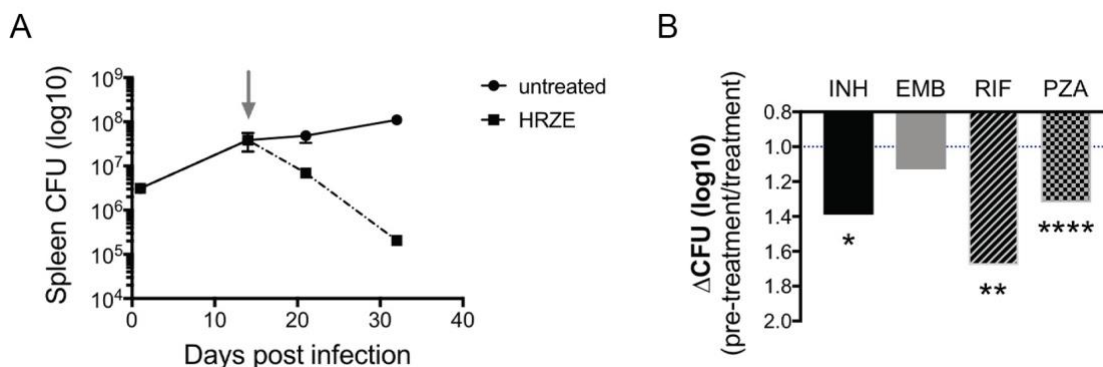


Figure 2.1 | Antibiotic treatment of *M. tuberculosis* infected mice.

A, Spleen CFU from BALB/c mice infected with transposon mutant library both untreated (circles) and after HRZE treatment (squares). Antibiotic treatment was started at 14 dpi (indicated by gray arrow). Plotted means from 3 biological replicates with standard deviations are shown. **B**, Change in CFU after treatment with the indicated antibiotic for 5 weeks. The change in CFU between pretreatment and posttreatment samples is presented. Significance was calculated using unpaired *t* test: *, $P = 0.03$; **, $P = 0.002$; ***, $P = 0.0002$; ****, $P < 0.0001$.

Mutant pools were collected from three groups of animals. A pretreatment pool was collected immediately before drug administration. One week later, pools from antibiotic-treated or untreated groups were collected. This study design allowed the relative fitness of each bacterial mutant to be assessed in the presence and absence of drug therapy. Pairwise analyses of the treated and untreated pools with the pretreatment library identified distinct sets of genes that altered bacterial representation under each condition (Appendix Tables A2.1 – A2.3). As many antibiotics act in a growth rate-dependent manner, we investigated whether bacterial fitness *in vivo* was an important determinant of antibiotic efficacy.

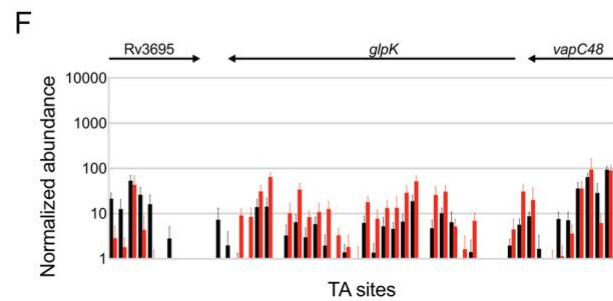
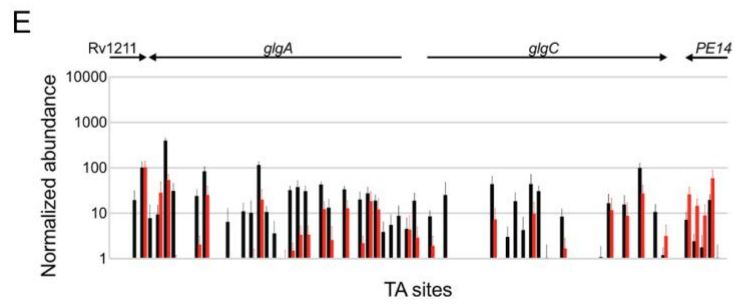
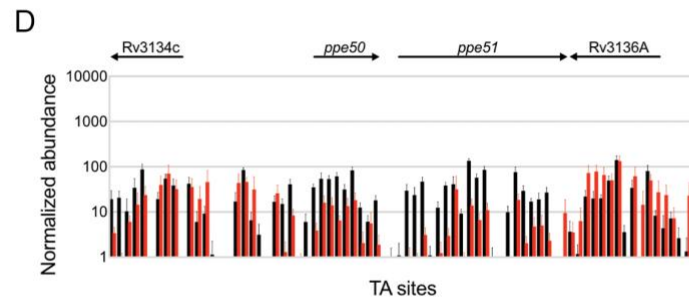
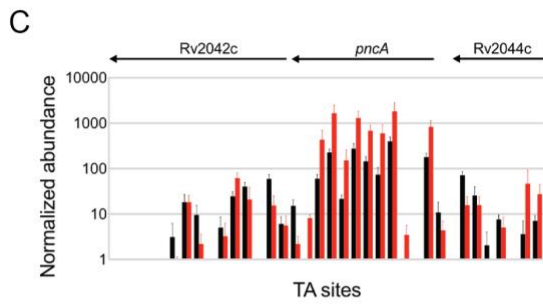
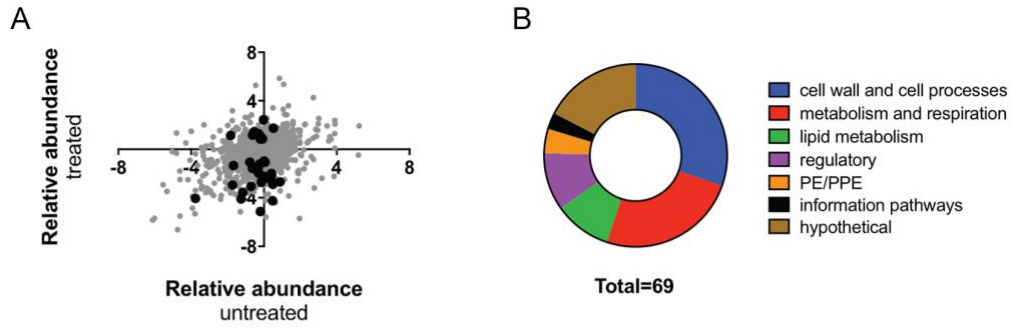


Figure 2.2 | Genetic strategy to define bacterial functions that limit drug efficacy.

A, Relative abundance of individual mutants, measured by \log_2 fold change, in untreated mice (*x* axis) and HRZE-treated mice (*y* axis). Significantly altered mutants after treatment are indicated in black. **B**, Functional classes of mutants with altered susceptibility in vivo. Classification from Mycobrowser. **C-F**, Normalized abundance of mutations in pretreatment (black) and after HRZE treatment (red) at individual TA dinucleotide insertion sites in *pncA* (**C**) *ppe50-ppe51* (**D**) *glgA-glgC* (**E**) and *glpK* (**F**). Shown are the average numbers of unique sequence reads (*y* axis) plotted versus TA sites (*x* axis).

When the relative abundance of each mutant in untreated animals was compared with their abundance in time-matched drug-treated mice, we found no global correlation between bacterial fitness in the presence and absence of antibiotic (Figure 2.2A). However, several individual mutations were observed that reduced fitness under both conditions. Thus, to more formally focus our study on drug-related phenotypes, we performed a three-way analysis to identify those mutations that alter fitness preferentially in antibiotic-treated animals. This analysis defined 61 mutants that increased, and 8 that reduced, the effect of therapy (Appendix Tables A2.4 and A2.5). These mutants corresponded to a variety of functional pathways (Figure 2.2B). In several cases mutation resulted in dramatic alterations in fitness after drug exposure, as the relative representation of these mutants under the pre- and posttreatment conditions varied by more than 100-fold.

A number of functions found to alter bacterial fitness in drug-treated mice were already known to impact drug efficacy. For example, mutants lacking PncA, which converts PZA into its active pyrazinoic acid form (31), were highly

overrepresented in the treated mice, highlighting the singular importance of PZA in the activity of this regimen (Figure 2.2C). In addition, we found that mutations in *mmaA1*, *mmaA2*, and *cmaA2* sensitized the bacterium to drug treatment. All of these genes encode functions necessary for mycolate modification, and chemical inhibition of these partially redundant activities has been shown to increase cellular permeability to antibiotics (154). Additional protein families associated with cell wall structure altered drug efficacy. PE/PPE family members have been implicated in cell envelope integrity (155), and we found that mutations in the *ppe50-ppe51* pair increased killing (Figure 2.2D). Conversely, the loss of enzymes (*ppsA*, *ppsC*, and *drrA*) necessary for the synthesis of the major cell envelope lipid, phthiocerol dimycocerosate, decreased clearance. Drug access appeared to be similarly limited by multiple classes of efflux pumps, as mutations in members of the ATP-binding cassette (*rv1747*), major facilitator superfamily (*rv3728*), and MmpL (*mmpL8* and *mmpL10*) families were found to increase bacterial clearance (Appendix Table A2.4).

In addition to these known mechanisms, we identified a number of novel functions that altered bacterial killing. Prominent among these were pathways involved in carbon metabolism. For example, mutation of both assayable steps of the glycogen synthetic pathway (*glgA* and *glgC*) increased antibiotic activity (Figure 2.2E). This pathway promotes carbon storage through carbohydrate anabolism, a general process that has been previously implicated in drug tolerance (143). In addition, we identified the *glpK* gene, which encodes the *sn-*

glycerol-3 kinase of *M. tuberculosis*. Twenty-six of the 29 insertional mutants in this gene showed a similar decrease in clearance rate upon drug treatment (Figure 2.2F). When pools isolated before and after treatment were directly compared, only *pncA* mutations produced a statistically significant reduction that was greater than those in *glpK* (Figure 2.3). This relatively dramatic phenotype was explored in more detail.

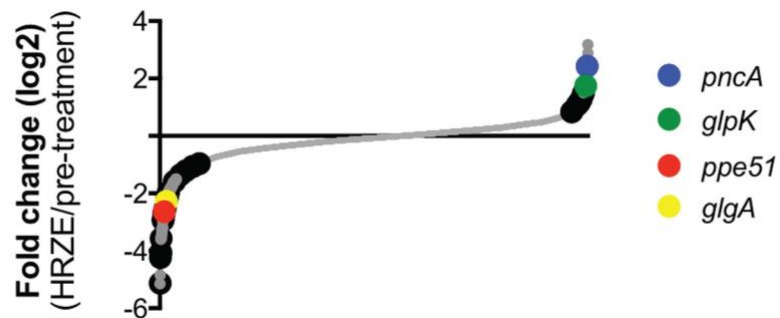


Figure 2.3 | Genes with altered susceptibility to HRZE treatment *in vivo*.

Log₂ fold change of individual mutants (gray dots) 1 week posttreatment compared to pretreatment. Significantly altered mutants are indicated by black circles.

Glycerol metabolism increases drug efficacy *in vitro* and during murine infection

GlpK is responsible for phosphorylating the 3-position of glycerol, which is necessary for its catabolism via the lower glycolytic pathway. To determine if glycerol catabolism *per se* was capable of enhancing the activity of TB drugs, the effects of INH, RIF, and moxifloxacin (MOX) were compared in media containing

glycerol or other carbon sources known to be used during infection, fatty acid and cholesterol (132, 156). These carbon sources supported different growth rates, which can confound endpoint- based determinations of antibiotic activity, such as standard MIC measurements. As a result, we quantified the growth rate (GR) of bacteria over a time course and determined the concentration of each drug that was necessary to decrease this rate by 50%, which is expressed as GR₅₀ (157). Using this approach, we found that glycerol catabolism produced a modest but reproducible decrease in the GR₅₀ for several drugs. Growth in glycerol significantly increased the efficacy of RIF and MOX compared to growth in valerate and enhanced the efficacy of INH and MOX compared to growth in cholesterol (Figure 2.4).

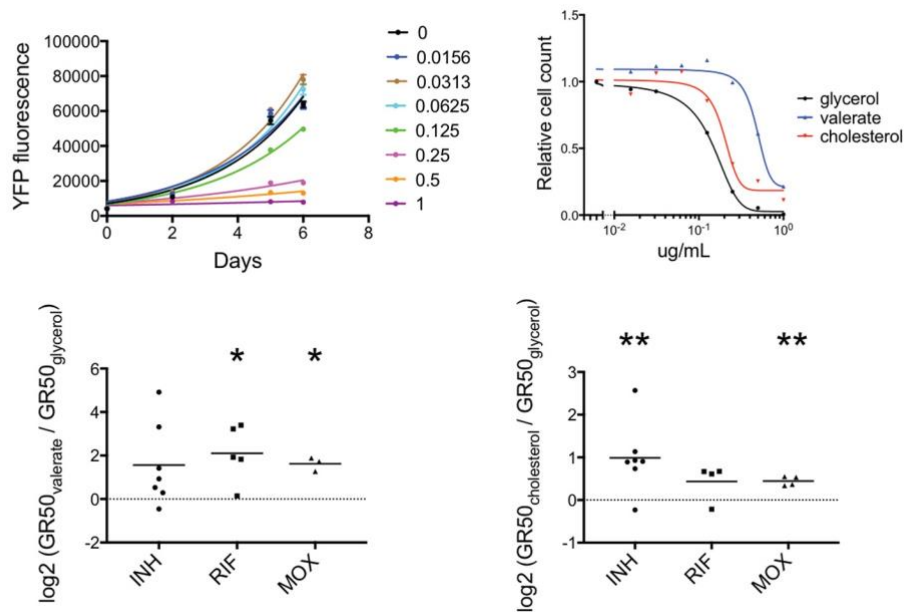


Figure 2.4 | Glycerol metabolism broadly increases drug efficacy *in vitro*.

Top left, Growth of H37Rv on cholesterol and treated with moxifloxacin at the indicated concentrations. Growth was measured by yellow fluorescent protein (YFP) fluorescence. **Top right**, GR₅₀ for moxifloxacin (MOX) in medium containing either glycerol, valerate, or cholesterol. **Bottom**, GR₅₀ ratios for INH (circles), RIF (squares), and MOX (triangles) grown on different carbon sources. Shown are valerate/glycerol (left) and cholesterol/glycerol (right). Significance was calculated using one-sample *t* test with a theoretical mean value of 0: *, P = 0.05; **, P = 0.01.

To further investigate the role of glycerol metabolism in drug efficacy, a *glpK* deletion mutant of *M. tuberculosis* was constructed. The $\Delta glpK$ mutant was unable to grow in media containing glycerol as the sole carbon source (Figure 2.5A), indicating that the deleted gene encodes the sole glycerol-3 kinase activity. The effect of antibiotics on the growth rates of *glpK*-sufficient and *glpK*-deficient strains was then compared in media containing different carbon sources. When glycerol was present in the medium, the $\Delta glpK$ mutant was significantly less sensitive to INH and RIF than the wild-type or the complemented mutant (Figure 2.5B). This difference largely disappeared when glycerol was replaced with either the nonglycolytic substrate, butyrate, or a glycolytic product that bypasses the triose phosphate pool, pyruvate. The differential effects of these carbon sources indicated that the assimilation of exogenous glycerol was primarily responsible for *glpK*'s influence on drug sensitivity. PZA sensitivity was assessed at pH 5.8 to maximize the *in vitro* efficacy of the drug. However, under these conditions, *glpK* deletion did not alter PZA sensitivity. As INH, RIF, and MOX have distinct mechanisms of action, the

effect of glycerol catabolism on antibiotic activity *in vitro* did not appear to be specific to a particular drug or target pathway.

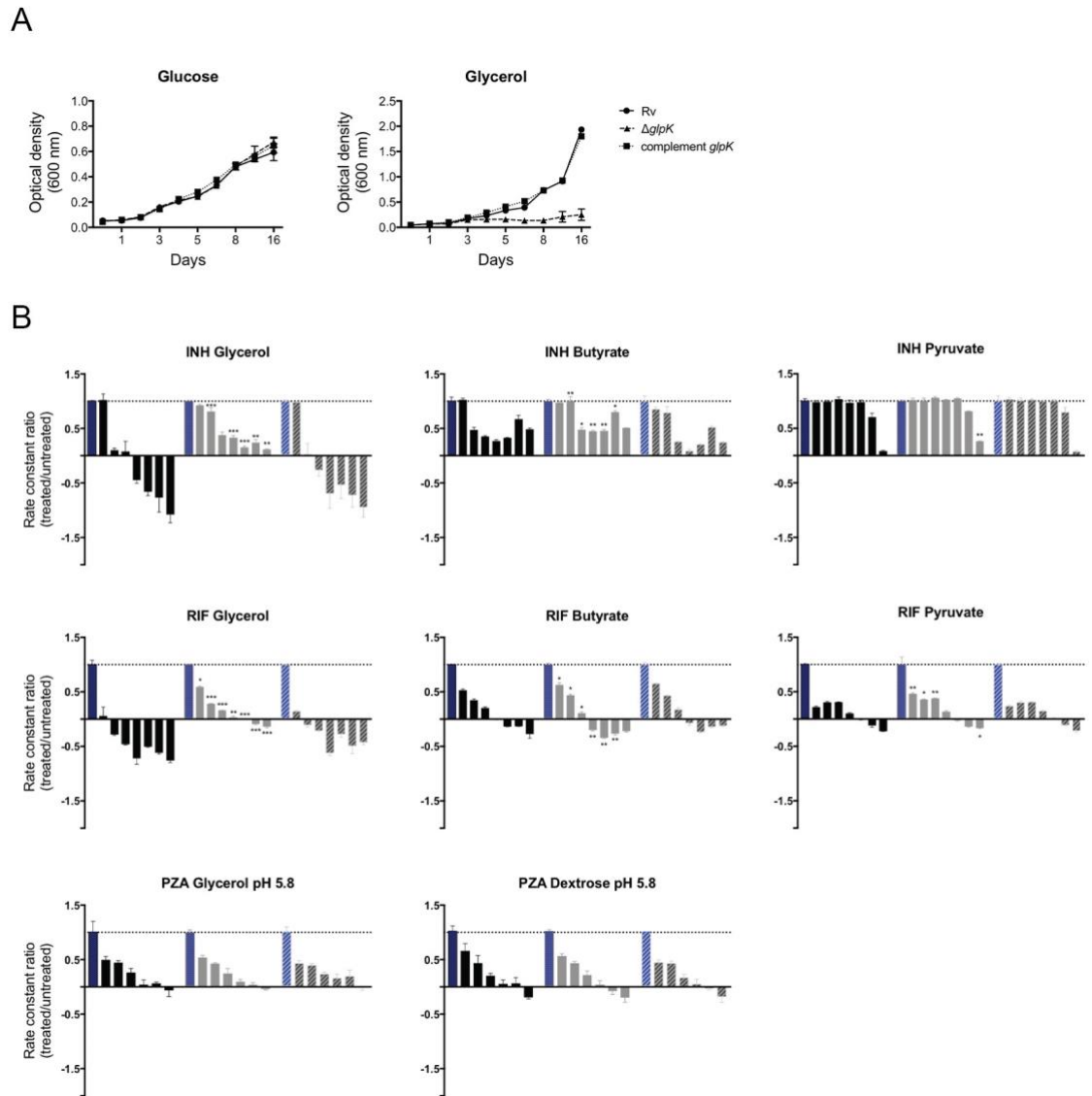


Figure 2.5 | $\Delta gfpK$ antibiotic susceptibility *in vitro*.

A, Growth kinetics of H37Rv (circles), $\Delta gfpK$ (triangles), and complement (squares) strains on glucose (left) and glycerol (right). Plotted means from 3 biological replicates with standard deviations are shown. **B**, Growth of H37Rv (black bars), $\Delta gfpK$ (gray bars), and complement *gfpK* (striped bars) strains after treatment with INH or RIF in media

containing glycerol, butyrate, or pyruvate and PZA in media containing glycerol or dextrose at pH 5.8. Growth was assessed by the growth constant, k , normalized to no-antibiotic controls and plotted as ratios (treated/untreated), where 1 is the growth constant without antibiotic (indicated by a dotted line). Antibiotic concentrations started at 2 $\mu\text{g/ml}$, 1 $\mu\text{g/ml}$, and 400 $\mu\text{g/ml}$ for INH, RIF, and PZA, respectively, and were serially diluted 2-fold for 6 dilutions. Significance was calculated using an unpaired t test with Benjamini-Hochberg multiple-testing correction. *, $P = 0.03$; **, $P = 0.002$; ***, $P = 0.0002$; ****, $P < 0.0001$.

The mouse model was then used to explore the role of *glpK* during infection. Consistent with both our TNseq data and previous work (158), deletion of the *glpK* gene did not affect the growth or persistence of *M. tuberculosis* in the lungs of mice after aerosol infection (Figure 2.6A). To quantify the effect of *glpK* deletion on the efficacy of individual drugs, mice were inoculated via the intravenous route with a mixture of wild-type and $\Delta\textit{glpK}$ bacteria and treated with antibiotics, as was done for the initial TNseq screen. Another mutant lacking the *ppe51* gene, which TNseq predicted to be hypersensitive to multidrug treatment (Figure 2.2D), was included as an additional control. Since this study did not require maintaining the complex mutant mixture needed in the TNseq study, more prolonged treatment regimens could be used. As we observed previously, all drug regimens reduced the bacterial burden, and PZA or combination therapy had the greatest effect (Figure 2.6B). Surviving bacteria were recovered by plating at the indicated time points, and the relative abundance of the three *M. tuberculosis* strains was determined by quantitative PCR. Both mutants demonstrated the predicted phenotypes in animals treated with the four-drug combination therapy for 2 weeks, as the $\Delta\textit{glpK}$ mutant was cleared significantly

more slowly and the $\Delta ppe51$ mutant significantly more rapidly than the wild-type (Figure 2.6C). These phenotypes were even more pronounced in animals treated with PZA alone. In contrast to the broadly sensitizing effect of glycerol catabolism *in vitro*, the $\Delta glpK$ mutant behaved similarly to the wild type in mice treated with RIF, INH, or EMB.

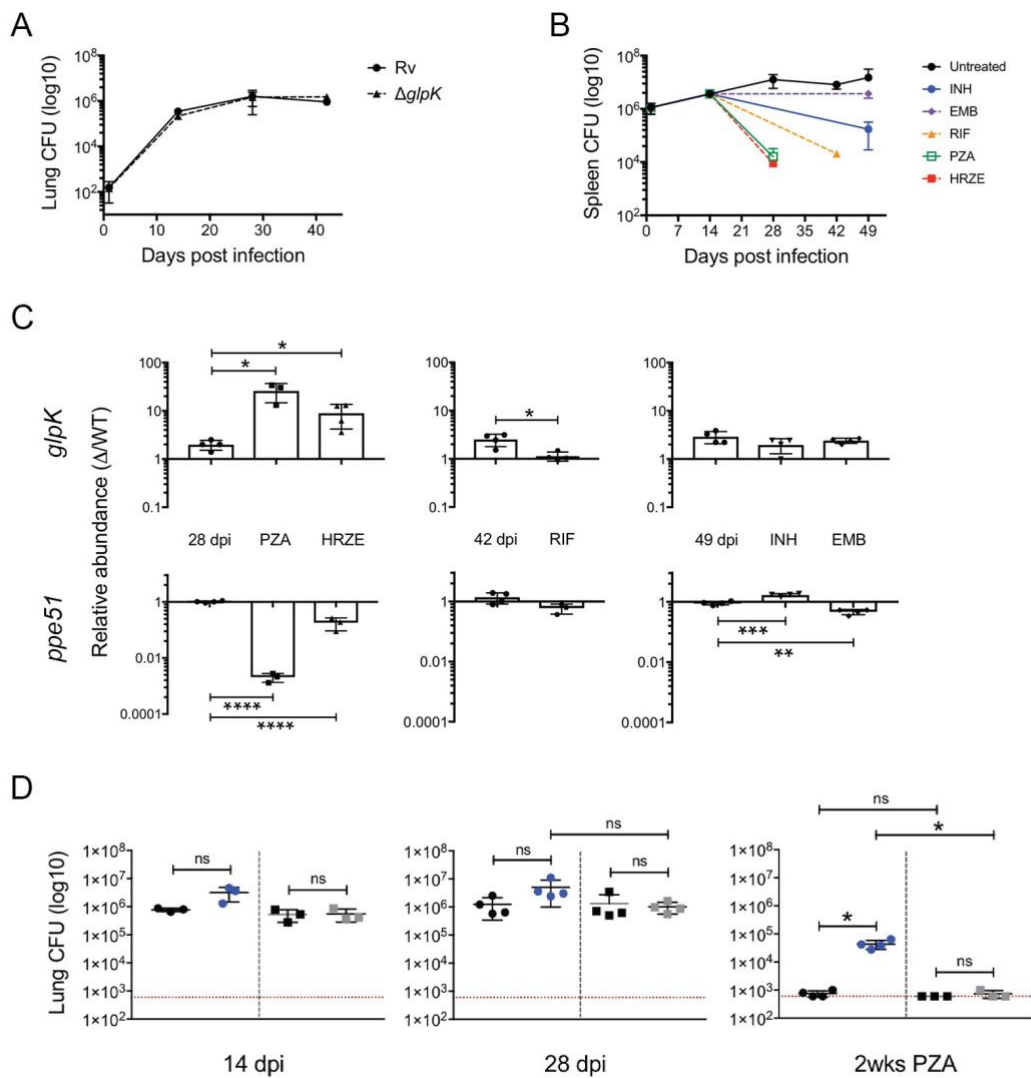


Figure 2.6 | Loss of glycerol kinase increases survival under PZA treatment *in vivo*.

A, Lung CFU of H37Rv (circles) and $\Delta glpK$ (triangles) strains from BALB/c mice after aerosol infection with a dose of 500 to 700 CFU/mouse. Shown are plotted means from 4 biological replicates with standard deviations. **B**, Spleen CFU from BALB/c mice after intravenous infection with pooled mutant strains both untreated (black circles) and treated with the indicated antibiotic. Plotted means from 4 biological replicates with standard deviations are shown. **C**, Relative abundance of $\Delta glpK$ (top) and $\Delta ppe51$ (bottom) strains compared to that of the wild-type *in vivo* after antibiotic treatment. Treatment times were 14 days for PZA and MIX, 28 days for RIF, and 35 days for INH and EMB. Individual points are biological replicates normalized to day 0 ratios. Significance was calculated using unpaired *t* test with Benjamini-Hochberg multiple testing correction: *, $P = 0.03$; **, $P = 0.002$; ***, $P = 0.0002$; ****, $P < 0.0001$. **D**, Lung CFU of H37Rv, $\Delta glpK$, and complement strains from BALB/c mice after aerosol infection and treatment with PZA. Data represent two competition infections: 1:1 H37Rv and $\Delta glpK$ (black and blue circles, respectively) strains, dose of 700 to 1,000 CFU/mouse, and 1:1 H37Rv and complement (black and gray squares, respectively) strains, dose of 300 to 500 CFU/mouse. Treatment with PZA was started at 21 dpi and continued to 35 dpi. Shown are plotted means and standard deviations, and individual points are biological replicates. Limits of quantification are indicated by dotted red lines. Significance was calculated using unpaired *t* test with Benjamini-Hochberg multiple testing correction: *, $P = 0.03$; **, $P = 0.002$; ***, $P = 0.0002$; ****, $P < 0.0001$; ns, not significant.

The decreased efficacy of PZA against the $\Delta glpK$ mutant was also found in the lungs of mice infected via aerosol. In this model, treatment with PZA between 21 and 35 days post infection reduced the bacterial burden of wild-type and $\Delta glpK$ complemented strains by at least 1,000-fold but had a significantly reduced effect on the *glpK*-deficient mutant (Figure 2.6D). Thus, while glycerol catabolism can nonspecifically alter antibiotic susceptibility *in vitro*, *glpK* deletion preferentially reduced the effect of PZA and a PZA-containing multidrug regimen in this animal model.

Glycerol catabolic defects are associated with extensive drug resistance in Korea

As the *glpK* deletion did not alter bacterial fitness during infection and conferred a benefit upon drug treatment, we hypothesized that mutations altering glycerol catabolism are positively selected during the evolution of drug resistance in natural populations. As a first test of this hypothesis, we characterized a panel of Korean *M. tuberculosis* isolates that varied in drug sensitivity profiles, from fully sensitive strains to extensively evolved clones that were phenotypically resistant to more than ten different antibiotics (Appendix Tables A2.6 and A2.7). To investigate whether glycerol catabolic defects were selected during the evolution of resistance in these strains, we subcultured a random subset of drug-sensitive or extensively resistant isolates in media containing glycerol as the sole carbon source. Drug-sensitive strains grew at a rate similar to that of a standard laboratory strain (H37Rv). However, while the extensively drug-resistant isolates could grow in butyrate, none of the tested isolates could grow in the glycerol-containing media (Figure 2.7).

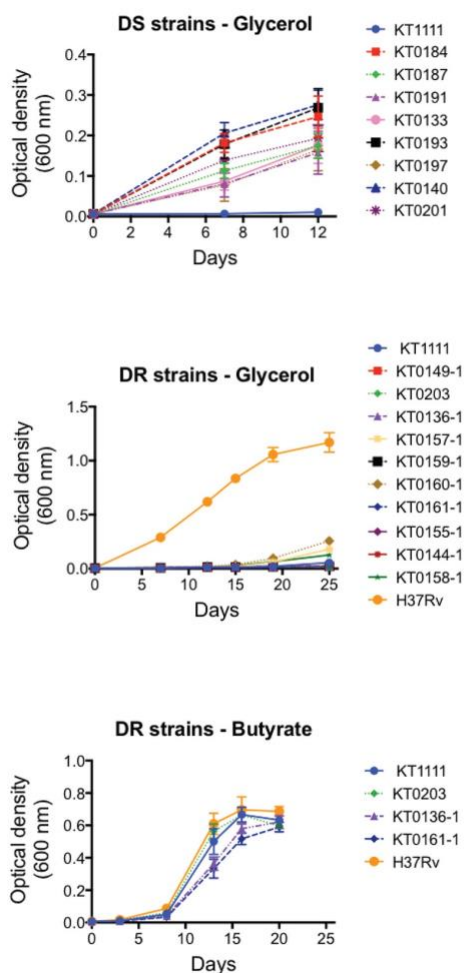


Figure 2.7 | Growth of extensively drug-resistant strains on individual carbon sources.

Growth kinetics of drug-susceptible (DS) and drug-resistant (DR) clinical isolates on glycerol- or butyrate-containing media. Shown are plotted means from 3 biological replicates with standard deviations.

The whole-genome sequences (WGS) of these isolates were determined. Based on WGS, this collection was predominantly comprised of a Korean sublineage of East Asian strains (159), and the multidrug-resistant (MDR) phenotypes could generally be attributed to known high-level resistance-conferring mutations. Inspection of the WGS data revealed that the glycerol catabolic defect in 9 of the 11 tested strains could be attributed to loss-of-function mutations in the *glpK* gene (Appendix Table A2.8). These strains all harbored a one-base expansion of the same homopolymeric sequence (GGGGGGG) in the

5' half of the *glpK* open reading frame. The sequence of the *glpK* homopolymer was verified in the entire panel by targeted Sanger sequencing (Figure 2.8A). This mutation is predicted to eliminate GlpK enzymatic activity, as it introduces a premature termination codon that eliminates the majority of the open reading frame, and the same homopolymer expansion has been previously observed in *M. bovis* strains lacking glycerol kinase activity (160). An additional missense mutation altering amino acid 169 was identified in an otherwise *glpK* wild-type allele, but the functional significance of this mutation is unclear. Two of the phenotypically glycerol-deficient strains carried no obvious mutations in *glpK* or other glycerol catabolic genes. Thus, while *glpK* frameshifts appear to be the most common lesion associated with glycerol catabolic defects in this collection, other mechanisms contribute in a fraction of isolates.

All ten of the *glpK* frameshifts identified in this panel were found in multidrug-resistant strains, particularly the highly evolved strains that were resistant to more than eight different drugs (Figure 2.8B). Based on the phylogenetic relationship between these strains, the identified *glpK* frameshifts represent at least three independent mutational events. Alternative tree topologies necessary to accommodate fewer mutational events were significantly less likely ($P < 10^{-4}$). Thus, in this relatively small collection of strains, inactivating mutations in *glpK* were frequent and associated with defective glycerol utilization and drug resistance.

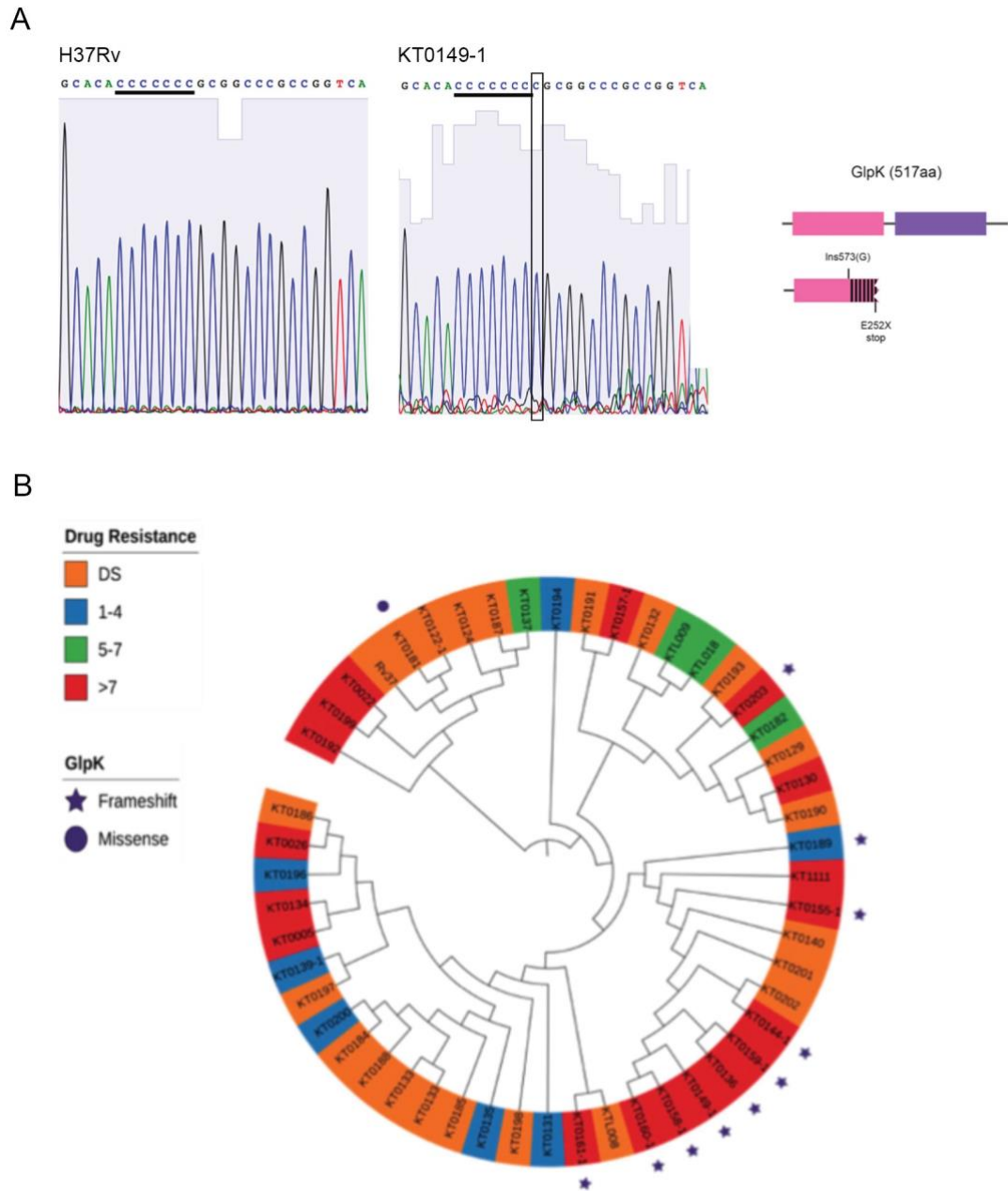


Figure 2.8 | Glycerol catabolic mutations associated with XDR strains.

A, Sanger sequencing of *glpK* from H37Rv and clinical isolate KT0149-1. The homopolymer region is in the first domain of the protein. One-bp insertion changes downstream amino acid sequence and introduces a premature stop codon at amino acid 252. **B**, Phylogenetic tree of *M. tuberculosis* isolates from Korea with various drug

susceptibility profiles: DS (orange); DR, 1 to 4 antibiotics (blue); DR, 5 to 7 antibiotics (green); and DR >7 antibiotics (red). Mutations in *glpK* gene are indicated: frameshift mutations, purple stars; missense mutations, purple circles.

GlpK frameshift mutations are common in *M. tuberculosis* isolates and associated with drug resistance in Peru

Frameshift mutations in homopolymeric DNA sequences can represent high-frequency and reversible events (112). To assess the frequency of this mutation in a larger population and to further explore its association with drug resistance, we analyzed the whole-genome sequences of a larger collection of isolates from Peru. Of 1,031 sequenced strains, 68 isolates harbored nonsynonymous variants in the *glpK* gene. Of these, 45 contained a single-base expansion of the *glpK* homopolymer and 2 contained a two-base expansion. These frameshifts were found in all phylogenetic clades of *M. tuberculosis*, indicating that this mutation has arisen through multiple distinct mutational events in different lineages of the pathogen (Figure 2.9A and B). In total, homopolymer expansion accounted for 66% of the nonsynonymous *glpK* variants, and 4.6% of all isolates harbored frameshift mutations disrupting the *glpK* open reading frame.

As we found in the smaller set of Korean strains, *glpK* frameshifts were significantly associated with drug resistance. No instances of *glpK* frameshifts were found in the 90 phenotypically drug-sensitive strains. In contrast, 44 of the 739 isolates that met the WHO criteria for MDR carried these mutations ($P = 3 \times$

10^{-5}). In this large collection, we were also able to test the association between *glpK* genotype and resistance to individual drugs and found significant associations with RIF, INH, and ethionamide (ETH) (Figure 2.9C). The lack of observed association with PZA resistance could have been due to the unreliability of this phenotypic assay. Indeed, using a genotypic assay we found a significant association between *glpK* frameshifts and nonsynonymous *pncA* variants ($P = 0.001$). Thus, the *glpK* homopolymer is the site of the majority of variation in this gene, and expansion of this hypervariable region is associated with the evolution of drug resistance.

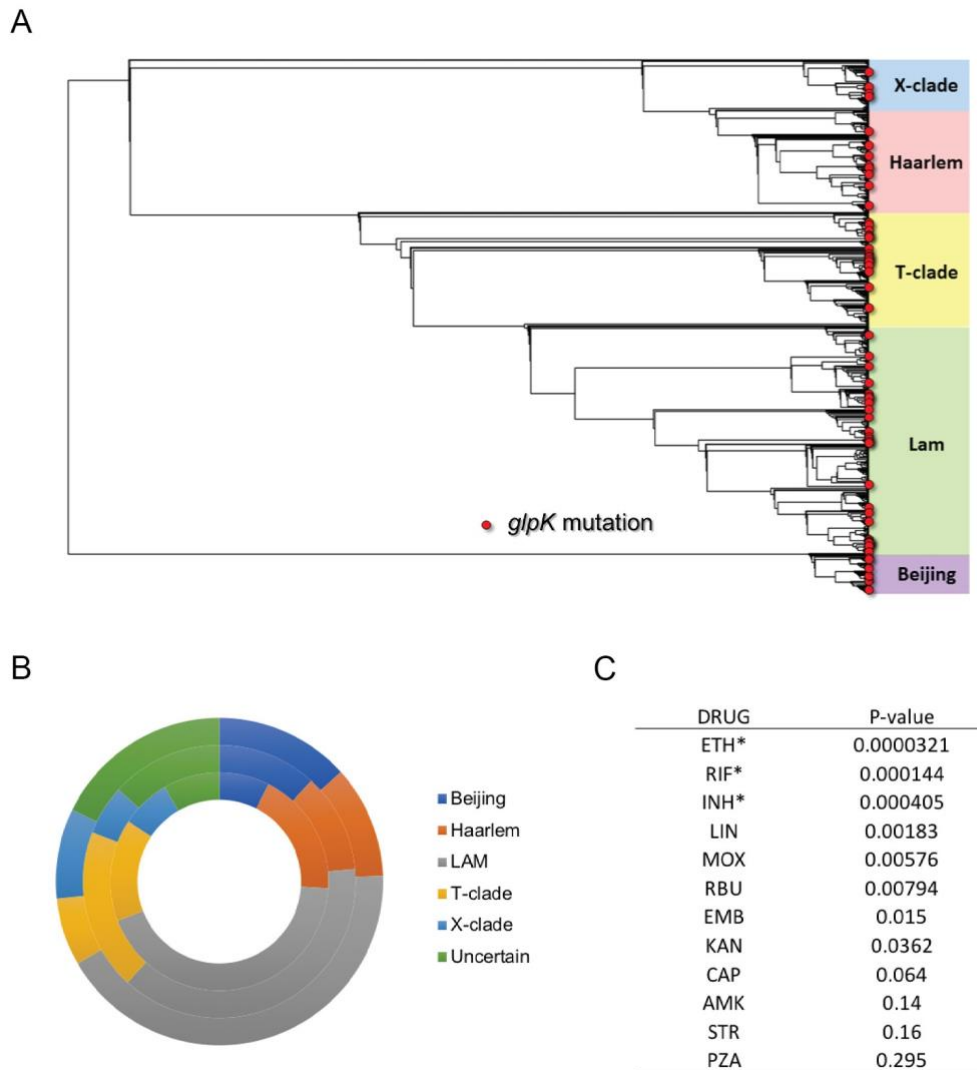


Figure 2.9 | GlpK mutations associated with drug resistance in clinical isolates from Peru.

A, Phylogenetic tree of *M. tuberculosis* isolates from Peru. GlpK mutations are indicated (red circles). **B**, Representation of GlpK mutations in different lineages: lineage distribution of 1,031 GWAS samples (outer); distribution of 68 *glpK* mutations (middle); distribution of 45 single-base expansions, T57GT, of the *glpK* homopolymer (inner). **C**, Association between *glpK* mutations and drug resistance. Statistical significance (*) based on Bonferroni correction with a type 1 error rate of 0.01. INH, isoniazid; RIF, rifampin; RBU, rifabutin; EMB, ethambutol; PZA, pyrazinamide; STR, streptomycin; LIN, linezolid; MOX, moxifloxacin; AMK, amikacin; KAN, kanamycin; CAP, capreomycin; ETH, ethionamide.

Discussion

Drug tolerance has been proposed to contribute to both relapsing TB disease and the emergence of drug-resistant clones (161). Most current models to explain tolerance in mycobacteria are largely restricted either to nonheritable processes, such as changes in gene expression or functionally asymmetric cell division, or stably heritable mutations (145). Our data provide a new mechanism by which alterations in a hypervariable region in the *glpK* gene produces bacteria that persist during antibiotic treatment and could contribute to the emergence of drug-resistant clones.

Insertions and deletions in a homopolymeric region of an open reading frame is a common mechanism to produce high-frequency reversible phenotypic variation in bacteria. These mutations are generally thought to result from slipped-strand mispairing during DNA replication. However, additional DNA repair mechanisms, such as mismatch repair (162) or base excision repair (163), can alter the frequency and directional bias of the process. The exclusive bias for +1 and +2 frameshifts in the *glpK* gene of clinical isolates argues for a more complex process than simple replicative error, and the ultimate frequency of mutants may also be influenced by the specific fitness effect of each frameshift. As a result, it is difficult to anticipate the rate of variation that occurs during infection.

Regardless, we identified +1 and +2 frameshifts in 6% of the Peruvian MDR isolates. Since clinical samples are routinely cultured in glycerol-containing media, which would be expected to select for reversion to the wild-type *glpK*

coding sequence, it is likely our data underestimate the frequency of *glpK* mutants. The observed prevalence of this mutation is clearly high enough to produce a significant population of *glpK*-deficient clones that alter drug efficacy.

Our studies in the mouse model demonstrate that *glpK*-deficient bacteria are drug tolerant during infection. The mechanism(s) that underlies the drug tolerance of *glpK*-deficient bacteria is likely to be complex. Common fates for glycerol-3-phosphate are catabolism via the lower glycolytic pathway, incorporation into anabolic pathways, and spontaneous degradation to methylglyoxal. As a result, glycerol assimilation can alter growth rate, metabolism, and cellular structure. While not yet conclusive, our *in vitro* studies argue against some of these mechanisms. Both the *in vitro* effects of glycerol supplementation and the *in vivo* effects of *glpK* expression were independent of growth rate (Figures 2.2 and 2.5), and the differential effect of *glpK* in glycerol versus pyruvate growth media indicates that glycolytic flux *per se* is not the major determinant of drug efficacy. Thus, we speculate that the abundance of the triose phosphate pool or some derivative of this pool is primarily responsible for the general enhancement of antibiotic efficacy that we observed upon glycerol assimilation *in vitro*.

The nonspecific effect of *glpK* on multiple drugs that we observed *in vitro* is consistent with previous studies that identified frameshifts in the *glpK* homopolymer in mutants selected for spontaneous resistance to investigational anti-mycobacterial compounds *in vitro* (158). Similarly, *glpK* mutations have also

been found in conjunction with additional mutations in strains selected to be drug tolerant (164) or PZA resistant (41) *in vitro*. Despite these relatively general effects on drug activity *in vitro*, *glpK* deletion preferentially reduced the efficacy of PZA-containing regimens in the mouse model used in this study. This apparent discrepancy could reflect differences in drug exposure, bacterial physiology, or GlpK functions in these two settings. The poor activity of PZA *in vitro*, where we observed no effect of *glpK* on PZA activity, makes it difficult to dissect these mechanisms in a more controlled system. Regardless, the identification of mutations that affect PZA efficacy only during infection highlights the importance of performing the original TNseq screen in an animal model.

The prevalence of *glpK*-deficient strains in natural populations and the preferential survival of these bacteria in drug-treated animals suggested that *glpK*-deficient clones contribute to the persistence of *M. tuberculosis* during therapy and provide precursors for the emergence of clones with high-level resistance-conferring mutations. It is unlikely that the effects of *glpK* variation would be noted in standard phenotypic drug susceptibility testing (DST). This situation is similar to common variation in the *prpR* gene, which specifically influences drug tolerance but not DST results (145). These observations raise the possibility that genotypic tests for common drug tolerance-inducing variants could predict treatment failure and eventually be used to tailor therapy. We note that our TNseq study identified a number of additional loss-of-function mutations that alter drug efficacy, and the genome contains more than 100 genes with

homopolymeric regions that are at least as long as the one found in *glpK* (165). Together, these observations suggest that many phenotypically distinct subpopulations arise via similar mechanisms and influence antibiotic efficacy.

Acknowledgments

We are thankful to the members of the laboratory of C.M.S. for both technical assistance and helpful discussions. This work was supported by the Office of the Assistant Secretary of Defense for Health Affairs through the Peer Reviewed Medical Research Program, Focused Program Award, under award no. W81XWH-17-1-0692. Opinions, interpretations, conclusions, and recommendations are those of the author and are not necessarily endorsed by the Department of Defense. M.M.B. received additional support from the NIH (AI007349).

CHAPTER III: Distinct Bacterial Pathways Influence the Efficacy of First-Line Tuberculosis Antibiotics

Michelle M. Bellerose,^a Megan K. Proulx,^a Clare M. Smith,^a Richard E. Baker,^a
Thomas R. Ioerger,^b Christopher M. Sassetti^a

^aDepartment of Microbiology and Physiological Systems, University of
Massachusetts Medical School. Worcester, Massachusetts, USA; ^bDepartment of
Computer Science and Engineering, Texas A&M University. College Station, TX,
USA.

This chapter is adapted from an unpublished manuscript.

MMB and CMS conceived projects, designed experiments, and prepared the
manuscript. MKP performed Illumina sequencing of pooled infections. REB and
TRI designed computational analyses for TNseq. MKP and CMS aided in animal
infections.

Introduction

The current regimen for tuberculosis (TB) chemotherapy was developed through a series of large clinical trials in the early 1970s (166). The resulting “short-course regimen” consists of four drugs, isoniazid (INH), rifampicin (RIF), pyrazinamide (PZA), and ethambutol (EMB) (15). Combining these agents reduced the duration of treatment from 12-18 months to as little as 6 months (14). The wide-scale application of this regimen is generally considered a public health success and is estimated to have cured 58 million patients in the last two decades (5). Despite this success, delivering the extended therapy necessary to prevent recurrent disease is difficult in many settings and TB remains a leading cause of infectious death worldwide (5). The rational design of more rapid and effective therapies would be facilitated by understanding the mechanisms that limit the efficacy of our current drugs.

It has been clear since the first animal treatment studies, that the requirement for prolonged therapy correlates with the relatively slow killing of *Mycobacterium tuberculosis* in tissue (32, 167). Both INH and RIF are rapidly bactericidal in laboratory culture, but these agents clear bacteria much more slowly from the lungs of infected animals (161). While drug penetration into TB lesions can be limiting (74), sub-optimal drug exposure alone is unlikely to fully account for persistence of viable bacteria. In addition, bacterial adaptations to the host environment have been proposed to limit drug efficacy via a number of mechanisms. For example, the rate at which most antibiotics kill is related to

growth rate and metabolic activity of bacteria (111, 128, 143), and the relatively slow replication of *M. tuberculosis* during infection correlates with reduced drug efficacy (168). More specific adaptations to this environment, such as the induction of stress responses (169), changes in cell wall permeability (170), and expression of efflux pumps (61), have also been proposed to play an important role.

In addition to these inducible adaptations to the host environment, the wide-spread application of TB chemotherapy has also selected for stable genetic variants that promote bacterial survival. Most obviously, strains harboring high-level resistance conferring mutations in drug targets or prodrug activators have become common (171). The resulting “resistance” increases the minimal inhibitory concentration (MIC) of the corresponding antibiotic *in vitro*. Recent studies have also shown that even small changes in MIC can negatively affect treatment outcome (172). In addition, recent bacterial genome-wide associations studies (GWAS) have identified genetic variants that are associated with drug-resistant phenotypes but do not directly affect MIC. Some of these mutations compensate for the fitness cost imposed by primary resistance conferring variants (96). In other cases, they may promote bacterial survival in the presence of antibiotic (145), a phenotype termed drug “tolerance”. While hundreds of drug resistance-associated variants have been described (145, 148-150), the vast majority have not been functionally characterized.

In order to more globally define bacterial pathways that alter drug efficacy during infection, we designed a study to identify efficacy-altering mutations directly during infection using transposon sequencing (TNseq) in an animal model of TB. TNseq provides an unbiased approach to study conditional gene essentiality by comprehensively comparing the effect of loss-of-function mutations in different environments. Unlike previous studies that focused on individual mechanisms that broadly alter drug efficacy *in vitro* (173-175), our unbiased study found that most drug tolerance altering mutations are antibiotic specific, unrelated to growth rate, and alter drug efficacy only in the *in vivo* environment. A number of these efficacy-altering genes harbor mutations that are associated with drug resistance in clinical *M. tuberculosis* isolates, indicating that similar mechanisms may influence treatment outcome.

Results

Selection of transposon mutant libraries in antibiotic treated mice

A differential selection strategy was designed to identify bacterial mutants that alter the efficacy of each of the first-line TB therapeutics, INH, EMB, RIF, and PZA. Mice were infected with a complex transposon mutant library representing >50,000 independent insertion events via the intravenous route. The infection was allowed to progress for two weeks to establish the adaptive immune responses that accentuate drug tolerance (152). We initially assessed bacterial survival in the spleen, since the representation of the entire library could

be maintained in each individual mouse at this site. Spleen infection is a model of intracellular growth in the presence of adaptive immunity, a combination of conditions that resembles the primary pulmonary site of infection (176-179). At the initiation of drug treatment, the bacterial population had expanded to an average of 2×10^7 CFU/spleen. As expected, different antibiotics cleared the bacteria at distinct rates (Figure 3.1A). However, each drug, even the bacteriostatic agent, EMB, significantly reduced bacterial burden over 5 weeks of therapy. At this time point all drugs had reduced the bacterial burden by >100 fold, but relatively complex libraries could still be recovered. Similar rates of clearance were observed in the lung (Figure 3.1B). Only in PZA-treated mice did we observe a decreased rate of killing between 2.5 and 5 weeks, suggesting the possible expansion of resistant clones.

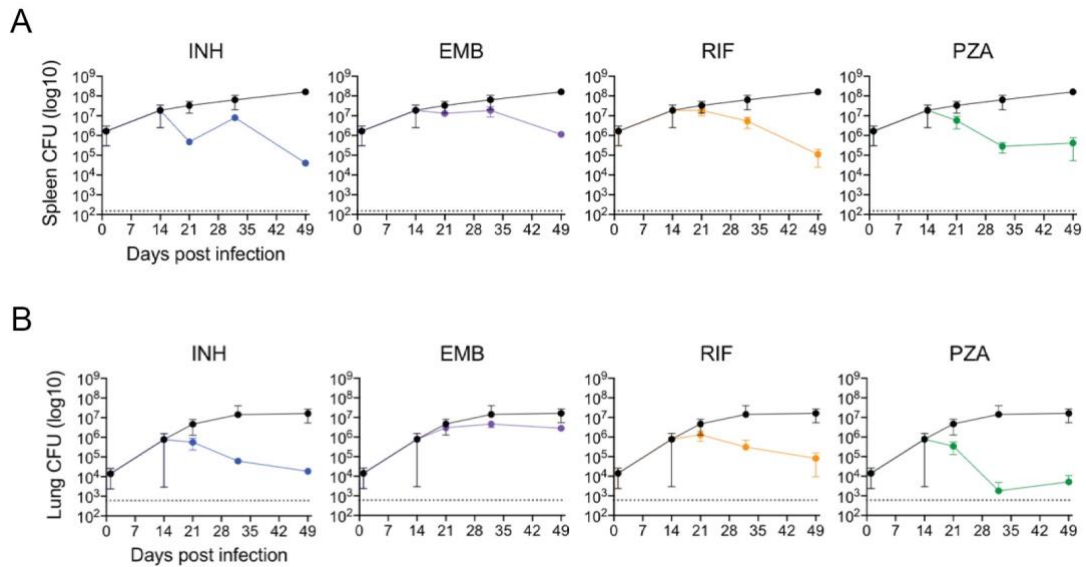


Figure 3.1| Antibiotic treatment of transposon mutant libraries *in vivo*.

CFU from spleens (**A**) and lungs (**B**) of BALB/c mice infected with transposon mutant library either untreated (black circles) or treated with indicated antibiotic. Treatment was started at 14 days post infection. Mean and standard deviation of biological replicates is plotted (n = 2-7 per time point).

To identify genes that alter bacterial fitness in this environment, we used TNseq to quantify the relative abundance of each transposon mutant in libraries recovered before infection, immediately before the initiation of therapy, from mice treated for 1, 2.5 or 5 weeks, or from untreated mice at the same time points (Figure 3.2). Surviving bacteria were recovered from the spleen of each mouse by plating and extracting genomic DNA. Transposon-chromosome junctions were ligated to unique molecular identifiers (UMI), amplified and sequenced (153). The relative abundance of each mutant in a pool is estimated based on the number of corresponding UMI sequences. This design allowed the independent

quantification of mutant fitness under the pressures imposed by the host and by the combined pressure of host immunity and antibiotic therapy.

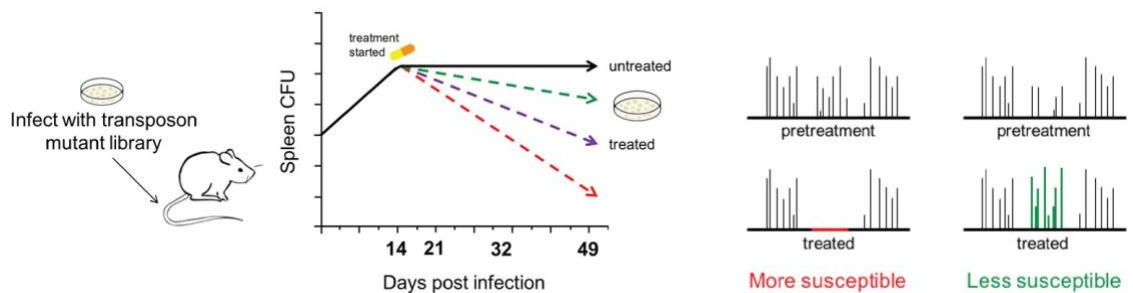


Figure 3.2 | Genetic strategy to identify mutations that alter susceptibility to antibiotic treatment in mice.

Diagram of TNseq screen design. BALB/c mice were infected via intravenous route with 2×10^6 bacteria/mouse. At 14 days post infection pretreatment libraries were collected, via plating, and treatment regimens were initiated. Time points were collected, via plating, from untreated and treated mice at 21, 32, and 49 days post infection. Comparison of transposon insertion abundance pre- and posttreatment identifies mutants more susceptible (decrease in insertions) and less susceptible (increase in insertions).

Identification of genes necessary for bacterial fitness in untreated animals

Initially, TNseq libraries recovered from the untreated mice were analyzed to determine the relative fitness of each mutant over the time course of our infection. Libraries recovered at each time point were compared to the input libraries used for the infection. In total, 562 genes were found to be required for optimal fitness *in vivo* by 49 days post infection (Figure 3.3A and Appendix Table A3.1). We observe up to 77% overlap with genes previously reported to be required for replication in the mouse model using similar approaches (176, 178,

180). These genes encode a wide variety of functions previously verified to be necessary for replication in mice, including type VII protein secretion (ESX1), cholesterol (Mce4) and fatty acid (Mce1) catabolism, and siderophore transport (IrtAB, MmpL4/S4). The 231 novel genes identified in our study likely reflects the longer period of infection, and more accurate quantification that resulted from greater number of animals used.

The availability of time-course data allowed the assessment of mutant fitness at different stages of infection. The two week time point captures the early expansion of the bacteria, before the onset of the adaptive response. The later time points reflect additional pressures imposed by T cells that control bacterial replication. As expected, we observed a progressive depletion of mutants over this time course (Figure 3.3B), and distinct sets of genes were found to be important in establishing infection or persisting at later time points. For example, biotin biosynthetic mutants were dramatically under-represented at the earliest time points, reflecting their known inability to replicate *in vivo* (181) (Figure 3.3C). In contrast, Mce4 mutants were well-represented at the early time point, but became progressively depleted from the pool, reflecting their specific deficit in fitness upon exposure to adaptive immunity (156) (Figure 3.3D). These data validated our methodology, and provide insight into the stresses *M. tuberculosis* may encounter during different times of infection independent of drug treatment.

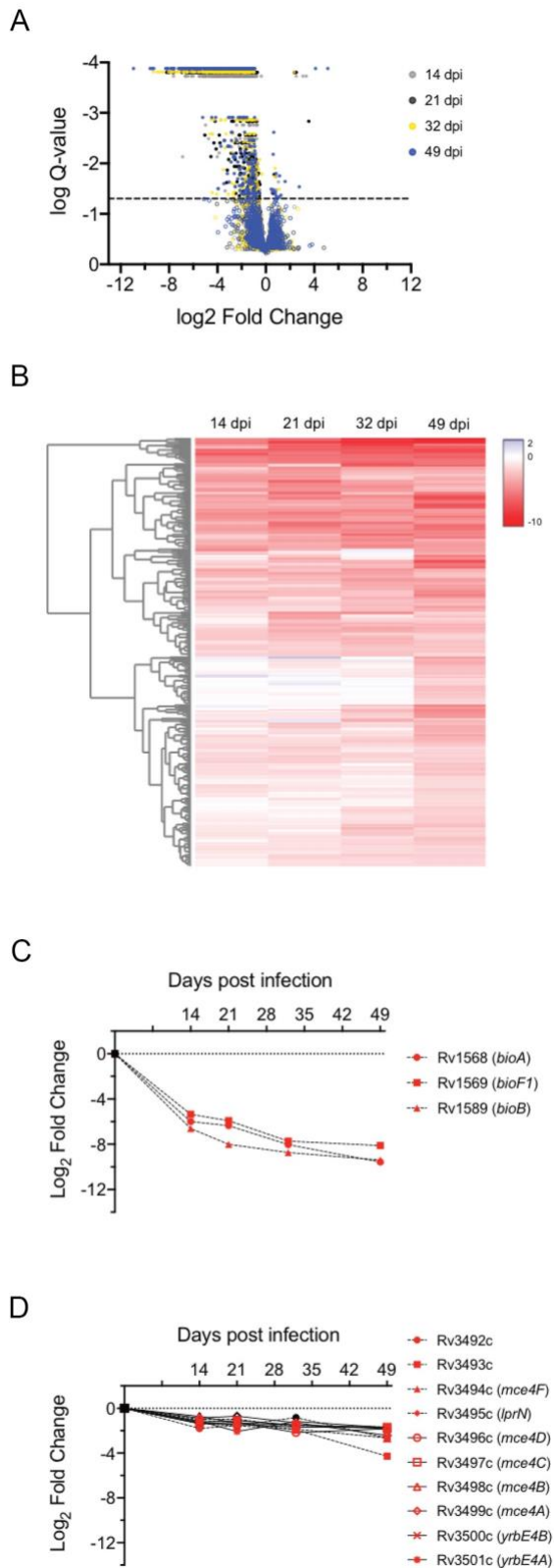


Figure 3.3 | Genes required for optimal fitness *in vivo*.

A, Volcano plot of *in vivo* libraries compared to *in vitro* input library at indicated time points. Q-value < 0.05 is indicated by dashed line. Genes meeting significance (Q-value < 0.05) are indicated by filled circles. **B**, Heatmap of the relative abundance of 293 genes significantly underrepresented *in vivo* at each time point over the untreated time course. Genes are hierarchical clustered based on log₂ fold change at individual time points. Time points are in order of infection length from shortest (left) to longest (right). **C and D**, TNseq phenotype of genes/operons significantly underrepresented *in vivo* at each time points: biotin biosynthesis genes, **(C)**; *mce4* operon, **(D)**. Significance (Q-value < 0.05) is indicated by red symbols.

Identification of mutants with altered susceptibility to antibiotics

A critical requirement for TNseq-based comparisons is maintaining the complexity of each library to reduce stochastic effects. Treatment decreases the number of viable bacteria, which could result in decreased representation of mutants across the genome. As a result, we first assessed the complexity of the libraries recovered from drug treated mice. Initial analyses, calculating the average reads derived from transposon insertions in each gene, indicated that libraries exposed to extended RIF or PZA treatments were less complex than the rest (Figure 3.4). This effect was particularly clear for PZA, where the library became dominated by mutants with a disrupted *pncA* gene, which encodes the activator for the prodrug. A similar, but less pronounced, effect was found upon RIF treatment, where mutations in the *cmaA2* gene became the most abundant strains in each sample from extended RIF treatments. The *cmaA2* gene encodes a cyclopropane synthase which modifies the mycolate layer of the cell wall and alters cellular permeability (154). In both cases, transposon insertions throughout these genes were enriched, indicating that the loss of gene function was directly related to decreased drug efficacy. While a small number of other mutants appeared to be enriched upon extended therapy, these were not consistent between samples and represented single insertion events, likely reflecting the presence of spontaneous resistance conferring mutations that are unlinked to the insertion. Thus, the lack of complexity in these libraries led to the exclusion of long-term RIF and PZA samples from the following comparative analyses.

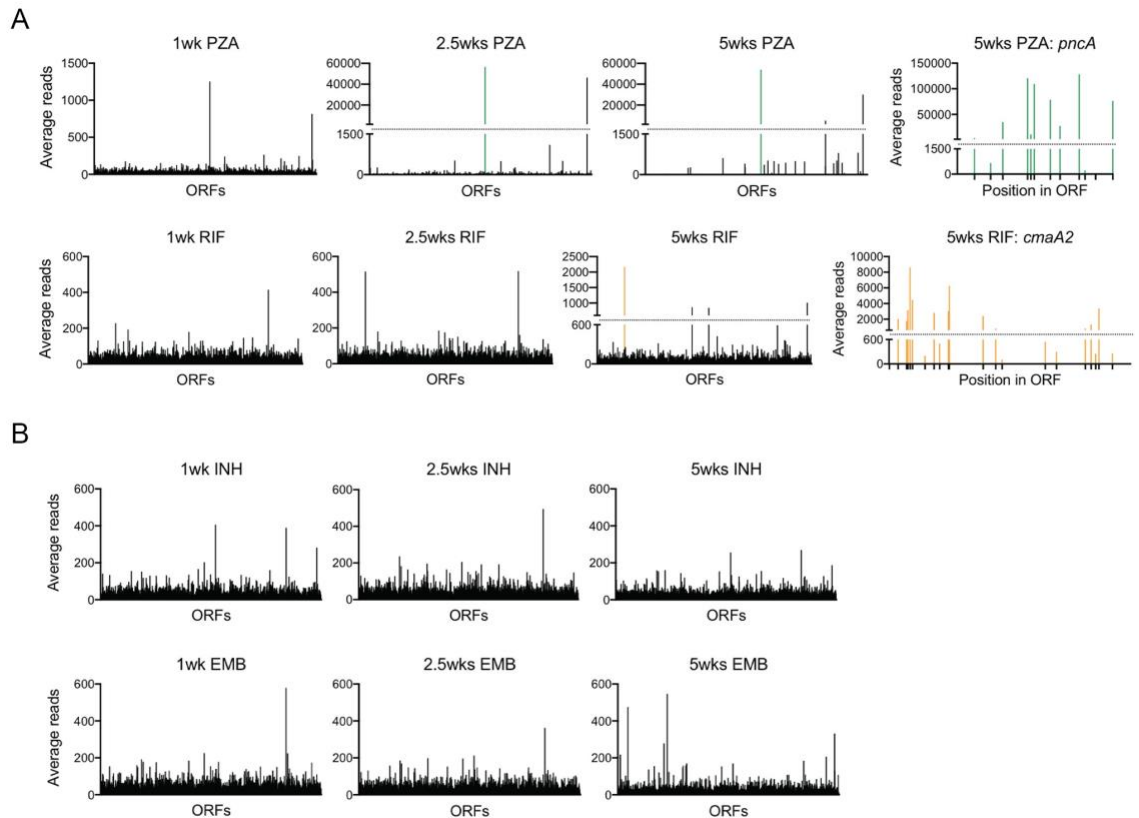


Figure 3.4 | Complexity of antibiotic treated libraries.

A, Average reads of transposon insertions for each open reading frame (ORF) in the H37Rv genome. Top: PZA treated libraries, *pncA* is indicated by the green line, and average reads for each TA site in *pncA* at 5 weeks posttreatment. Bottom: RIF treated libraries, *cmaA2* is indicated by the orange line, and average reads for each TA site in *cmaA2* at 5 weeks posttreatment. **B**, Average reads of transposon insertions for each ORF in the H37Rv genome in INH treated libraries (top) and EMB treated libraries (bottom).

We next compared mutant abundance between pre- and post-treatment samples to quantify mutant survival during therapy (Figure 3.5A and Appendix Tables A3.2 – A3.9). We first compared mutant fitness in treated versus untreated animals, by comparing each time point to the pretreatment control

sample, to estimate the relationship between replication rate and drug efficacy (Figure 3.5B). We observed the most overlap in the context of INH, a drug with clear growth rate dependent effects *in vitro* (182). However, this effect was not apparent for other drugs, indicating that distinct bacterial functions influence survival in the presence and absence of drugs.

We next assessed the number of mutants with altered susceptibility to treatment. For each antibiotic regimen we observed mutants that were both under- or over-represented in the posttreatment samples (Figure 3.5C). The genes identified are involved in a range of distinct functions and include genes in pathways known to alter antibiotic efficacy. For example, *pncA*, the pyrazinamidase that activates PZA, and *glpK* mutants were found to be less sensitive to PZA treatment, consistent with previous studies in Chapter II (183). Conversely, mutants increasing efficacy included *ppe50/51*, previously shown to increase efficacy of combination treatment (183). We also identified multiple transporter mutants which are putative antibiotic efflux pumps, including ABC-transporters Rv1747 and Rv1273 which were more susceptible to INH and RIF, respectively. Overall, we found 160 mutants that altered efficacy of antibiotic treatment (Appendix Tables A3.2 – A3.9).

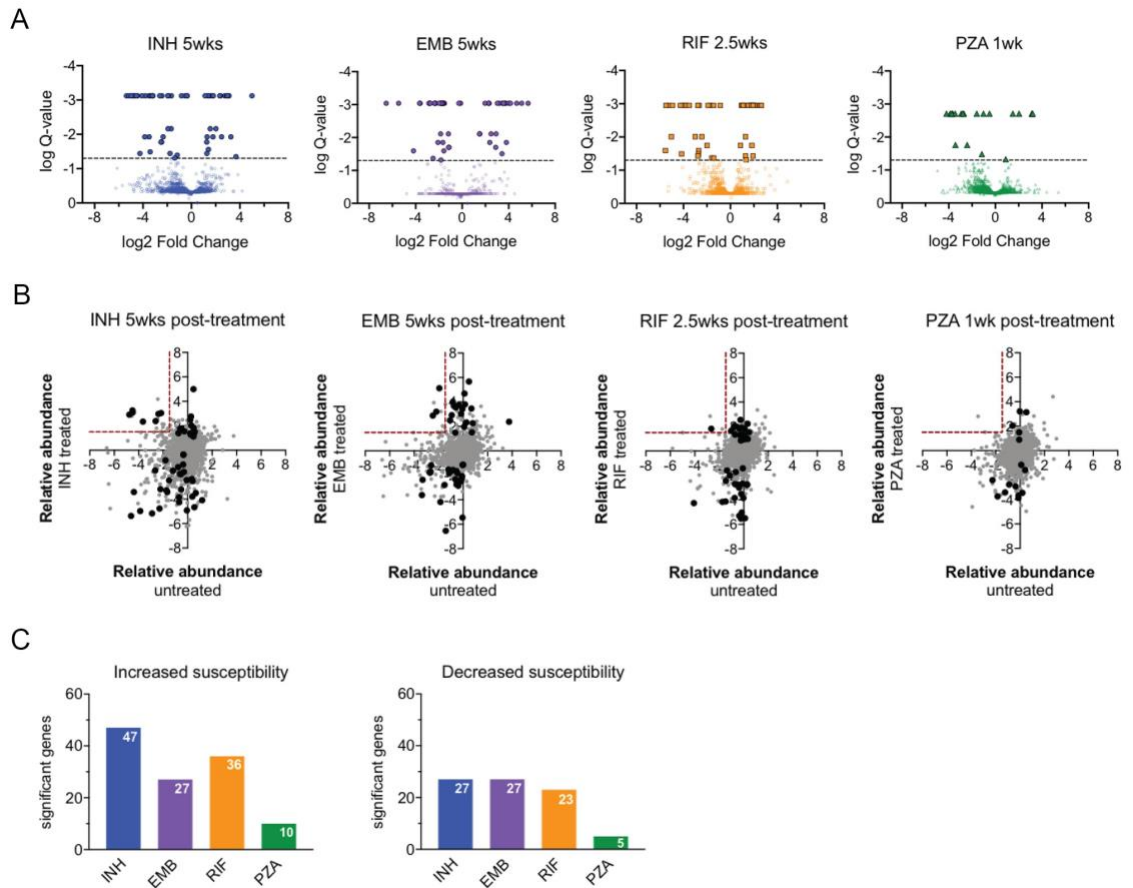
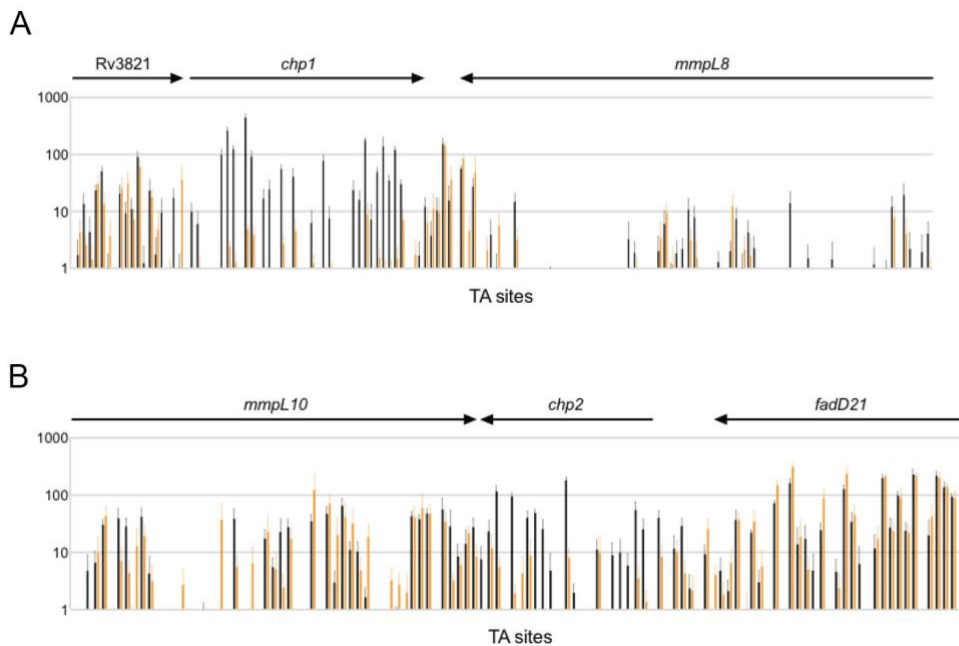


Figure 3.5 | Mutants with altered susceptibility to antibiotics.

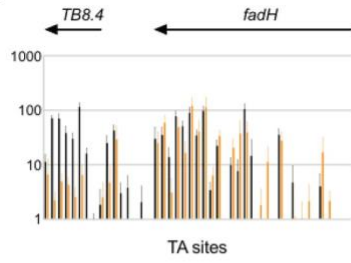
A, Volcano plots of treated libraries at individual time points compared to pretreatment libraries. Treatment lengths indicated by symbol: triangles 1 week; squares, 2.5 weeks; circles, 5 weeks. Negative log₂ fold change = underrepresented posttreatment. Positive log₂ fold change = overrepresented posttreatment. Q-value < 0.05 is indicated by dashed line. Genes meeting significance (Q-value < 0.05) are indicated by filled symbols. **B**, Scatterplot plotting the relative abundance, log₂ fold change, for each gene in untreated libraries (x axis) or treated libraries (y axis). Genes significantly altered posttreatment are in black. The red dotted line indicates the threshold for genes that are attenuated *in vivo* and less susceptible to antibiotic treatment. **C**, Number of genes with a significant decrease in transposon insertions (left) and a significant increase in transposon insertions (right), under each treatment condition.

Validation of mutant phenotypes in an aerosol infection model

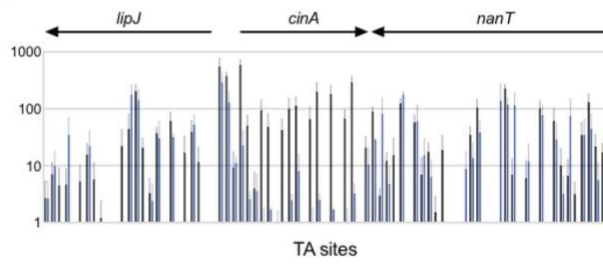
To determine how well the TNseq study predicted the phenotype of loss-of-function mutations, a series of deletion mutants were generated: *rv3822* (*chp1*); *rv1184* (*chp2*); *rv1174c* (TB8.4); *rv1901* (*cinA*); *rv1747*; *rv1273c*; *rv3136* (*ppe51*); *rv0248c*; *rv0503c* (*cmaA2*). These genes were selected based on statistical criteria that consider each distinct transposon insertion in a gene to be an independent assessment of the loss-of-function phenotype. As a result, genes that are predicted to alter drug efficacy, contain a number of independent insertions that all produce a similar effect (Figure 3.6A-I).



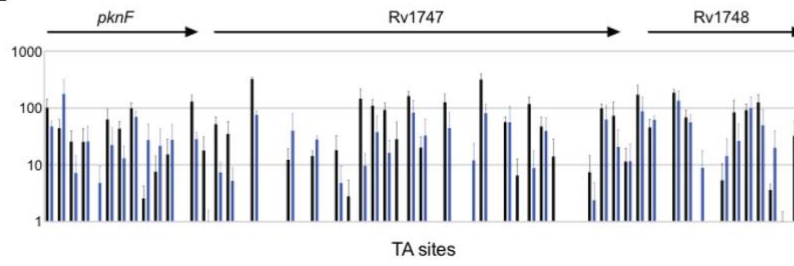
C



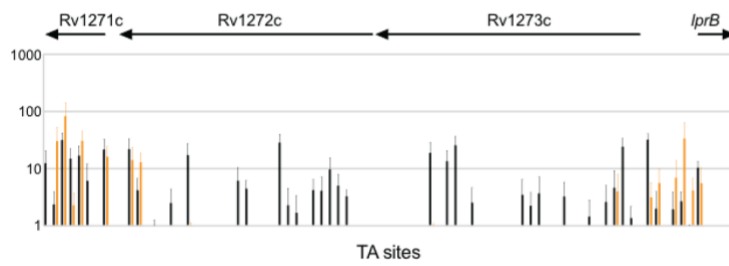
D



E



F



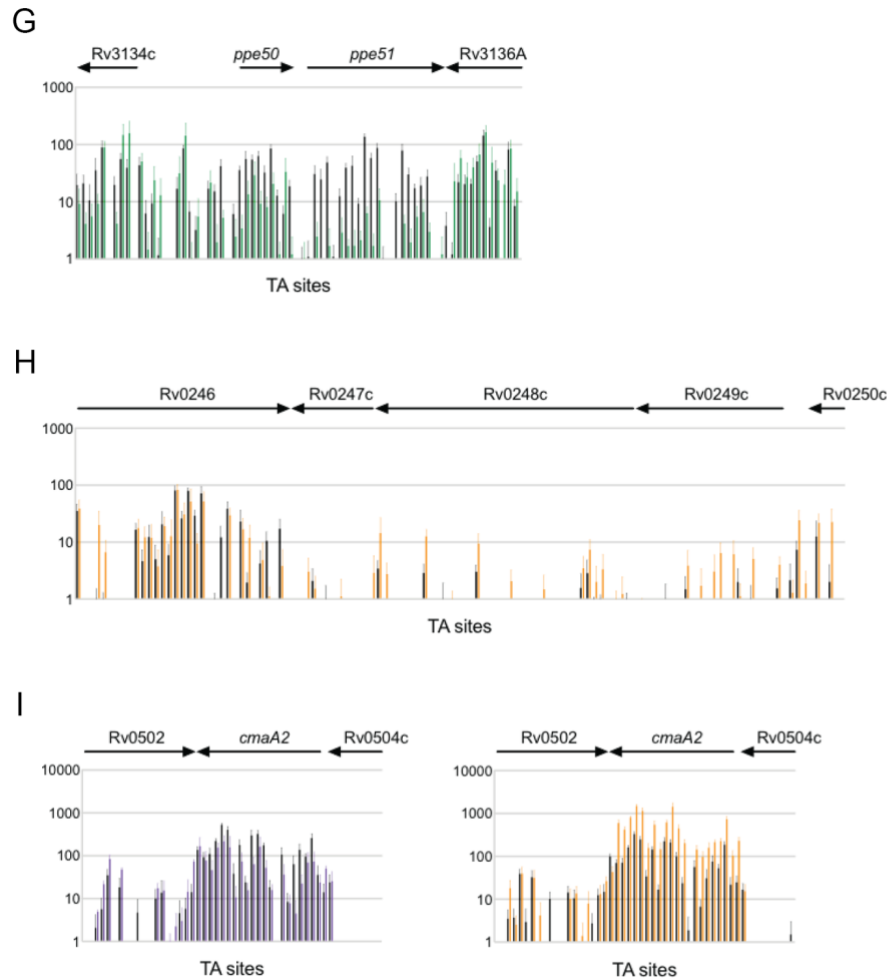


Figure 3.6 | Transposon insertions pre- and post-treatment in genes with altered susceptibility.

Average number of unique sequencing reads (*y* axis) plotted versus the TA sites in the genome (*x* axis) for pretreatment (black) and posttreatment (INH, blue; EMB, purple; RIF, orange; PZA, green). Mean and standard deviation of biological replicates are plotted. **A**, *chp1* (*rv3822*) **B**, *chp2* (*rv1184c*) **C**, *TB8.4* (*rv1174c*) **D**, *cinA* (*rv1901*) **E**, *rv1747* **F**, *rv1273c* **G**, *ppe51* **H**, *rv0248c* **I**, *cmaA2* (*rv0503c*)

We also included mutants that disrupt different cellular functions and produce both qualitatively and quantitatively distinct phenotypes. For this analysis we included data from Chapter II, TNseq from mice treated with the combination

regimen HRZE (consisting of INH, RIF, EMB, and PZA) using a parallel treatment regimen (183).

Individual deletion strains were constructed to contain a barcode at the site of deletion which served as an identifier for downstream quantification via sequencing. To measure susceptibility of the knockout strains, mutant and wild-type strains were mixed into a pool of nine strains for infection via either intravenous (i.v.) or aerosol routes. Treatment was initiated at two weeks post infection, and the duration was adjusted to produce a similar decrease in CFU for each of the bactericidal regimens and maintain library complexity (Figure 3.7). At indicated time points, bacteria were isolated via plating the spleen or lung for i.v. and aerosol infections, respectively. The relative abundance of each mutant to wild-type was calculated for each strain and normalized to their pretreatment abundance, allowing a direct comparison to the TNseq data (Figure 3.8A-I).

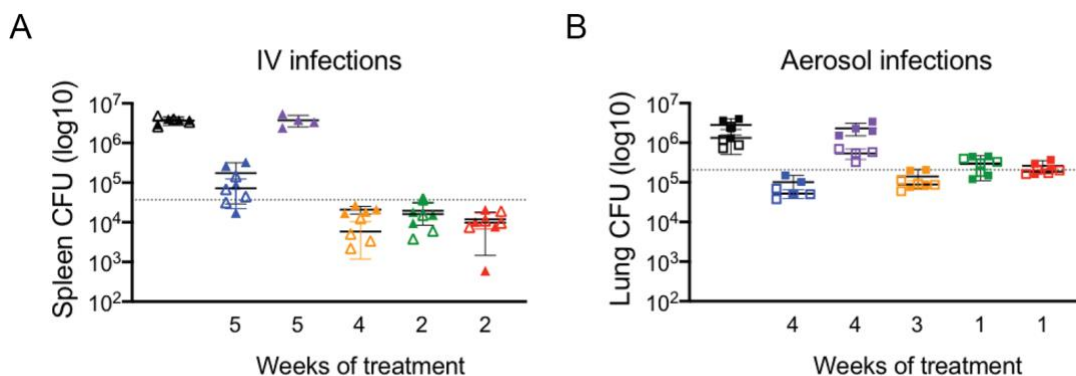


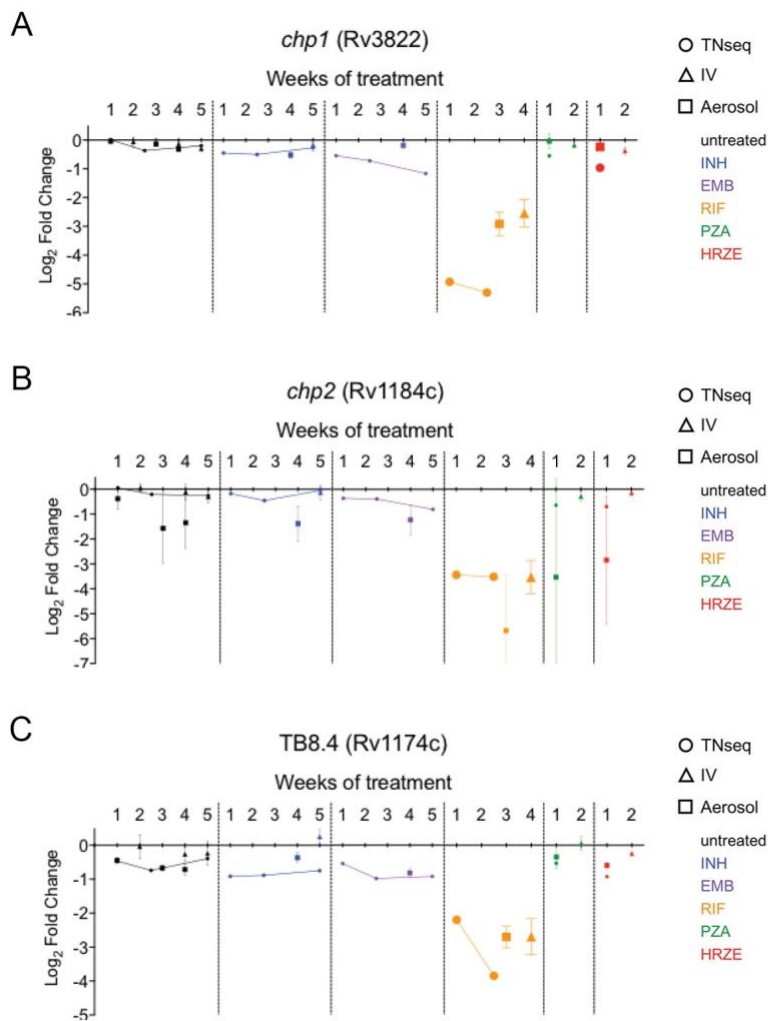
Figure 3.7 | Antibiotic treatment of mutant and wild-type pooled infections.

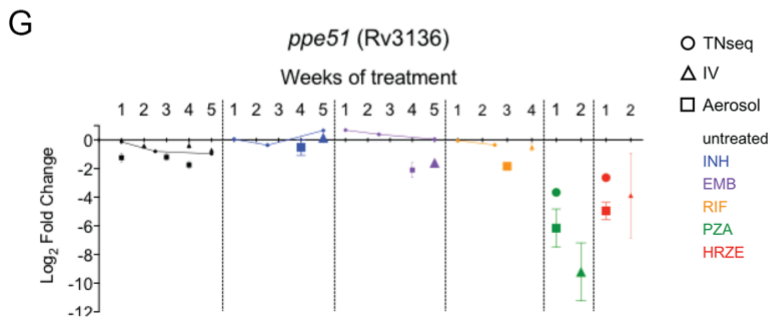
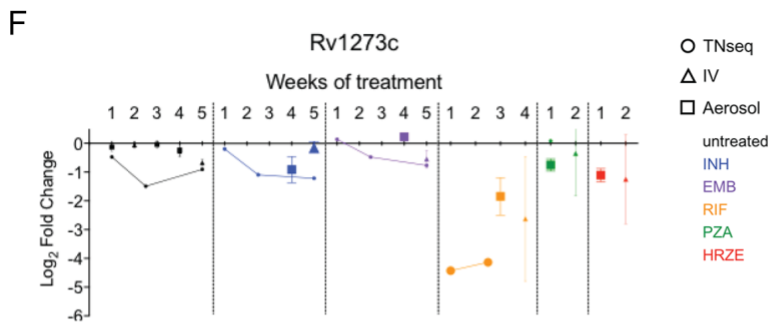
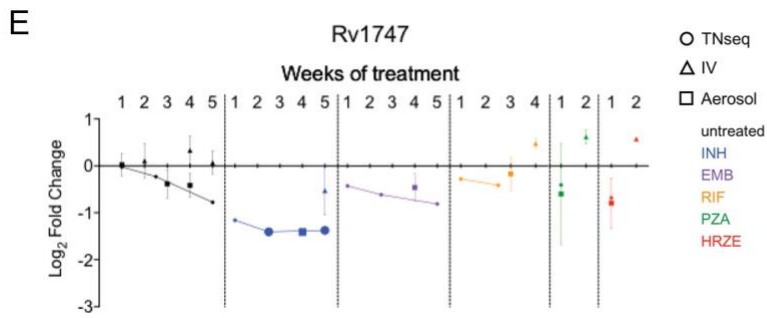
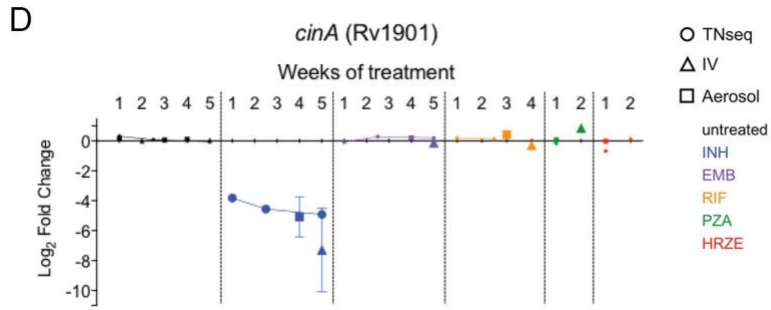
A, Spleen CFU from BALB/c mice post intravenous infection. Treatment was started at 14 days post infection. The data represents two infections, indicated by closed and open triangles. Mean and standard deviation are plotted, individual points are biological

replicates. Treatment conditions are indicated by color: untreated (black), INH (blue), EMB (purple), RIF (orange), PZA (green), HRZE(red). **B**, Lung CFU from BALB/c mice post aerosol infection. Treatment was started at 21 days post infection. The data represents two infections, indicated by closed and open squares. Mean and standard deviation are plotted, individual points are biological replicates. Treatment conditions are indicated by color: untreated (black), INH (blue), EMB (purple), RIF (orange), PZA (green), HRZE(red).

In almost every case, the altered susceptibility phenotypes predicted by TNseq were validated using deletion mutants upon i.v. and/or aerosol infection. Many mutants were predicted to enhance the efficacy of individual antibiotics. These included genes that were among the ten strongest hypersusceptible phenotypes for RIF (*rv1184c*, *rv3822*, and *rv1174c*) and INH (*cinA*) (Figures 3.8A-D). Additionally, mutations affecting two ABC transporters, Rv1747 and Rv1273c, indicated that these proteins could function as efflux pumps for INH and RIF, respectively (Figures 3.8E and 3.8F). PZA specific effects were observed as well. We confirmed *ppe51* mutant strains have increased susceptibility to PZA containing regimens (Figure 3.8G), consistent with previous work in Chapter II (183). Other mutations were predicted to decrease efficacy. For example, mutants lacking the succinate dehydrogenase component, Rv0248c, were consistently cleared less rapidly than wild-type bacteria. This phenotype was observed upon treatment with different regimens (INH, RIF, and HRZE), suggesting that this mutation produces tolerance to many unrelated antibiotics (Figure 3.8H). CmaA2 mutants were predicted to have a complex phenotype, with opposing susceptibilities to EMB and RIF (Figure 3.8I). We

validated CmaA2 mutants as more susceptible to EMB treatment, consistent with previous studies (154), and less susceptible to RIF, consistent with our initial analyses of library complexity (Figure 3.3). These opposing phenotypes may compensate for each other during combination therapy, as we observe a neutral phenotype in the HRZE regimen.





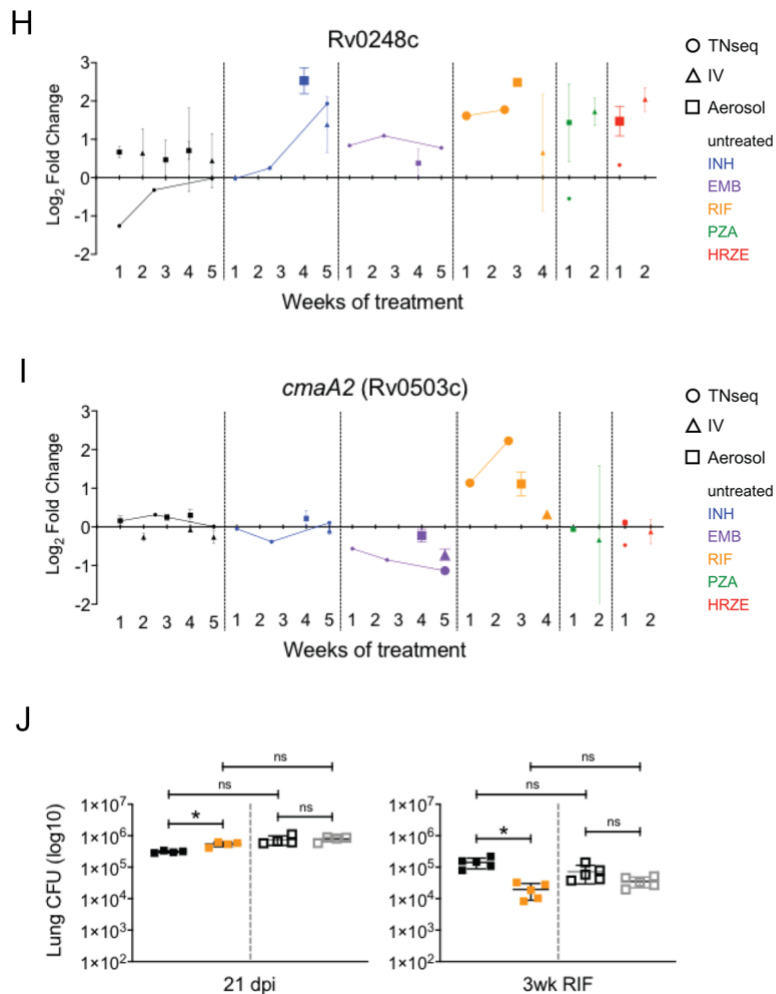


Figure 3.8 | Validation of mutant phenotypes.

A-I, The relative abundance, \log_2 fold change, of mutants post TNseq (circles), i.v. (triangles), or aerosol (squares) infections. Mean and standard deviation of biological replicates for i.v. and aerosol infections are plotted. Significance is indicated by increased symbol size: TNseq, resampling Q-value <0.05 ; i.v. and aerosol, unpaired t test with Benjamini-Hochberg multiple testing correction $P < 0.05$. Conditions are indicated by color: untreated (black); INH (blue); EMB (purple); RIF (orange); PZA (green); HRZE (red). HRZE data was obtained from Chapter II (183). **J**, Lung CFU of H37Rv (black), Δ Rv1273c (orange), and complement (grey) strains post aerosol infection and treatment with RIF. Data represents two aerosol infections of combined bacterial strains, 1:1 Rv and Δ (filled squares) and 1:1 Rv and complement (open squares). Treatment was administered starting at 21 days post infection. RIF treatment was for 3 weeks. Mean and standard deviation are plotted, individual points are

biological replicates. Significance was determined using unpaired *t* test with Benjamini-Hochberg multiple testing correction: *(0.03); **(0.002); ***(0.0002).

To assess whether the relative abundance determined by sequencing mutant pools reflected genuine differences in viable bacteria, we mixed the putative efflux pump mutant strain, $\Delta rv1273c$, and its complemented strain and performed additional infections using CFU as a measure of abundance. Using a competitive model in which each mutant was mixed at a 1:1 ratio with wild-type and inoculated via the aerosol route we observed that the $\Delta rv1273c$ mutant was cleared more rapidly than wild-type or the complemented strain by RIF treatment, as anticipated (Figure 3.8J). We conclude that the TNseq data provide an accurate assessment of relative mutant abundance in this system.

Mutations produce drug-specific effects

Having validated the accuracy of the TNseq data, we analyzed the composite dataset to understand more broadly how bacterial functions alter drug efficacy. Again, we included a previously generated HRZE treatment condition from Chapter II, that was produced using identical methodology (183). When compared to the pretreatment time point, the number of mutants identified with altered abundance varied for each antibiotic condition (Figure 3.9A). The majority of mutations only had significantly altered susceptibility to a single agent, while a smaller subset had effects in multiple conditions (Figure 3.9A). The largest

overlap, 13 genes, was observed between INH and EMB, two drugs that inhibit cell wall synthesis by interrupting mycolate or arabinogalactan production.

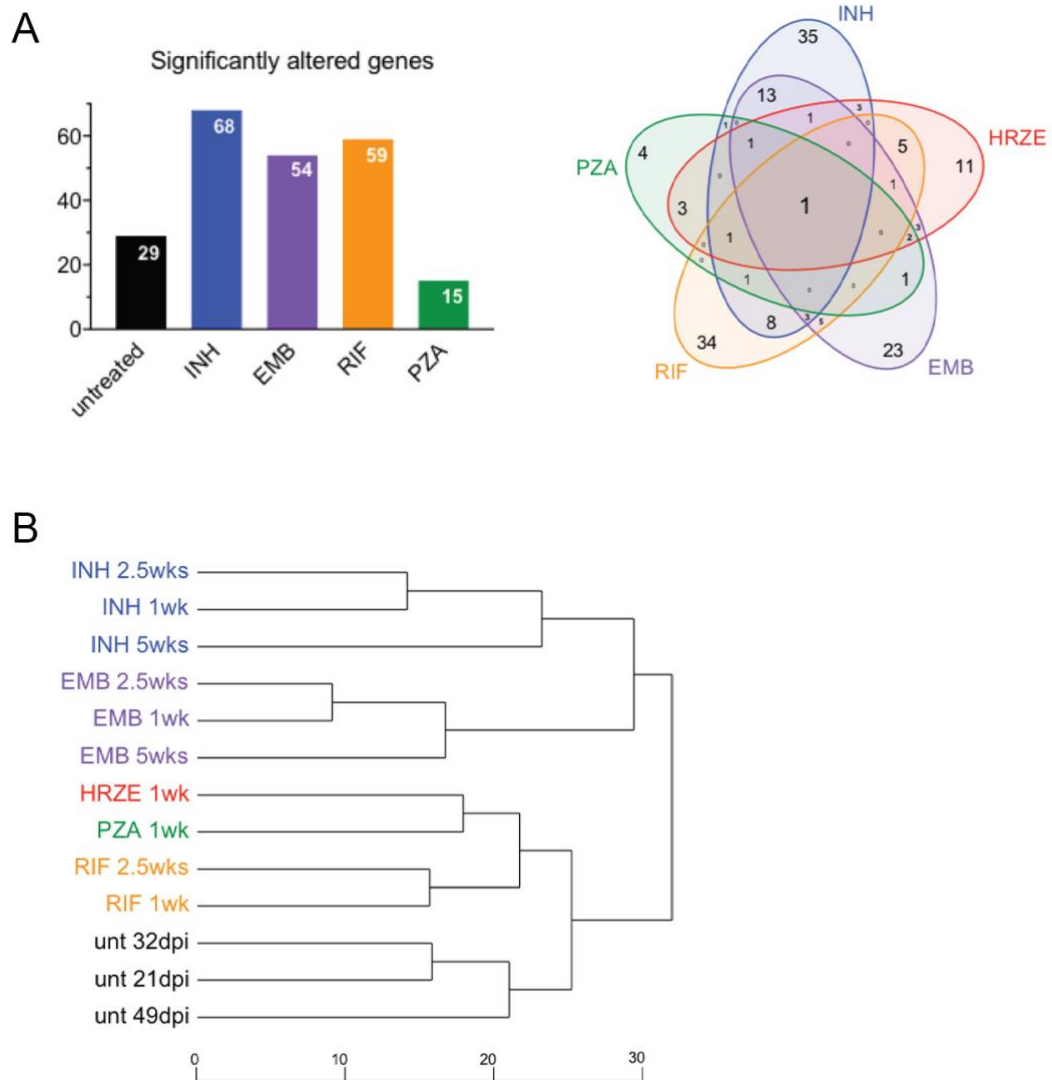


Figure 3.9 | Mutants with altered susceptibility to treatment are specific to individual treatment regimens.

A, Left: the number of genes with a significant change in transposon insertions under each condition. Right: Venn diagram displaying the overlap between treatment conditions. **B**, Dendrogram displaying the relationship between treatment conditions and individual time points. Relationship was determined by hierarchical clustering of

significantly altered genes based on TNseq log₂ fold change at each time point. HRZE data was obtained from Chapter II (183).

Similarities between conditions was also evident upon hierarchical clustering of significantly altered genes (Figure 3.9B). Conditions clustered primarily based on regimen. Higher order similarities based on mechanism of action were also seen, as the cell wall inhibitors (INH and EMB) were found in a branch distinct from the other conditions. In addition, PZA clustered closely with HRZE, suggesting that the bactericidal activity of the combination regimen is largely driven by PZA.

While these simple comparisons indicated that each treatment generally selected a distinct set of mutants, this analysis was insufficient to clearly define bacterial functions that were selectively affected by each treatment. We therefore devised a multidimensional analysis to identify the bacterial genes that are most responsible for defining the treatments. Principle component analysis (PCA) was applied to transposon insertion counts of genes across conditions to map them onto orthogonal axes (linear combinations of conditions). We then performed a varimax rotation (184) to maximally re-align the first principle components with treatment conditions, resulting in six abstract dimensions that differentiate the antibiotics based on their effects on conditional gene essentiality. All treatment groups were assigned to a distinct dimension, except for PZA and HRZE which were similar enough to share one (Figure 3.10A). This analysis also identified a clear inverse correlation between INH treatment and the untreated condition that we previously inferred (Figure 3.5B). The bacterial genes most closely aligned

with each varimax dimension were identified based on their rotated PCA loadings, and the significance of these associations was determined using a projection resampling approach (see Appendix A1: Materials and Methods). This analysis identified between 1 and 20 genes that are significantly associated with individual treatment conditions (Figure 3.10B and Appendix Tables A3.10 – A3.14). For example, mutations in an operon consisting of *ppe1*, *rv0097*, and *nrp*, were found to increase survival in the presence of INH, an effect that is consistent with previous work (182). Increased abundance of mycobactin mutants distinguishes EMB from the other treatment conditions. Genes associated with the RIF dimension include previously validated genes *rv1184c*, *rv3822*, and *cmaA2* (Figure 3.8). Prominent among these 9 genes were 7 that are involved in cell wall, lipid, or arabinan metabolism (*pks2*, *phoR*, *mmaA3*, *mmaA2*, *cmaA2*, *ephD*, *rv1635*) (185-189), suggesting that the permeability of the mycobacterial envelope is a primary determinant of RIF activity during infection. The PZA/HRZE dimension is associated with *pncA*, the activator of the PZA prodrug, as well as mutations in the *ppe51* genes that are involved in glycerol/glucose uptake (190) and was previously found to enhance the activity of HRZE (183). In addition, mutations in several genes dedicated to the synthesis of the cell envelope lipid, phthiocerol dimycocerosate (PDIM), decreased HRZE efficacy. The untreated dimension is associated with a single gene, *rv2563*, that enhances susceptibility in all drug treated conditions, which encodes a predicted glutamine transporter.

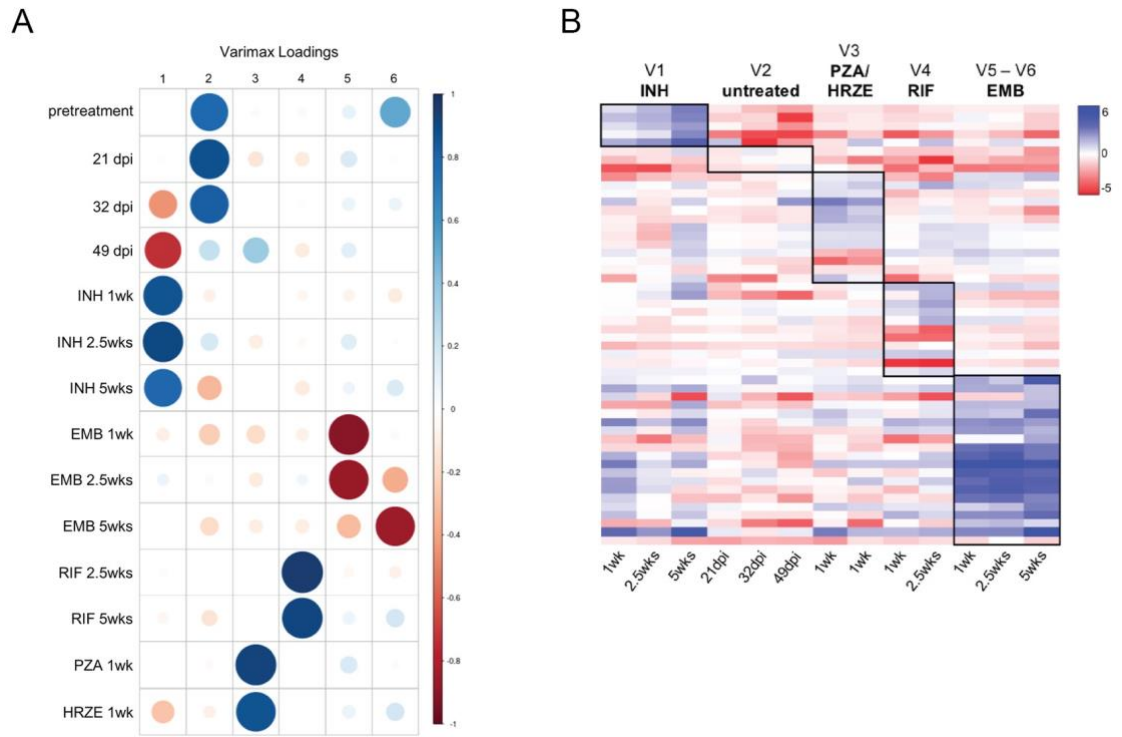


Figure 3.10 | Multi-dimensional analysis to identify mutations associated with individual antibiotic treatments.

A, Correlation between individual time points and conditions with each varimax loading. **B**, Heatmap of genes significantly associated with a varimax dimension. Signal is based on TNseq log₂ fold change. Boxes indicate genes significantly associated (Q-value < 0.05) with dimensions. HRZE data was obtained from Chapter II (183).

Many susceptibility phenotypes are specific to the *in vivo* environment

To evaluate the importance of the infection environment in shaping the mechanisms of drug susceptibility, we investigated whether mutations found to alter efficacy in animals also had an effect in standard culture conditions. We first compared the mutants found in our *in vivo* study with those previously found to alter the MICs of INH, EMB, or RIF *in vitro* using an analogous TNseq approach

(175). We observed a small but significant overlap of genes post INH (*in vivo* = 68 genes, *in vitro* = 90 genes, overlap = 8 genes, $P = 0.0004$), EMB (*in vivo* = 54 genes, *in vitro* = 67 genes, overlap = 4 genes, $P = 0.02$), and RIF treatment (*in vivo* = 59 genes, *in vitro* = 75 genes, overlap = 10 genes, $P = 4 \times 10^{-7}$), identifying pathways that alter treatment efficacy both *in vitro* and during infection. The 8 gene overlap between *in vivo* and *in vitro* INH treatments included the validated *cinA* gene (Figure 3.8) that increases susceptibility when mutated. Despite these similarities, the majority of mutations found to alter *in vivo* efficacy do not appear to alter *in vitro* MIC values.

To more directly quantify *in vitro* effects, we took advantage of our deletion mutant set (Figure 3.8). Each mutant was exposed to the antibiotic that resulted in the most differential selection for that strain *in vivo* (RIF or INH), and both the MIC₅₀ and rate of killing was determined *in vitro*. While MIC differences between wild-type and three mutants met statistical significance, none differed by more than 2-fold (Table 3.1). When the rate of killing was measured, no differences were observed under RIF treatment. In INH treatment only a single mutant, $\Delta cinA$ displayed increased killing that was consistent with the *in vivo* phenotype (Figure 3.11). Thus, consistent with the TNseq comparison, this analysis indicated that many of the mutations that alter *in vivo* drug efficacy have little effect during *in vitro* culture.

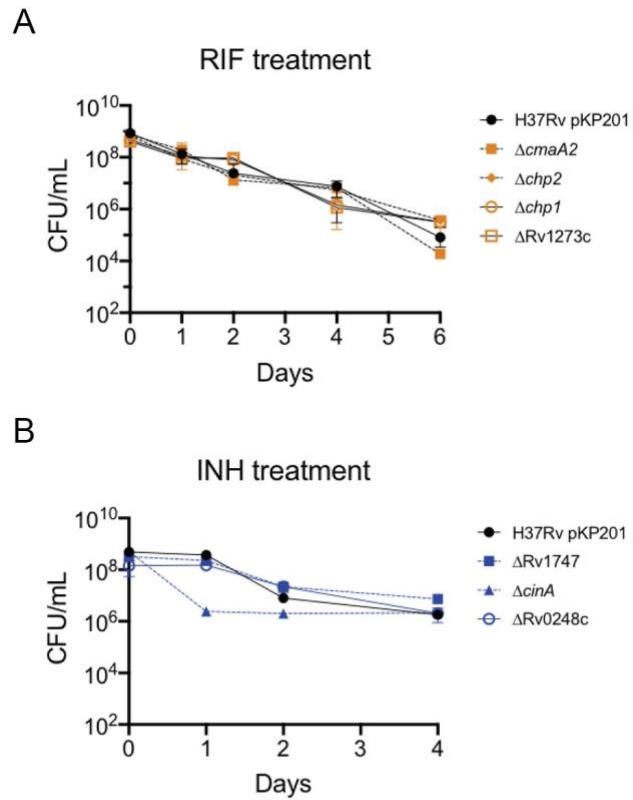


Figure 3.11 | Rate of killing of mutants *in vitro*.

Viable bacteria determined by CFU of H37Rv and deletion mutants post RIF treatment (0.5 $\mu\text{g}/\text{mL}$) **(A)** or INH treatment (0.6 $\mu\text{g}/\text{mL}$) **(B)**. Mean and standard deviation of triplicates are plotted.

Table 3.1 | Antibiotic susceptibility of deletion strains *in vitro*.

Strain	IC ₅₀ (µg/mL ± SD)	
	INH	RIF
H37Rv	0.03 ± 0.002	0.0033 ± 0.0003
Δrv0248c	0.04 ± 0.005 *	0.0035 ± 0.0002
ΔcmaA2	0.03 ± 0.001	0.0025 ± 0.0003 *
Δrv1174c	0.03 ± 0.001	0.0033 ± 0.0004
Δchp2	0.03 ± 0.001	0.0029 ± 0.0007
Δrv1273c	0.03 ± 0.005	0.0032 ± 0.0006
Δrv1747	0.03 ± 0.004	0.0028 ± 0.0009
Δppe51	0.05 ± 0.005 *	0.0041 ± 0.0001 *
Δchp1	0.03 ± 0.002	0.0030 ± 0.0003

IC₅₀ = mean of three individual experiments. **P* < 0.05

Natural variants in efficacy-altering genes are associated with drug resistance

In the mouse model, we identified many genes that have the capacity to alter antibiotic efficacy (Figure 3.5C and Appendix Tables A3.2 – A3.9). Reasoning that naturally-occurring polymorphisms in these genes might be selected in the context of antibiotic exposure, we investigated if there was overlap between genes identified our mouse studies and those previously found to contain resistance-associated single nucleotide polymorphisms (SNPs) in clinical isolates. We utilized data from three published GWAS studies (145, 148, 150) that identified genes that are subject to convergent evolution in drug resistant isolates. We compared these genes to the loss-of-function mutations that we found to either increase or decrease antibiotic killing in the mouse, since

naturally occurring polymorphisms could increase, decrease, or alter the functions of these genes. Of the 328 genes identified by GWAS, 14 were also identified in our TNseq study with a Q-value of < 0.05, and 21 overlapped with a Q-value less than 0.1 (Figure 3.12 and Table 3.2). Genes known to alter drug sensitivity (*pncA*) and tolerance (*glpK*) were identified, along with a number of genes that have not been shown to influence drug efficacy. For example, we find that disruption of the nonribosomal peptide synthase, *nrp*, produces tolerance to INH in the mouse, which likely explains the association of *nrp* variants with clinical INH resistance (145). Similarly, loss of *pks2* function reduced RIF killing in mice, and SNPs in the *pks2* gene are associated with clinical ofloxacin resistance (148). As individual resistance traits in multi-drug resistant isolates are linked, these observations are consistent with *pks2* mutations contributing to this phenotype either by increasing RIF tolerance or influencing the effects of multiple drugs, including fluoroquinolones, which were not tested in the mouse. While the overlap between these datasets was relatively small, this analysis allowed us to functionally implicate variants in at least 14 *M. tuberculosis* genes in the evolution of drug resistance. As many of the efficacy altering mutations found in the mouse model have little effect *in vitro* (Figure 3.11 and Table 3.1), we speculate that the effects of these natural variants may not be apparent under similar *in vitro* conditions. If so, these variants could represent cryptic determinants of treatment outcome that preferentially alter drug efficacy in the appropriate environments.

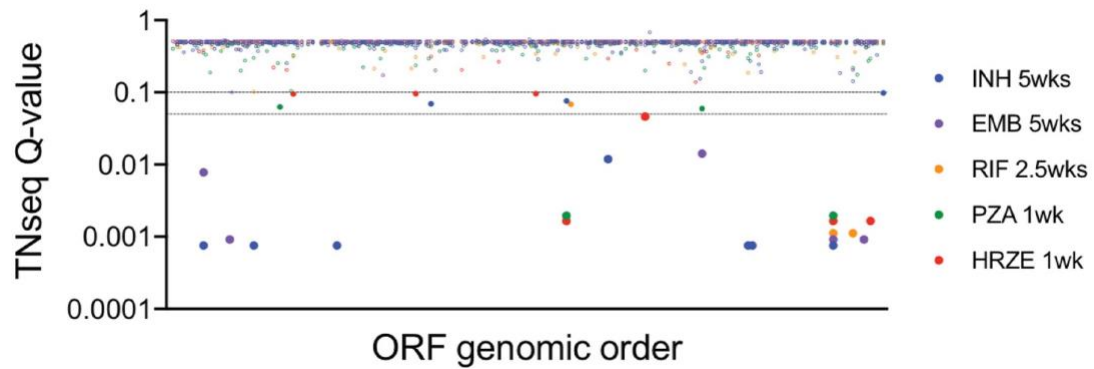


Figure 3.12 | Comparison between *in vivo* susceptibility and association with clinical resistance.

328 genes associated with clinical resistance are plotted by genomic order, x axis, and Q-value from TNseq conditions are indicated, y axis. Dashed lines indicate Q-value < 0.05 and < 0.01. TNseq hits overlapping with genes associated with clinical resistance are indicated by filled circles.

Table 3.2 | Genes that alter drug susceptibility in mice and contain resistance-associated SNPs in clinical isolates

Gene	Phenotypes	GWAS dataset	GWAS phenotype
Rv0101 (<i>npr</i>)	INH; EMB	Hicks et al. (145)	INH
Rv0244c (<i>fadE5</i>)	EMB	Zhang et al. (148)	KAN
Rv0353 (<i>hspR</i>)	INH	Farhat et al. (150)	RIF; INH; EMB; CAP
Rv0859 (<i>fadA</i>)	INH	Zhang et al. (148)	OFX; KAN
Rv2043c (<i>pncA</i>)	PZA; HRZE	Farhat et al. (150)	AMI; CAP; EMB; ETA; INH; KAN; MXF; PZA; RFB; RIF; STR; LIN
Rv2344c (<i>dgt</i>)	INH	Hicks et al. (145)	INH
Rv2571c	HRZE	Farhat et al. (150)	KAN; CAP; AMI; ETA; PZA; STR; RFB

Rv2942 (<i>mmpL7</i>)	INH; EMB	Farhat et al. (150)	RIF
Rv3211 (<i>rhIE</i>)	INH	Hicks et al. (145)	INH
Rv3267	INH	Hicks et al. (145)	INH
Rv3696c (<i>glpK</i>)	INH; EMB; RIF; PZA; HRZE	Farhat et al. (150)	AMI; INH; KAN; RFB; RIF; CAP; LIN; EMB; ETA; PZA
Rv3825c (<i>pks2</i>)	RIF	Zhang et al. (148)	OFX
Rv3859c (<i>gltB</i>)	EMB	Farhat et al. (150)	STR
Rv3877 (<i>eccD1</i>)	HRZE	Zhang et al. (148)	CAP
Rv0560c *	PZA	Hicks et al. (145)	INH
Rv0600c *	HRZE	Zhang et al. (148)	KAN
Rv1282c (<i>oppC</i>) *	HRZE	Hicks et al. (145)	INH
Rv1330c (<i>pncB1</i>) *	INH	Farhat et al. (150)	KAN; CAP; ETA; RIF; STR
Rv1860 (<i>apa</i>) *	HRZE	Farhat et al. (150)	STR,RIF
Rv2080 (<i>lppJ</i>) *	RIF	Zhang et al. (148)	ETH; KAN
Rv3919c (<i>gid</i>) *	INH	Farhat et al. (150)	EMB; INH; MXF; PZA; RFB; RIF; STR; CAP; LIN; ETA; KAN

Red = underrepresented in drug treated TNseq samples; Green = overrepresented in drug treated TNseq samples; “GWAS phenotype” = the drug resistance pattern associated with SNPs. INH (isoniazid); EMB (ethambutol); RIF (rifampicin); PZA (pyrazinamide); KAN (kanamycin); CAP (capreomycin); OFX (ofloxacin); MXF (moxifloxacin); AMI (amikacin); ETA (ethionamide); STR (streptomycin); RFB (rifabutin); LIN (linezolid). *Q-value < 0.1.

Discussion

Many studies investigating antibiotic efficacy and new drug target discovery are performed *in vitro*. While it is possible to change discrete aspects of the culture conditions to mimic individual stresses (123, 144, 175, 191, 192),

these models do not fully recapitulate the complex environment encountered by the bacterial population during infection. In this study, we identified genes important for bacterial survival under antibiotic pressure in the mouse model of TB, where the bacteria grow intracellularly (179) in the presence of a fully functional adaptive immune response. By collecting data across several time points, we were able to discern a number of new insights into the processes necessary to sustain an infection and persist through antibiotic treatment.

This time-resolved study provides the most detailed assessment of *M. tuberculosis* genes necessary to persist in the mouse model to date, identifying 562 genes (Figure 3.3 and Appendix Table A3.1). Our data are consistent with previous studies, and identified a large number of known virulence factors. We also identified 231 genes that were not found in previous TNseq studies, reflecting the increased accuracy of UMI based quantification of transposon insertions and increased number of replicates and time points. These included functions already known to be important, such as a number of genes encoded in a large genomic region dedicated to cholesterol catabolic functions (*kshA*, *rv3538*, *rv3549c*, *echA20*, *rv3557c*, *rv3562*, *rv3570c*, *rv3575c*) (136, 193). Similarly, several additional genes related to Type VII protein secretion were identified, *cyp143*, *ppe27*, and *esxN* are components of the ESX5 system (194), *esxW* is homologous to ESX substrates and has been associated with TB transmission (195), and *rv3866* (*espG*) is a component of the ESX1 system (196). A number of novel functions were identified as well. For example, we

found genes encoding a succinate dehydrogenase complex (*sdhA*, *sdhB*, *sdhD*), the proton translocating NADH dehydrogenase (*nuoE*, *nuoK*), and the Mce3 transporter that is homologous to lipid importers (*mce3A*, *mce3B*, *mce3C*, and *lprM*). Overall, this dataset enhances our understanding of the genomic requirements for infection.

When infected animals were treated with antibiotics, we only found a small number of genes that broadly alter drug efficacy. These included *glpK*, which is necessary for glycerol metabolism and has been shown to alter the effect of HRZE *in vivo* in Chapter II (183), and several drugs *in vitro*. Similarly, the mutation of the putative glutamine transporter encoded by *rv2563* and *rv2564* broadly sensitizes the bacterium to different drugs. These observations highlight the importance of primary metabolic functions in general alterations in drug sensitivity. A much larger collection of mutations produced relatively drug-specific effects (Figure 3.9), and suggested primary mechanisms that determine the efficacy of some antibiotics. For example, the majority of genes associated with RIF treatment are likely to be involved in cell wall formation, such as acyltransferases Rv1184c and Rv3822 and cyclopropane synthase CmaA2. While *rv1184c* and *rv3822* mutants are more susceptible to RIF, mutations in *cmaA2* result in increased survival, indicating that changes in permeability can affect RIF efficacy in multiple ways. More generally, the abundance of cell wall modifying enzymes indicates that permeability is an important determinant of RIF efficacy during infection, which is consistent with previous *in vitro* observations

(197-199). Similarly, mutants in the mycobactin biosynthesis pathway were overrepresented specifically post-EMB treatment, indicating a role for iron utilization in EMB efficacy. Finally, the specific correlation between *in vivo* fitness and drug efficacy for INH, a drug known to be affected by growth rate *in vitro* (143, 182), suggested that INH is preferentially affected by the decreased replication rate of the bacterium during infection.

Drug efflux may also produce drug-selective effects. For example, Rv1273c is predicted to be a multi-drug transporter based on sequence homology (200), and we found this mutant was only hypersusceptible to RIF. Similarly, loss of the ABC transporter encoded by Rv1747 specifically increased INH susceptibility. Despite these *in vivo* effects we found no evidence that mutating these genes altered drug susceptibility *in vitro*, suggesting that both systems are regulated. Indeed, Rv1747 is an unusual ABC transporter that is controlled via phosphorylation by PknF (201), indicating a potential mechanism of inducing INH tolerance in response to environmental cues. In contrast, Rv1273c expression is increased in clinical isolates (63), leading to the hypothesis that this may be an inducible efflux pump, similar to a previously identified mycobacterial drug efflux system that is expressed during intracellular growth (61).

While we did not globally assess the effect of transposon mutations on antibiotic efficacy *in vitro*, we compared our *in vivo* dataset to a previous TNseq study (175) and directly measured *in vitro* effects for a selection of mutants. Both efforts indicated that many of the efficacy-altering mutations that we identified in

the mouse model have a minimal effect on *in vitro* MIC or rate of killing (Figure 3.11 and Table 3.1), suggesting that the observed chemical-genetic synergies are specific to the host environment. This observation has important implications, as it suggests the possibility that many genetic variants that alter treatment outcome do not produce an effect that is measurable in standard drug susceptibility testing (DST).

Genetic variants that are selected by drug exposure, can be identified via GWAS approaches, using the thousands of available whole-genome sequences from *M. tuberculosis* clinical isolates (145, 148, 150). While these data are immediately useful for genotypic drug susceptibility assessment (202, 203), the functional roles played by the majority of these variants remains unknown. In this work, we leveraged our TNseq data to identify a number of variants that are likely to directly alter drug efficacy, suggesting new mechanisms that are relevant to treatment outcome (Figure 3.12 and Table 3.2). As many of the efficacy altering mutations found in the mouse model have little effect *in vitro*, these variants could represent cryptic determinants of treatment outcome that only alter drug efficacy in the appropriate environments. However, the relatively modest overlap between the TNseq and GWAS datasets was also notable. It is possible that this observation indicates that only a small fraction of the variants identified by GWAS directly alter drug efficacy. However, this conclusion should be approached with caution, as there are significant physiological differences between human and mouse TB, and the TNseq approach only assesses the effect of loss-of-function

mutations. Thus, the ultimate functional assessment of natural genetic polymorphisms still requires the individual investigation of each variant.

Understanding how *Mycobacterium tuberculosis* survives prolonged antibiotic pressure also suggests new strategies to improve treatment. Our data indicate that a large number of potential synergies exist that could be exploited to accelerate bacterial clearance. While we do not assess sterilization or ultimate “cure” in this model, rapidly eliminating viable bacteria remains an important goal. While the relatively drug-selective effects of these synergies represents a potential challenge, our data indicate that more effective regimens are possible and their development could be facilitated by this type of unbiased chemical-genetic study.

Acknowledgments

We are thankful to members of the Sasseti lab, both past and present, for insightful discussions related to the project and technical support. This work was supported by the Office of the Assistant Secretary of Defense for Health Affairs through the Peer Reviewed Medical Research Program, Focused Program Award, under award no. W81XWH-17-1-0692. Opinions, interpretations, conclusions, and recommendations are those of the author and are not necessarily endorsed by the Department of Defense. The work was additionally supported by the NIH (AI142793 and AI095208).

CHAPTER IV: Discussion

Mycobacterium tuberculosis is an ancient pathogen, evolving in parallel with humans, that remains a modern-day global health problem. As with many bacterial infections, the discovery and introduction of antibiotics revolutionized the treatment of tuberculosis - leading some scientists to believe that tuberculosis (TB) would be eradicated. Famously, Selman Waksman, who was involved in the discovery of streptomycin, stated: “the ancient foe of man, known as consumption, the great white plague, tuberculosis, or by whatever other name, is on the way to being reduced to a minor ailment of man. The future appears bright indeed, and the complete eradication of the disease is in sight” (204). However, the development of antibiotic resistance, the lack of an effective vaccine, the increase in active disease due to co-morbidities such as HIV and diabetes, and multiple hurdles with transmission control have all contributed to TB becoming the largest global cause of death due to a single infectious agent.

Antibiotic treatment of TB remains an effective weapon against disease and transmission. Diagnosis and treatment of latent infection helps prevent progression to active disease, therefore preventing spread, and treatment of active disease has an 85% cure rate (5). However, these treatments require months of antibiotics, three to four months for latent infections and six months of multiple drugs for drug-susceptible (DS) TB, creating a burden on the patient and the healthcare system. Additionally, we have been using the same treatment regimen for decades, resulting in bacterial mutations that cause high-level

resistance against these antibiotics. Multi-drug resistant (MDR) and extensively-drug resistant (XDR) infection rates have risen over the past years, each requiring longer treatment regimens with more toxic antibiotics and decreased cure rates.

Improving our current treatment regimens and developing new antibiotics effective against *M. tuberculosis* remain important goals in the fight against TB. Drug discovery for effective anti-mycobacterials is difficult and, in the past decades, only two antibiotics have been approved for use: bedaquiline and pretomanid. A number of factors contribute to the lack of success in drug development, starting with the bacteria. *M. tuberculosis* is effective at preventing killing by decreasing antibiotic import, by modifying antibiotics to prevent activity, and by exporting antibiotics out of the cell. Additionally, *M. tuberculosis* is an obligate human pathogen and alters its physiology to adapt to multiple environments and stresses that are impossible to replicate *in vitro*, creating an obstacle in identifying antibiotics that are as effective *in vivo*. The use of the mouse model in our studies to understand *M. tuberculosis* mechanisms of survival allows us to identify potential targets for new and synergistic treatments in a physiologically relevant disease model that mimics the complex disease pathology found in humans.

Using knowledge about our current antibiotics to discover new treatments has had prior success. Notably, derivatives of the rifamycin antibiotic class have variable efficacies against susceptible and drug-resistant *M. tuberculosis* (205-

207). However, our current regimen for DS-TB treatment was implemented with minimal knowledge about the mechanism of action of the antibiotics or resistance mechanisms. Improved understanding of the efficacy of the current antibiotic regimen and *M. tuberculosis* survival during prolonged antibiotic exposure in the context of an *in vivo* infection is crucial to improving treatment. In these studies, we used unbiased, comprehensive genetic approaches and the mouse model of TB to identify bacterial mechanisms which alter treatment efficacy, providing insight to *M. tuberculosis* antibiotic tolerance and the development of resistance during infection.

Treatment is always administered as combination therapy; therefore, we first aimed to identify mutants with altered susceptibility to the standard DS-TB combination regimen, commonly referred to as HRZE (Chapter II). We observed many mutants with increased susceptibility. These are potential new targets for synergistic treatments (Appendix Tables A2.1 and A2.4). We also observed a small number of mutants with decreased clearance (Appendix Tables A2.2 and A2.5), including glycerol kinase mutants. Mutations in *glpK* have no observed fitness defect *in vivo* and result in increased survival under pyrazinamide containing regimens, including combination therapy (Figure 2.6). Our observation of loss of function mutants, with no fitness cost, and prolonged survival led to the hypothesis that *glpK* mutations would be present in clinical isolates. We confirmed our hypothesis with the observation that *glpK* mutations evolve independently in multiple strains and lineages of TB in two distinct geographical

cohorts (Figure 2.8 and 2.9). These mutations are also significantly associated with drug resistance phenotypes. The majority of these mutations were +1bp frameshift mutations in a homopolymer region of the open reading frame, providing a potential new genetic mechanism of antibiotic tolerance in *M. tuberculosis*.

Phase variation, such as frameshifting, has not been previously described in *M. tuberculosis*. Previous work has shown selection against long mononucleotide regions (165), indicating that the presence of remaining homopolymeric regions in *M. tuberculosis* may be genetic mechanisms of regulation that confer a fitness advantage. Therefore, phase variation in a small number of genes may have a greater role in adaptation to environments and prolonged survival under antibiotic treatment. Reducing the rate of clearance of *M. tuberculosis* allows for the potential accumulation of mutations, thus increasing the risk of high-level resistance-conferring mutations. Loss-of-function mutations which prolong survival were previously described in clinical isolates (145), and the high prevalence of *glpK* frameshift mutations in drug-resistant strains indicates that this mechanism may be an efficient method for producing tolerant populations. Preliminary investigation has identified a number of genes with homopolymers that contain SNPs associated with drug-resistant phenotypes. Further investigation into the rate of frameshifting within the *glpK* gene and other homopolymeric regions will provide a platform to study the

function of phase variation in *M. tuberculosis* and how it may influence infection and treatment outcomes.

Discovery of new effective combination therapies for treatment of TB is essential for improving therapy. Since the addition of RIF and PZA to the standard regimens, the length of treatment has remained at six months. Previous clinical trials aiming to shorten DS-TB treatment length have had minimal success in reducing relapse rates (49, 208-210). Here, we identified mutations with altered susceptibility to individual first-line antibiotics (Chapter III). We observed that a majority of mutant phenotypes were specific to an individual antibiotic (Figure 3.9). This confirms mechanism-of-action studies showing that these antibiotics target different essential pathways (Figure 1.1). However, it also indicates that a majority of tolerance mechanisms are distinct for each antibiotic. Multidimensional analyses, of these datasets identified bacterial genes/pathways responsible for defining the bacterial response to the different treatments (Figure 3.10). For example, we observed a number of enzymes involved in cell wall modification associated with RIF treatment, indicating permeability as a potential determinant of RIF efficacy. Insight into *M. tuberculosis* physiology and survival under mono-therapy treatment could improve our knowledge on desired characteristics of new drugs for new combinations.

A potential caveat of high-throughput genetic screening is that observed phenotypes are the result of the screen and not the mutations generated. To determine how well our TNseq studies predict mutant phenotypes under more

defined infection conditions, we generated a series of deletion mutants. Between the two studies (Chapter II and III), we have validated the observed phenotypes using deletion mutants in multiple infections for several genes of interest using a variety of experimental techniques (Figure 2.6 and 3.8). These phenotypes are genuine differences in viable bacteria, as we have also validated two genes of interest via colony forming unit (CFU) plating as a measure of abundance. Additionally, we observed that the majority of phenotypes were specific to the *in vivo* environment, through *in vitro* minimum inhibitory concentration (MIC) and rate of killing assays (Figure 3.11 and Table 3.1) and overlap with previously published datasets (175).

Comparing bacterial genome-wide association studies (GWAS) with our *in vivo* studies, we identified a number of genes which alter susceptibility to antibiotics *in vivo* that contain mutations in clinical isolates associated with resistance phenotypes (Figure 3.12 and Table 3.2). A majority of SNPs associated with clinical resistance identified have yet to be functionally characterized. Utilizing overlap with genetically tractable *in vivo* studies, such as those performed here, could aid in identification of variants relevant to treatment outcome. For example, we identified loss-of-function mutants that are more and less susceptible to antibiotic treatment, and this knowledge could provide mechanistic insight into observed genetic variation. Additionally, these data provide a list of clinically-relevant genes which could be further studied in tractable lab models.

Small changes in antibiotic efficacy can have negative impacts on treatment outcome (172). In our studies, we identified multiple loss-of-function mutations altering drug efficacy which have the potential to produce distinct drug tolerant populations (Appendix Tables A2.2; A2.5; A3.3; A3.5; A3.7; A3.9). Identification of mutations that result in prolonged survival under antibiotic therapy, like those identified in these and other studies (145), have the potential to expand genotypic testing for drug tolerant variants that alter treatment outcome (202, 203). Through clinical trial studies, it has been observed, that for some patients, the six month regimen is longer than necessary (49, 209-211). However, it is near impossible to predict which patients can benefit from a shorter treatment and which patients require longer regimens. Identifying patients who are at risk of relapse through testing for drug tolerant variants could allow for more personalized treatment, through alterations of regimens to prevent negative outcomes.

Here, we describe the identification of *M. tuberculosis* mechanisms of survival during antibiotic treatment which are specific to the infection environment and clinically relevant. While decades of research has provided a wealth of knowledge on TB infections and *M. tuberculosis* survival, there are still many unknowns inhibiting improvement of treatment and control of TB. Combining comprehensive genetic tools previously used to identify conditionally-essential genes in *M. tuberculosis* and the highly developed mouse model of TB to mimic the infection environment, we have provided a foundation for the identification of

a new genetic mechanism of antibiotic tolerance, many potential targets for new synergistic treatments, and the characterization of clinically-relevant mutations associated with resistance.

APPENDIX A1: Materials and Methods

Transposon sequencing

BALB/cJ (stock no. 000651) mice were purchased from the Jackson Laboratory (Bar Harbor, ME, USA). Housing and experimentation were in accordance with the guidelines set forth by the Department of Animal Medicine of University of Massachusetts Medical School and Institutional Animal Care and Use Committee and adhered to the laws of the United States and regulations of the Department of Agriculture. Eight- to 12-week-old female animals were infected with 10^6 CFU of a *himar1* transposon library (131) via the intravenous route. Groups of mice were treated with antibiotics starting at 14 days post infection. Antibiotics were administered via drinking water at the following concentrations: 0.1 g/liter isoniazid (Sigma), 0.6 g/liter ethambutol (Sigma), 0.1 g/liter rifampin (Sigma), and 15 g/liter pyrazinamide (Sigma). At the indicated time points, mice were sacrificed, spleens and lungs were isolated and homogenized, and CFU numbers were determined by plating dilutions on 7H10 agar with 10 μ g/ml kanamycin. For library recovery, approximately one million CFU per mouse were plated on 7H10 agar with kanamycin (10 μ g/ml). Genomic DNA was extracted (153), and the relative abundance of each mutant was estimated as described previously (153). Statistical analysis of \log_2 fold change (\log_2 FC) in counts between conditions (two-way analysis) was performed by resampling (212).

In Chapter II, a three-way analysis was used. The three-way analysis measures the difference in $\log_2\text{FC}$ ($\Delta\log_2\text{FC}$) measured under two selective conditions relative to a common starting condition:

$$\Delta\log_2\text{FC} = \log_2\text{FC}(\text{condition 1}) - \log_2\text{FC}(\text{condition2})$$

In the present case, condition 1 was 14 days post infection plus 7 days of antibiotic treatment, condition 2 was 21 days post infection, and the starting condition was 14 days post infection (the start of drug treatment). Statistical significance was assessed by resampling. For each gene, the sampling distribution of $\Delta\log_2\text{FC}$ was obtained by resampling with replacement of the insertion counts at each TA within the gene (after normalization across all libraries). Counts for replicates were pooled prior to resampling. For each of 10,000 resamples, $\Delta\log_2\text{FC}$ was calculated. The P value was taken as the fraction of the cumulative frequency distribution of $\Delta\log_2\text{FC}$ falling outside $\Delta\log_2\text{FC} = 0$, on the negative side for values measured as $\Delta\log_2\text{FC} > 0$, or on the positive side for values measured as $\Delta\log_2\text{FC} < 0$ (equivalent to a 1-tailed test). The resulting P values were adjusted for multiple testing by Benjamini-Hochberg false discovery rate.

In Chapter III, libraries were analyzed via hierarchical clustering and multi-dimensional analyses. Hierarchical clustering (using *hclust()* in R, with average-linking clustering) was applied to vectors of $\log_2\text{FC}$ for each gene across all conditions. PCA and Varimax rotation were performed on log-fold-changes LFCs using the procedures *prcomp()* and *varimax()* in R, where the LFC for each

condition was calculated as the \log_2 of the ratio of the mean insertion count in that condition relative to the grand mean across all conditions.

Projection resampling

In order to identify genes significantly associated with individual Varimax dimensions in Chapter III, we devised a sampling-based version of the permutation test. For a given gene G , we collected the normalized insertion counts at all TA sites in the gene across all replicates in all conditions (drug treatments). Let $W[c,v]$ be the matrix of weights (loadings) of each condition c (i.e. drug) projected onto each Varimax dimension v . The normalized insertion counts in each condition were randomly re-distributed onto the Varimax dimensions with probability proportional to the loadings, where the weights $W[.,v]$ were converted to a probability distribution by dividing by $\sum_i W[.,i]$. Let D be the Varimax dimension of interest for testing the association of gene G . The re-distributed observations for g were divided into two groups, A: those counts associated with dimension D , and B: those counts not associated with dimension D . Finally, the significance of the difference in mean counts in A versus B was determined by a permutation test, where a null distribution on the difference in means was generated by randomly permuting the counts between groups A and B 10,000 times, from which a p -value for the association of gene G with dimension D was derived. P values were adjusted post-hoc by the Benjamini-

Hochberg procedure (213) for multiple tests correction (to limit the false-discovery rate to 5%).

***Mycobacterium tuberculosis* strains and culturing**

M. tuberculosis H37Rv was maintained in Middlebrook 7H9 medium containing oleic acid-albumin-dextrose-catalase (OADC), 0.2% glycerol, and 0.05% Tween 80 and grown with shaking (200 rpm) at 37°C. Hygromycin (50 µg/ml) or kanamycin (20 µg/ml) was added when necessary. All work with *M. tuberculosis* adhered to the CDC-NIH *Guide for Biosafety in Microbiological and Biomedical Laboratories* (214). Deletion strains were constructed by allelic exchange as previously described (215) and this work adhered to NIH Guidelines for research involving recombinant DNA molecules. Genes were replaced by the vector pKM464 carrying one of seven unique q-Tag sequences to identify each mutant for deep sequencing (216), for strain details see Table A1.1.

Table A1.1 | Deletion strains constructed in this study.

Strain	Organism	Reference genome	Nucleotides deleted	Plasmid ¹	Barcode ²
ΔRv0248c	<i>M.tb</i>	H37Rv	298898 - 300763	pKM464	qTag-19
ΔcmaA2 (Rv0503c)	<i>M.tb</i>	H37Rv	593901 - 594779	pKM464	qTag-19
ΔRv1174c	<i>M.tb</i>	H37Rv	1305699 - 1305984	pKM464	qTag-22
Δchp2 (Rv1184c)	<i>M.tb</i>	H37Rv	1324562 - 1325588	pKM464	qTag-23
ΔRv1273c	<i>M.tb</i>	H37Rv	1422332 - 1424020	pKM464	qTag-24
ΔRv1747	<i>M.tb</i>	H37Rv	1973660 - 1976197	pKM464	qTag-29
Δppe51 (Rv3136)	<i>M.tb</i>	H37Rv	3501829 - 3502901	pKM464	qTag-26
ΔglpK (Rv3696c)	<i>M.tb</i>	H37Rv	4138237 - 4139720	pKM464	qTag-22
ΔcinA (Rv1901)	<i>M.tb</i>	H37Rv	2147692 - 2148924	pKM464	qTag-25
Δchp1 (Rv3822)	<i>M.tb</i>	H37Rv	4286751 - 4287905	pKM464	qTag-27

Strain indicated by gene deleted. ¹ORBIT plasmid (215). ²qTag sequences (216).

ΔglpK mutant characterization

In Chapter II, the ΔglpK strain *in vitro* growth and antibiotic susceptibility was determined. The ΔglpK strain was cultured in glycerol-free 7H9. Glycerol-dependent growth was assessed in minimal medium containing asparagine (0.5 g/liter), KH₂PO₄ (1 g/liter), Na₂HPO₄ (2.5 g/liter), ferric ammonium citrate (50 mg/liter), MgSO₄·7 H₂O (0.5 g/liter), CaCl₂ (0.5mg/liter), ZnSO₄ (0.1mg/liter), 0.1% tyloxapol, and either 0.1% glycerol or 0.1% dextrose. For *in vitro* antibiotic susceptibility testing, isoniazid (INH) and rifampin (RIF) were used at 2 and 1 μg/ml, respectively, and serially diluted 2-fold. Bacteria were inoculated to a starting optical density at 600nm (OD₆₀₀) of 0.05 in 96-well plates with 7H9 medium containing OADC, 0.05% Tween 80, and 0.2% glycerol, butyrate, or

pyruvate. Pyrazinamide (PZA) was used at 400 μ g/ml and serially diluted 2-fold. Bacteria were inoculated to a starting OD₆₀₀ of 0.01 in inkwells containing 7H9 medium supplemented with OADC, 0.2% glycerol, and 0.05% tyloxapol at pH 5.8 and grown with shaking. Growth was monitored by OD₆₀₀. Conditions were assessed in triplicate. Antibiotic efficacy was determined by comparing growth rate under increasing drug concentrations. OD₆₀₀ was plotted and the rate constant (k) value was determined for all conditions using an exponential growth model. Rate constants posttreatment were normalized to levels for no-antibiotic controls.

In Chapter II, $\Delta glpK$ mutant fitness *in vivo* was determined. Mice were inoculated with a 1:1 mixture of $\Delta glpK$ (hygromycin resistant) and H37Rv (harboring pJEB402 chromosomally integrated plasmid encoding kanamycin resistance) strains via the aerosol route. At the indicated time points, mice were sacrificed and CFU numbers in spleen and lung homogenate were determined by plating on 7H10 agar. Fitness in the presence of antibiotic was assessed by a similar competitive assay. Mice were infected with a pool of strains at equal ratios via the intravenous route (10^6 total CFU/mouse). Groups of mice were treated with antibiotics starting at 14 days post infection, as described for the TNseq study. At the indicated time points, approximately 10,000 CFU from the spleen homogenate of each mouse were plated on 7H10 agar. Genomic DNA was extracted for quantitative real-time PCR analysis (216). Briefly, the abundance of the constant and variable regions of the q-Tag present in each mutant was

determined by TaqMan PCR assay, as described previously (216), and used to calculate a variable/constant region ratio for each strain. The abundance of each mutant strain was then plotted relative to that of wild-type H37Rv (mutant/wild type). Values were normalized to initial day 0 ratios.

GR₅₀ determination

In Chapter II, the GR₅₀ values were determined for H37Rv. Bacteria were grown in minimal medium with 0.1% glycerol, 0.1% valeric acid, or 0.1% cholesterol on 96-well plates. Isoniazid (INH), rifampin (RIF), and moxifloxacin (MOX) were used at 1, 0.062, and 1 µg/ml, respectively, and serially diluted 2-fold. A no-antibiotic control was included in each experiment. Bacteria were inoculated to a starting OD₆₀₀ of 0.05, and growth was monitored by OD₆₀₀ and fluorescence. Conditions were prepared in triplicates. Antibiotic efficacy was determined by growth rate inhibition. The exponential growth constant (*k*) value was determined for all conditions. The *k* value of each antibiotic concentration was normalized to the *k* value of the no-drug control. The GR₅₀ value was determined as the concentration of antibiotic that resulted in a 50% decrease in growth rate, as previously described (157).

***In vitro* antibiotic susceptibility**

In Chapter III, MIC testing was performed. Bacteria were inoculated to a starting OD₆₀₀ 0.05 in 96-well plates with 7H9 medium containing OADC, 0.2%

glycerol and 0.05% Tween 80. Isoniazid (INH) and rifampin (RIF) were used at 0.4 and 0.05 $\mu\text{g}/\text{mL}$, respectively, and serially diluted 2-fold for a total of 6 dilutions. Growth was monitored by OD_{600} and conditions were assessed in triplicate. IC_{50} was determined by plotting OD versus concentration of antibiotic and plotting a curve using [inhibitor] versus response model.

For kill curves performed in Chapter III, bacteria were inoculated to a starting OD_{600} 0.05 in inkwells containing 7H9 medium containing OADC, 0.2% glycerol and 0.05% Tween 80. At OD_{600} ~0.8-1.0 antibiotics were added to a final concentration of 0.6 and 0.5 $\mu\text{g}/\text{mL}$ for INH and RIF respectively. At indicated time points samples from the cultures were taken and CFU/mL was determined by plating on 7H10 agar with 50 $\mu\text{g}/\text{mL}$ hygromycin. Conditions were assessed in triplicate.

***In vivo* antibiotic susceptibility**

In Chapter III, mice were infected with pools of strains at equal ratios via the intravenous route (10^6 total CFU/mouse) or aerosol route (500-1000 CFU/mouse). Groups of mice were treated with antibiotics, as described for the TNseq study. Treatment was administered starting at 14 days post infection for i.v. infections and 21 days post infection for aerosol infections. At indicated time points, approximately 10,000 CFU from the spleen or lung (for i.v. and aerosol infections, respectively) homogenate of each mouse were plated on 7H10 agar. Genomic DNA was extracted for sequencing as described previously (153).

Sequencing libraries spanning the variable region of each qTag were generated using PCR primers binding to regions common among all qTags, similar to previously described protocols (217), see Table A1.2 for primer details. During this PCR, a unique molecular identifier was incorporated into the sequence to allow for the accurate counting of input templates and account for PCR jackpotting. The libraries were sequenced to 1000-fold coverage on an Illumina NextSeq platform using a 150 cycle Mid-Output kit with single end reads. Total abundance of each mutant in the library was determined by counting the number of reads for each q-Tag with a unique molecular counter. Relative abundance of each mutant in the pool was then calculated by dividing the total abundance of a mutant by the total abundance of reads for wild-type H37Rv. This value was then normalized to the relative abundance at the pretreatment time point to obtain the final relative abundance for each mutant in the pool. Statistical significance was determined by unpaired *t* test with Benjamini-Hochberg multiple testing correction.

Table A1.2 | qTag sequencing primers.

ID	Dir.	Round	Sequence
Ftotal1	FW	1	CCCTACACGACGCTCTCCGATCTGCCNNNCNNNCNNNggagcgtgtccatctggtgt
Ftotal2	FW	1	CCCTACACGACGCTCTCCGATCTTCNNNCNNNCNNNggagcgtgtccatctggtgt
Ftotal3	FW	1	CCCTACACGACGCTCTCCGATCTCNNNCNNNCNNNggagcgtgtccatctggtgt
Ftotal4	FW	1	CCCTACACGACGCTCTCCGATCTAACNNNCNNNCNNNggagcgtgtccatctggtgt

Ftotal5	FW	1	CCCTACACGACGCTCTTCCGATCTCTGCNNNCNNNCNNNggagcgtgtccatctggtgt
Rtotal1	RV	1	GTGACTGGAGTTCAGACGTGTGCTCTTCCGATCTGAgaccacaacggttccatag
Rtotal2	RV	1	GTGACTGGAGTTCAGACGTGTGCTCTTCCGATCGAgaccacaacggttccatag
Rtotal3	RV	1	GTGACTGGAGTTCAGACGTGTGCTCTTCCGATCAGAgaccacaacggttccatag
Rtotal4	RV	1	GTGACTGGAGTTCAGACGTGTGCTCTTCCGATCCGGAgaccacaacggttccatag
Rtotal5	RV	1	GTGACTGGAGTTCAGACGTGTGCTCTTCCGATCCATGAgaccacaacggttccatag
F501	FW	2	AATGATACGGCGACCACCGAGATCTACAC TATAGCCT ACACTCTTCCCTACACGAC GCTCTTCC
F502	FW	2	AATGATACGGCGACCACCGAGATCTACAC ATAGAGGC ACACTCTTCCCTACACGAC GCTCTTCC
F503	FW	2	AATGATACGGCGACCACCGAGATCTACAC CCTATCCT ACACTCTTCCCTACACGAC GCTCTTCC
F504	FW	2	AATGATACGGCGACCACCGAGATCTACAC GGCTCTGA ACACTCTTCCCTACACGAC GCTCTTCC
F505	FW	2	AATGATACGGCGACCACCGAGATCTACAC AGGCGAAG ACACTCTTCCCTACACGAC GCTCTTCC
F506	FW	2	AATGATACGGCGACCACCGAGATCTACAC TAATCTTA ACACTCTTCCCTACACGAC CTCTTCC
F507	FW	2	AATGATACGGCGACCACCGAGATCTACAC CAGGACGT ACACTCTTCCCTACACGAC GCTCTTCC
F508	FW	2	AATGATACGGCGACCACCGAGATCTACAC GTA CTGAC ACACTCTTCCCTACACGAC GCTCTTCC
R701	RV	2	CAAGCAGAAGACGGCATAACGAGAT CGAGTAAT GTGACTGGAGTTCAGACGTGTGC
R702	RV	2	CAAGCAGAAGACGGCATAACGAGAT TCTCCGGA GTGACTGGAGTTCAGACGTGTGC
R703	RV	2	CAAGCAGAAGACGGCATAACGAGAT AATGAGCG GTGACTGGAGTTCAGACGTGTGC
R704	RV	2	CAAGCAGAAGACGGCATAACGAGAT GGAATCTC GTGACTGGAGTTCAGACGTGTGC
R705	RV	2	CAAGCAGAAGACGGCATAACGAGAT TTCTGAAT GTGACTGGAGTTCAGACGTGTGC
R706	RV	2	CAAGCAGAAGACGGCATAACGAGAT ACGAATTC GTGACTGGAGTTCAGACGTGTGC
R707	RV	2	CAAGCAGAAGACGGCATAACGAGAT AGCTTCAGG GTGACTGGAGTTCAGACGTGTGC
R708	RV	2	CAAGCAGAAGACGGCATAACGAGAT GCGCATTAG GTGACTGGAGTTCAGACGTGTGC
R709	RV	2	CAAGCAGAAGACGGCATAACGAGAT CATAGCCG GTGACTGGAGTTCAGACGTGTGC

R710	RV	2	CAAGCAGAAGACGGCATACGAGATTT CGCGGA GTGACTGGAGTTCAGACGTGTGC
R711	RV	2	CAAGCAGAAGACGGCATACGAGAT GCGGAGA GTGACTGGAGTTCAGACGTGTGC
R712	RV	2	CAAGCAGAAGACGGCATACGAGAT CTATCGCT GTGACTGGAGTTCAGACGTGTGC

“ID” = primer identifier name. “Dir.” = annealing direction of the primer. “Round” = the PCR reaction the primer is used (1 or 2). Purple = annealing sequence. Red = unique molecular identifier (UMI). Blue = Illumina index.

In Chapter III, competition infections were performed by infecting mice with a 1:1 mixture of Δ Rv1273c and H37Rv (harboring pJEB402 chromosomally integrated plasmid encoding kanamycin resistance) or 1:1 mixture of Δ Rv1273c complement strain and kanamycin-resistant H37Rv via the aerosol route (500-1000 CFU/mouse). After 21 days post infection RIF was administered to groups of mice. At indicated time points mice were sacrificed and CFU in lung and spleen homogenate was determined by plating on 7H10 agar containing either hygromycin (50 μ g/ml) or kanamycin (20 μ g/ml).

Phenotypic and genotypic analysis of Korean strains

Strains were collected from the National Culture Collection for Pathogens, which is maintained by the Korea Centers for Disease Control and Prevention. Phenotypic DST testing for each strain was conducted by an absolute concentration method using Löwenstein-Jensen agar with critical concentrations of TB drugs (in μ g/ml): isoniazid (0.2), rifampin (40), ethambutol (2), streptomycin (10), kanamycin (40), prothionamide (40), cycloserine (30), para-aminosalicylic

acid (1), ofloxacin (2), pyrazinamide (50; pH 4.65), capreomycin (40), moxifloxacin (2), amikacin (40), levofloxacin (2), *p*-nitrobenzoic acid (500), and rifabutin (40). Strains were classified as resistant if drug-containing media produced more than 1% of the CFU observed in control cultures. To test growth on glycerol, *M. tuberculosis* was grown in Middlebrook 7H9 broth with 0.5% glycerol, 0.05% tyloxapol, catalase, and fatty acid-free bovine serum albumin (Sigma). Inocula were cultivated in 7H9-OADC-Tween 80 to an OD of 0.1 to 0.2, washed with phosphate-buffered saline plus tyloxapol (0.05%), and diluted to ~10⁶ CFU/ml.

Genomic DNA was sequenced either by Ion Torrent (yielding an average read length of 170 bases) or Illumina (300-base paired-end reads) platforms. In both cases, reads were aligned using *bwa mem* (version 0.7.12) against *Mycobacterium tuberculosis* H37Rv reference GenBank accession no. [NC_018143.2](#). Variants were called using GATK 3.3-0 (218, 219) by following the developer's best practices: (i) *picard* 1.96 MarkDuplicates, (ii) GATK Realigner Target Creator, (iii) GATK IndelRealigner, (iv) GATK BaseRecalibrator, (v) GATK UnifiedGenotyper, and (vi) GATK GenotypeGVCFs. Base recalibration was performed iteratively using the initial Ion variant calls, obtained without recalibration, to obtain a set of polymorphic sites for use in step 4. Final filtering was performed separately for single-nucleotide polymorphism (SNP) and insertion/deletion (indel) calls: for SNPs, FS of >60.0, MQ of <40.0, MQRankSum of < -12.5, and ReadPosRankSum of < -8.0; for indels, FS of >200.0 and

ReadPosRankSum of < -20.0 . Call-passing filters were combined and a final filter QD of < 20.0 was applied. Only calls passing all filters were combined into the final vcf file (a total of 7,418 variants). For phylogenetic analysis, only variant SNPs were used. The final alignment (which included the corresponding NC_181843.2 reference bases) consisted of 51 taxa X 7,247 positions. A maximum likelihood phylogeny was obtained using PHYML version 20120412 (220) with the generalized time-reversible model. Trees were visualized with iTOL (221). Alternative tree topologies were generated using PHYLIP retree (222), and SH tests were performed using PAML baseml, version 4.8 (223).

Phenotypic and genotypic analysis of Peruvian strains

Drug-resistant phenotypes were determined by measuring MICs to 12 anti-tuberculosis drugs. For strains found to be sensitive at the critical concentration recommended by the WHO for each drug (224), we tested two MIC levels below the critical concentration, and for those resistant at the critical concentration, we tested six levels above it. The testing concentrations deviated from the traditional doubling in order to better detect intermediate-level MICs that are theoretically achievable levels in patient sera.

Strains were sequenced on the Illumina platform to produce 100 to 150 paired-end reads and coverage of at least 50-fold. The paired-end raw sequence data were mapped to the H37Rv reference genome using the BWA mem algorithm. We used SAMtools (default settings) (225) and pilon (226) to identify

single-nucleotide variants and insertions and deletions up to approximately 100bp using a coverage-based approach. We assigned a variant call as missing if the valid depth of coverage at a specific site was less than 10 reads, if the mean read-mapping quality at the site did not reach 7, or if none of the alternative alleles accounted for at least 90% of the valid coverage. The genotype of *glpK* was determined by a binary burden score that represented the presence of any nonsynonymous single-nucleotide variant, insertion, or deletion observed in that gene. *M. tuberculosis* genetic lineages were determined using a previously published SNP barcode (227). A neighbor-joining tree was derived using <https://cran.r-project.org/web/packages/ape/index.html>.

A linear mixed model was used to examine the associations between *glpK* genotype and the rank-transformed MICs phenotypes of 12 drugs and *pncA* genotype. We adjusted for the population structure using a genetic relatedness matrix (GRM), calculated from a pairwise distance matrix using synonymous single-nucleotide variants of the complete genome using the software GEMMA. The type I error rate was set at 0.01 after a Bonferroni correction accounting for the multiple comparisons. The linear mixed model was also performed using GEMMA (228).

**APPENDIX A2: List of genes with altered susceptibility to HRZE
treatment *in vivo* and strain characteristics of Korean Isolates**

Table A2.1 | Significantly underrepresented genes post HRZE treatment compared to pretreatment

ID	gene	HRZE 1wk	
		LFC	Q-value
Rv0111		-1.5986	0.0016
Rv0407	<i>fgd1</i>	-1.9510	0.0016
Rv0757	<i>phoP</i>	-2.7132	0.0016
Rv0989c	<i>grcC2</i>	-4.2399	0.0016
Rv0998		-2.9370	0.0016
Rv1006		-1.3537	0.0224
Rv1099c	<i>glpX</i>	-4.0453	0.0016
Rv1212c	<i>glgA</i>	-2.2771	0.0016
Rv1213	<i>glgC</i>	-2.2245	0.0016
Rv1244	<i>lpqZ</i>	-1.9977	0.0121
Rv2048c	<i>pks12</i>	-1.0648	0.0016
Rv2605c	<i>tesB2</i>	-5.1316	0.0016
Rv2936	<i>drrA</i>	-1.5669	0.0121
Rv3135	<i>ppe50</i>	-2.1230	0.0016
Rv3136	<i>ppe51</i>	-2.6363	0.0016
Rv3419c	<i>gcp</i>	-2.6857	0.0461
Rv3484	<i>cpsA</i>	-4.0845	0.0016
Rv3494c	<i>mce4F</i>	-1.2131	0.0461
Rv3560c	<i>fadE30</i>	-3.5686	0.0432
Rv3578	<i>arsB2</i>	-1.0654	0.0461
Rv3693		-2.5123	0.0121
Rv3822		-0.9614	0.0461
Rv3877	<i>eccD1</i>	-2.8876	0.0016

LFC = log₂ fold change. Q-value = significance adjusting for multiple tests. Red = LFC ≥ -1.5.

Table A2.2 | Significantly overrepresented genes post HRZE treatment compared to pretreatment

ID	gene	HRZE 1wk	
		LFC	Q-value
Rv0465c		1.1459	0.0121
Rv1538c	<i>ansA</i>	1.2808	0.0224
Rv2043c	<i>pncA</i>	2.4300	0.0016
Rv2476c	<i>gdh</i>	1.1678	0.0016
Rv2571c		1.4486	0.0461
Rv2931	<i>ppsA</i>	1.0627	0.0016
Rv2933	<i>ppsC</i>	0.8416	0.0121
Rv2940c	<i>mas</i>	0.8539	0.0121
Rv3696c	<i>glpK</i>	1.7453	0.0016

LFC = log₂ fold change. Q-value = significance adjusting for multiple tests. Green = LFC ≥ 1.5.

Table A2.3 | Significantly underrepresented genes 21 days post infection compared to pretreatment

ID	gene	21 dpi	
		LFC	Q-value
Rv0465c		-1.8249	0.0031
Rv0485		-1.6265	0.0031
Rv0806c	<i>cpsY</i>	-1.5816	0.0031
Rv1701		-3.2905	0.0031
Rv2115c	<i>mpa</i>	-1.0712	0.0031
Rv3193c		-2.1654	0.0031
Rv3849	<i>espR</i>	-3.2237	0.0031
Rv3855	<i>ethR</i>	-2.2626	0.0031

LFC = log₂ fold change. Q-value = significance adjusting for multiple tests. Red = LFC ≥ -1.5.

Table A2.4 | Significantly underrepresented genes post HRZE treatment using three-way analysis

ID	gene	HRZE 1wk	
		Δ LFC	Q-value
Rv0051		-2.0407	0.0000
Rv0086	<i>hycQ</i>	-2.6265	0.0111
Rv0111		-1.5684	0.0000
Rv0125	<i>pepA</i>	-1.9922	0.0111
Rv0158		-1.4512	0.0194
Rv0190		-4.9787	0.0329
Rv0205		-1.5591	0.0456
Rv0271c	<i>fadE6</i>	-0.9635	0.0465
Rv0399c	<i>lpqK</i>	-1.5470	0.0277
Rv0407	<i>fgd1</i>	-1.9285	0.0194
Rv0503c	<i>cmaA2</i>	-0.9200	0.0000
Rv0600c		-4.4031	0.0000
Rv0644c	<i>mmaA2</i>	-2.2617	0.0000
Rv0645c	<i>mmaA1</i>	-1.6194	0.0000
Rv0727c	<i>fucA</i>	-1.1885	0.0465
Rv0757	<i>phoP</i>	-2.8317	0.0000
Rv0758	<i>phoR</i>	-1.3104	0.0329
Rv0908	<i>ctpE</i>	-1.3085	0.0329
Rv0941c		-1.5596	0.0493
Rv0946Ac		-2.2355	0.0371
Rv0989c	<i>grcC2</i>	-5.0461	0.0000
Rv1006		-1.3664	0.0493
Rv1183	<i>mmpL10</i>	-1.1943	0.0194
Rv1212c	<i>glgA</i>	-2.7661	0.0000
Rv1213	<i>glgC</i>	-2.4998	0.0000
Rv1244	<i>lpqZ</i>	-2.7024	0.0111
Rv1336	<i>cysM</i>	-1.9840	0.0000
Rv1387	<i>ppe20</i>	-1.4186	0.0000
Rv1508c		-0.7442	0.0456
Rv1732c		-1.9263	0.0436
Rv1745c	<i>idi</i>	-3.2513	0.0371
Rv1747		-0.9466	0.0194
Rv1905c	<i>aao</i>	-0.9624	0.0493
Rv1924c		-1.9230	0.0456

Rv2565		-1.2265	0.0465
Rv2605c	<i>tesB2</i>	-5.2356	0.0111
Rv2721c		-1.3514	0.0000
Rv2745c	<i>clgR</i>	-2.2730	0.0465
Rv2938	<i>drrC</i>	-1.3242	0.0194
Rv2945c	<i>lppX</i>	-2.6995	0.0111
Rv2994		-1.3044	0.0000
Rv3047c		-2.5337	0.0111
Rv3135	<i>ppe50</i>	-2.8176	0.0000
Rv3136	<i>ppe51</i>	-2.7915	0.0000
Rv3217Ac		-4.7511	0.0371
Rv3223c	<i>sigH</i>	-1.7085	0.0456
Rv3241c		-1.6016	0.0111
Rv3339Ac		-3.2444	0.0329
Rv3419c	<i>gcp</i>	-3.8452	0.0371
Rv3492c		-2.8399	0.0111
Rv3495c	<i>lprN</i>	-1.5819	0.0493
Rv3509c	<i>ilvX</i>	-1.0097	0.0000
Rv3578	<i>arsB2</i>	-1.4009	0.0371
Rv3689		-1.4143	0.0111
Rv3692	<i>moxR2</i>	-2.8581	0.0465
Rv3693		-3.1830	0.0000
Rv3728		-0.9618	0.0000
Rv3821		-1.7274	0.0456
Rv3822		-1.2510	0.0000
Rv3823c	<i>mmpL8</i>	-1.9440	0.0465
Rv3877	<i>eccD1</i>	-3.6560	0.0000

Δ LFC = difference between log₂ fold change in HRZE treated and untreated animals compared to pretreatment. Q-value = significance adjusting for multiple tests. Red = LFC \geq -1.5.

Table A2.5 | Significantly overrepresented genes post HRZE treatment using three-way analysis

ID	gene	HRZE 1wk	
		Δ LFC	Q-value
Rv0465c		2.6766	0.0000
Rv0805		1.7278	0.0456
Rv2043c	<i>pncA</i>	2.1607	0.0000
Rv2476c	<i>gdh</i>	1.5181	0.0000
Rv2571c		1.6985	0.0111
Rv2931	<i>ppsA</i>	0.9703	0.0329
Rv2933	<i>ppsC</i>	0.7721	0.0277
Rv3696c	<i>glpK</i>	0.9551	0.0465

Δ LFC = difference between log₂ fold change in HRZE treated and untreated animals compared to pretreatment. Q-value = significance adjusting for multiple tests. Green = LFC \geq 1.5.

Table A2.6 | Phenotypic drug sensitivity of Korean *M. tuberculosis* isolates determined by LJ Agar Assay

Sample	Lineage	Drug Sensitivity by LJ Agar Assay														
		INH	RIF	EMB	PZA	SM	KAN	PTH	PAS	CS	OFX	MXF	CPM	LEV	RBU	AMK
KT0005	Beijing (others)	R	R	R	R	R	R	R	S	R	R	S	R	S	R	R
KT0022	Beijing (others)	R	R	R	R	S	S	R	R	R	R	R	S	R	S	S
KT0026	Beijing (K)	R	R	R	R	R	R	S	S	R	R	R	S	R	R	R
KT0122-1	Non-Beijing	S	S	S	S	S	S	R	S	S	S	S	S	S	S	S
KT0124	ND	S	S	S	S	S	S	S	S	S	S	S	S	S	S	S
KT0129	Beijing	S	S	S	S	S	S	R	S	R	S	S	S	S	S	S
KT0130	ND	R	R	R	R	R	S	R	R	R	R	R	R	R	R	S
KT0131	Beijing	R	R	S	S	S	S	S	S	S	S	S	S	S	R	S
KT0132	Beijing	S	S	S	S	S	S	R	S	S	S	S	S	S	S	S
KT0133	Beijing	S	S	S	S	S	S	S	S	S	S	S	S	S	S	S
KT0133	Beijing (K)	S	S	S	S	S	S	S	S	S	S	S	S	S	S	S
KT0134	Beijing	R	R	R	S	S	R	R	R	R	R	S	S	R	R	S
KT0135	Beijing	R	R	R	S	S	S	S	S	S	S	S	S	S	S	S
KT0136	ND	R	R	R	R	R	R	R	R	R	R	R	R	R	R	R
KT0137	Non-Beijing	R	R	R	S	S	S	R	S	R	S	S	S	S	R	S
KT0139-1	Beijing	R	R	S	R	R	S	S	S	S	S	S	S	S	R	S
KT0140	Beijing (M)	S	S	S	S	S	S	S	S	S	S	S	S	S	S	S
KT0144-1	ND	R	R	S	R	S	R	R	R	R	R	R	R	R	R	R
KT0149-1	Beijing	R	R	R	R	R	R	R	R	S	R	R	R	R	R	R
KT0155-1	Beijing	R	R	R	R	S	R	R	R	R	R	R	R	R	R	R
KT0157-1	Beijing	R	R	R	S	R	R	R	R	R	R	R	R	R	S	R
KT0158-1	Beijing	R	R	R	R	R	R	R	R	R	R	R	R	R	R	R
KT0159-1	Beijing	R	R	R	R	R	R	R	R	R	R	S	R	S	R	R
KT0160-1	Beijing	R	R	R	R	R	R	R	R	R	R	R	R	R	R	R
KT0161-1	Beijing	R	R	R	R	R	R	R	R	R	R	R	R	R	R	R
KT0181	Non-Beijing	S	S	S	S	S	S	R	S	S	S	S	S	S	S	S
KT0182	Beijing	R	R	R	R	R	S	S	R	S	S	S	S	S	R	S
KT0184	Beijing	S	S	S	S	S	S	S	S	S	S	S	S	S	S	S
KT0185	Beijing (others)	S	S	S	S	S	S	R	S	S	S	S	S	S	S	S
KT0186	Beijing (K)	S	S	S	S	S	S	R	S	S	S	S	S	S	S	S
KT0187	Beijing (others)	S	S	S	S	S	S	S	S	S	S	S	S	S	S	S
KT0188	Beijing (others)	S	S	S	S	S	S	S	S	S	S	S	S	S	S	S
KT0189	Beijing (M)	R	R	R	S	R	S	S	S	S	S	S	S	S	S	S
KT0190	Beijing (others)	S	S	S	S	S	S	S	S	S	S	S	S	S	S	S

KT0191	Beijing (others)	S	S	S	S	S	S	S	S	R	S	S	S	S	S	S
KT0192	Non-Beijing	R	R	R	R	R	S	R	R	R	R	S	S	R	R	S
KT0193	Beijing (others)	S	S	S	S	S	S	S	S	S	S	S	S	S	S	S
KT0194	Non-Beijing	R	S	S	S	S	S	R	S	S	S	S	S	S	S	S
KT0196	Beijing (K)	R	R	R	S	S	S	S	S	S	R	R	S	R	S	S
KT0197	Beijing (K)	S	S	S	S	S	S	S	S	S	S	S	S	S	S	S
KT0198	Beijing (K)	S	S	S	R	S	S	S	S	S	S	S	S	S	S	S
KT0199	Non-Beijing	R	R	R	R	R	S	R	S	R	R	S	S	R	R	S
KT0200	Beijing (K)	R	R	S	S	R	S	S	S	S	S	S	S	S	R	S
KT0201	Beijing (M)	S	S	S	S	S	S	S	R	S	S	S	S	S	S	S
KT0202	Beijing (M)	S	S	S	S	S	S	S	S	S	S	S	S	S	S	S
KT0203	Beijing (others)	R	R	R	R	R	R	R	R	R	R	S	S	R	R	S
KT1111	Beijing	R	R	R	R	R	R	R	R	R	R	ND	ND	ND	ND	ND
KTL008	ND	ND	ND	ND	ND	ND	ND	ND	ND	ND	ND	ND	ND	ND	ND	ND
KTL009	ND	R	R	R	R	S	S	R	S	R	R	R	S	R	R	S
KTL018	ND	R	R	R	S	R	S	R	S	R	R	R	S	R	R	S

“ND” = not determined. “R”, red filled = resistant. “S”, green filled = susceptible. INH, isoniazid; RIF, rifampin; EMB, ethambutol; PZA, pyrazinamide; SM, streptomycin; KAN, kanamycin; PTH, prothionamide; PAS, *para*-aminosalicylic acid; CS, cycloserine; OFX, ofloxacin; MFX, moxifloxacin; CPM, capreomycin; LEV, levofloxacin; RBU, rifabutin; AMK, amikacin.

Table A2.7 | Phenotypic drug sensitivity of Korean *M. tuberculosis* isolates determined by MGIT assay

Sample	Lineage	Drug Sensitivity by LJ Agar Assay								
		INH	RIF	EMB	PZA	SM	KAN	OFX	MXF	CPM
KT0005	Beijing (others)	R	R	S	R	S	R	R	S	R
KT0022	Beijing (others)	R	R	S	R	S	S	R	R	S
KT0026	Beijing (K)	R	R	R	S	R	R	R	R	R
KT0122-1	Non-Beijing	S	S	S	S	S	S	S	S	R
KT0124	ND	S	S	S	S	S	S	S	S	R
KT0129	Beijing	S	S	S	S	S	S	S	S	S
KT0130	ND	R	R	R	R	R	R	R	R	R
KT0131	Beijing	R	R	S	S	S	S	S	S	S
KT0132	Beijing	S	S	S	S	S	S	S	S	R
KT0133	Beijing	S	S	S	S	S	S	S	S	S
KT0133	Beijing (K)	S	S	S	S	S	S	S	S	S
KT0134	Beijing	R	R	S	S	S	R	R	R	S
KT0135	Beijing	R	R	S	S	S	S	S	S	S
KT0136	ND	R	R	S	R	R	R	R	R	R
KT0137	Non-Beijing	R	R	S	S	S	S	S	S	S
KT0139-1	Beijing	R	R	S	S	S	S	S	S	S
KT0140	Beijing (M)	S	S	S	S	S	S	S	S	S
KT0144-1	ND	R	R	S	ND	R	R	R	R	R
KT0149-1	Beijing	R	R	R	R	R	R	R	R	R
KT0155-1	Beijing	R	R	R	R	S	R	S	R	R
KT0157-1	Beijing	R	R	R	R	R	R	R	R	R
KT0158-1	Beijing	R	R	R	R	R	R	R	R	R
KT0159-1	Beijing	R	R	S	R	R	R	S	R	R
KT0160-1	Beijing	R	R	S	R	R	R	R	R	R
KT0161-1	Beijing	R	R	S	R	R	R	R	R	R
KT0181	Non-Beijing	S	S	S	S	S	S	S	S	R
KT0182	Beijing	R	R	S	R	R	S	S	S	S
KT0184	Beijing	S	S	S	S	S	S	S	S	S
KT0185	Beijing (others)	S	S	S	S	S	S	S	S	S
KT0186	Beijing (K)	S	S	S	S	S	S	S	S	R
KT0187	Beijing (others)	S	S	S	S	S	S	S	S	S
KT0188	Beijing (others)	S	S	S	S	S	S	S	S	S
KT0189	Beijing (M)	R	R	S	S	R	S	S	S	S
KT0190	Beijing (others)	S	S	S	S	S	S	S	S	R

KT0191	Beijing (others)	S	S	S	S	S	S	S	S	S
KT0192	Non-Beijing	R	R	R	R	R	S	R	R	S
KT0193	Beijing (others)	S	S	S	S	S	S	S	S	S
KT0194	Non-Beijing	R	S	S	S	S	S	S	S	S
KT0196	Beijing (K)	R	S	S	S	S	S	R	R	S
KT0197	Beijing (K)	S	S	S	S	S	S	S	S	S
KT0198	Beijing (K)	S	S	S	R	S	S	S	S	S
KT0199	Non-Beijing	R	R	S	R	R	S	R	R	S
KT0200	Beijing (K)	R	R	S	S	S	S	S	S	S
KT0201	Beijing (M)	S	S	S	S	S	S	S	S	S
KT0202	Beijing (M)	R	S	S	S	S	S	S	S	S
KT0203	Beijing (others)	R	R	R	R	R	R	R	R	S
KT1111	Beijing	ND	ND	ND	ND	ND	ND	ND	ND	ND
KTL008	ND	ND	ND	ND	ND	ND	ND	ND	ND	ND
KTL009	ND	ND	ND	ND	ND	ND	ND	ND	ND	ND
KTL018	ND	ND	ND	ND	ND	ND	ND	ND	ND	ND

“ND” = not determined. “R”, red filled = resistant. “S”, green filled = susceptible. INH, isoniazid; RIF, rifampin; EMB, ethambutol; PZA, pyrazinamide; SM, streptomycin; KAN, kanamycin; OFX, ofloxacin; MFX, moxifloxacin; CPM, capreomycin.

Table A2.8 | Growth on glycerol and *glpK* genotype of Korean *M. tuberculosis* isolates

Sample	Lineage	growth on glycerol	<i>glpK</i> genotype
KT0005	Beijing (others)	ND	WT
KT0022	Beijing (others)	ND	WT
KT0026	Beijing (K)	ND	WT
KT0122-1	Non-Beijing	ND	WT
KT0124	ND	ND	WT
KT0129	Beijing	ND	WT
KT0130	ND	ND	WT
KT0131	Beijing	ND	WT
KT0132	Beijing	ND	WT
KT0133	Beijing	ND	WT
KT0133	Beijing (K)	ND	WT
KT0134	Beijing	ND	WT
KT0135	Beijing	ND	WT
KT0136	ND	negative	frameshift
KT0137	Non-Beijing	ND	WT
KT0139-1	Beijing	ND	WT
KT0140	Beijing (M)	positive	WT
KT0144-1	ND	negative	frameshift
KT0149-1	Beijing	negative	frameshift
KT0155-1	Beijing	negative	frameshift
KT0157-1	Beijing	negative	WT
KT0158-1	Beijing	negative	frameshift
KT0159-1	Beijing	negative	frameshift
KT0160-1	Beijing	negative	frameshift
KT0161-1	Beijing	negative	frameshift
KT0181	Non-Beijing	ND	missense
KT0182	Beijing	ND	WT
KT0184	Beijing	positive	WT
KT0185	Beijing (others)	ND	WT
KT0186	Beijing (K)	ND	WT
KT0187	Beijing (others)	positive	WT
KT0188	Beijing (others)	ND	WT
KT0189	Beijing (M)	ND	frameshift
KT0190	Beijing (others)	ND	WT

KT0191	Beijing (others)	positive	WT
KT0192	Non-Beijing	ND	WT
KT0193	Beijing (others)	positive	WT
KT0194	Non-Beijing	ND	WT
KT0196	Beijing (K)	ND	WT
KT0197	Beijing (K)	positive	WT
KT0198	Beijing (K)	ND	WT
KT0199	Non-Beijing	ND	WT
KT0200	Beijing (K)	ND	WT
KT0201	Beijing (M)	positive	WT
KT0202	Beijing (M)	ND	WT
KT0203	Beijing (others)	negative	frameshift
KT1111	Beijing	negative	WT
KTL008	ND	ND	WT
KTL009	ND	ND	WT
KTL018	ND	ND	WT

“ND” = not determined. “positive” = growth on glycerol.
“negative” = no growth on glycerol. “WT” = wild-type *glpK* genotype. “frameshift” = +1bp indel in *glpK* homopolymer region. “missense” = missense mutation in *glpK* open reading frame.

Appendix A3: List of genes with altered susceptibility to antibiotic treatment *in vivo*

Table A3.1 | Genes required for optimal fitness *in vivo*

ID	gene	14 dpi		21 dpi		32 dpi		49 dpi	
		LFC	Q-value	LFC	Q-value	LFC	Q-value	LFC	Q-value
Rv0007		-0.0736	0.5005	-0.8733	0.3390	0.2311	0.4949	-2.3103	0.0094
Rv0012		-0.9110	0.0243	-1.0468	0.0185	-0.9631	0.0508	-1.0029	0.0839
Rv0013	<i>trpG</i>	-1.1802	0.4717	-3.2395	0.0241	-2.8004	0.0248	-2.5896	0.0001
Rv0018c	<i>pstP</i>	-0.7002	0.5005	-1.7374	0.0742	-1.6992	0.1065	-2.8692	0.0094
Rv0019c	<i>fhaB</i>	-0.7355	0.4997	-4.0004	0.0002	-0.4306	0.4949	-4.7337	0.0001
Rv0040c	<i>mtc28</i>	-1.2886	0.0033	-0.9499	0.1054	-0.9612	0.1595	-2.6279	0.0001
Rv0043c		-1.1238	0.0033	-1.4789	0.0002	-1.7750	0.0002	-0.0676	0.4931
Rv0047c		-0.7765	0.4760	-0.3889	0.4993	-0.8607	0.3634	-2.8475	0.0024
Rv0049		-0.0797	0.5005	-0.0497	0.5189	-0.4726	0.4907	-2.1385	0.0168
Rv0050	<i>ponA1</i>	-0.5317	0.2612	-0.9956	0.0317	-0.1378	0.4949	-1.4469	0.0001
Rv0056	<i>rplI</i>	-1.5100	0.0663	-1.9828	0.0040	-2.4378	0.0002	-2.4448	0.0001
Rv0069c	<i>sdaA</i>	0.1169	0.5005	-0.3226	0.4875	-0.3267	0.4907	-2.7088	0.0001
Rv0078		-0.2505	0.5005	-2.7601	0.0002	-2.2503	0.0002	-1.1039	0.0834
Rv0081		-0.1719	0.5005	0.5280	0.3818	-1.1528	0.0049	-0.6125	0.1416
Rv0083		-0.0949	0.5005	-0.2571	0.4709	-0.7781	0.0301	-0.7966	0.0448
Rv0086	<i>hycQ</i>	-0.5142	0.4498	-0.0880	0.4993	-0.0662	0.4949	-1.2465	0.0141
Rv0088		-0.5664	0.4725	-0.8086	0.3048	-0.7737	0.3123	-2.4082	0.0035
Rv0092	<i>ctpA</i>	-0.8076	0.0002	-0.8346	0.0002	-0.1686	0.4824	-0.4786	0.1313
Rv0096	<i>ppe1</i>	-1.6387	0.0002	-2.1597	0.0002	-3.1672	0.0002	-3.8170	0.0001
Rv0097		-1.8453	0.0002	-2.9783	0.0002	-2.8133	0.0002	-6.5418	0.0001
Rv0098	<i>fcoT</i>	-1.9332	0.0017	-1.8107	0.0040	-3.9879	0.0002	-6.3198	0.0001
Rv0099	<i>fadD10</i>	-1.8030	0.0002	-1.4446	0.0040	-3.6219	0.0002	-4.2028	0.0001
Rv0101	<i>nrp</i>	-1.4123	0.0002	-1.6367	0.0002	-2.5136	0.0002	-4.0199	0.0001
Rv0111		-0.4950	0.1047	-0.8049	0.0116	-1.3985	0.0002	-1.3072	0.0001
Rv0119	<i>fadD7</i>	-4.7277	0.0033	-4.8284	0.0002	-4.3985	0.0026	-2.6434	0.0899
Rv0126	<i>treS</i>	-1.8426	0.1579	-2.5049	0.0568	-3.2871	0.0026	-4.2863	0.0001
Rv0129c	<i>fbpC</i>	-0.1546	0.5005	-0.7896	0.0453	-0.2192	0.4907	-1.6284	0.0001
Rv0135c		-1.8422	0.0243	-2.2867	0.0116	-2.3565	0.0038	-0.8465	0.3903
Rv0147		0.4135	0.1609	0.2498	0.4185	0.7173	0.0182	0.3148	0.2952

Rv0154c	<i>fadE2</i>	-0.5898	0.3111	-0.5163	0.3346	-1.6059	0.0002	-1.6914	0.0001
Rv0155	<i>pntAa</i>	-1.0288	0.0825	-3.6244	0.0002	-1.5716	0.0417	-0.8017	0.3329
Rv0157	<i>pntB</i>	-1.5891	0.0002	-3.5245	0.0002	-2.7045	0.0002	-3.3195	0.0001
Rv0158		-0.7556	0.0033	0.1962	0.4928	-0.6826	0.0266	-0.9992	0.0035
Rv0161		-0.6008	0.3450	-0.3155	0.4736	-1.2208	0.0238	-2.0137	0.0001
Rv0168	<i>yrbE1B</i>	-1.0934	0.0002	-0.5484	0.0515	-1.0055	0.0014	-1.1822	0.0001
Rv0169	<i>mce1A</i>	-1.0300	0.0002	-0.8155	0.0002	-0.6417	0.0124	-0.9750	0.0001
Rv0170	<i>mce1B</i>	-1.8030	0.0002	-1.0735	0.0015	-0.4776	0.3402	-1.5752	0.0001
Rv0171	<i>mce1C</i>	-1.4157	0.0002	-1.1665	0.0015	-0.9394	0.0014	-1.9520	0.0001
Rv0172	<i>mce1D</i>	-1.1196	0.0002	-0.7589	0.0002	-0.9944	0.0002	-1.1064	0.0001
Rv0173	<i>lprK</i>	-1.7113	0.0002	-0.7826	0.1107	-1.3334	0.0002	-1.3912	0.0001
Rv0174	<i>mce1F</i>	-1.2829	0.0002	-1.0273	0.0002	-1.0352	0.0002	-1.1897	0.0001
Rv0175		-1.8104	0.0002	-2.3451	0.0002	-1.1083	0.0266	-1.5609	0.0012
Rv0176		-0.7049	0.0433	-0.6101	0.1305	-0.4647	0.3351	-0.8928	0.0510
Rv0177		-1.5123	0.0002	-2.0679	0.0002	-1.7321	0.0014	-2.1518	0.0001
Rv0178		-1.4193	0.0033	-1.6473	0.0028	-0.6535	0.3140	-1.0691	0.1329
Rv0179c	<i>lprO</i>	-0.1851	0.5005	-0.3477	0.3870	0.0078	0.5003	-0.8495	0.0094
Rv0180c		-1.9813	0.0155	-2.1673	0.0116	-1.4426	0.1219	-2.1288	0.0345
Rv0191		-0.4619	0.2074	-0.4856	0.1781	-0.8268	0.0172	-0.4253	0.3006
Rv0199		-2.2204	0.0002	-5.3603	0.0002	-3.7123	0.0002	-2.5105	0.0001
Rv0200		-1.6498	0.0538	-3.2438	0.0002	-3.0138	0.0002	-7.7617	0.0001
Rv0201c		-1.4510	0.0002	-1.1499	0.0249	0.0724	0.4949	-0.2405	0.4653
Rv0202c	<i>mmpL11</i>	-1.4734	0.0002	-1.5023	0.0002	-1.2760	0.0002	-2.5460	0.0001
Rv0204c		-2.3014	0.0002	-1.8011	0.0002	-2.5335	0.0002	-5.5986	0.0001
Rv0206c	<i>mmpL3</i>	-3.7015	0.0002	-0.7451	0.4952	-2.5821	0.0266	-1.3448	0.2745
Rv0211	<i>pckA</i>	-2.0515	0.1101	0.8378	0.4862	-2.2603	0.0495	-3.1188	0.0046
Rv0216		-0.6889	0.4146	-1.7643	0.0125	-2.2476	0.0014	-2.0911	0.0012
Rv0234c	<i>gabD1</i>	-0.4250	0.4340	-0.6830	0.0936	-0.2346	0.4907	-1.0684	0.0159
Rv0238		-0.6234	0.5005	-4.3769	0.0002	-4.4319	0.0380	-1.6790	0.2984
Rv0242c	<i>fabG4</i>	-1.4669	0.0033	-1.6821	0.0063	-1.1924	0.0874	-0.6272	0.3269
Rv0243	<i>fadA2</i>	-0.7754	0.0615	-1.1223	0.0074	-1.1823	0.0038	-0.8184	0.1013
Rv0244c	<i>fadE5</i>	-4.0744	0.0002	-4.0101	0.0002	-2.5009	0.0002	-3.9392	0.0001
Rv0247c		-3.2252	0.0002	-4.2422	0.0002	-5.1526	0.0002	-3.4015	0.0035
Rv0248c		-3.7168	0.0002	-4.9509	0.0002	-4.0333	0.0002	-3.7416	0.0001
Rv0249c		-4.0550	0.0002	-3.4412	0.0002	-4.8405	0.0002	-3.8440	0.0001
Rv0256c	<i>ppe2</i>	-0.6634	0.0102	-1.0733	0.0002	-1.1288	0.0002	-0.5425	0.1083
Rv0259c		-0.6939	0.4250	0.1102	0.4993	-1.3110	0.0457	-0.3278	0.4439
Rv0270	<i>fadD2</i>	-1.7117	0.0002	-1.4878	0.0002	-1.7482	0.0002	-0.9139	0.0001
Rv0296c		-0.4097	0.2424	-0.8786	0.0028	-0.7690	0.0124	-1.5452	0.0001

Rv0317c	<i>glpQ2</i>	0.0400	0.5005	-0.8607	0.0308	-0.0914	0.4949	-0.2479	0.4283
Rv0321	<i>dcd</i>	-0.0844	0.5005	-0.9813	0.1516	-1.6966	0.0026	-0.8357	0.2921
Rv0323c		-0.4612	0.4986	0.3194	0.4809	0.4215	0.4501	-1.2960	0.0235
Rv0348		-2.4752	0.0033	-0.5203	0.4952	-2.1998	0.0192	-1.0728	0.3862
Rv0353	<i>hspR</i>	-3.3678	0.0002	-3.8145	0.0002	-3.8608	0.0002	-7.1072	0.0001
Rv0361		-0.2670	0.5005	-1.3152	0.1516	-2.2727	0.0133	0.7068	0.4726
Rv0364		-1.4382	0.2628	-2.5360	0.0084	1.1020	0.4112	0.7844	0.4250
Rv0380c		-1.2282	0.2854	-1.3173	0.2893	-2.7131	0.0038	-3.4558	0.0035
Rv0381c		-0.8649	0.0017	-1.0813	0.0002	-1.6017	0.0002	-2.6891	0.0001
Rv0385		-0.1833	0.5005	-0.1020	0.4993	-0.2506	0.4907	-1.3164	0.0001
Rv0390		-1.4056	0.0074	-1.5706	0.0015	-1.9794	0.0014	-3.2481	0.0001
Rv0391	<i>metZ</i>	-2.1560	0.0002	-2.2789	0.0002	-2.9601	0.0002	-2.8661	0.0001
Rv0400c	<i>fadE7</i>	-1.0015	0.2631	-2.3040	0.0040	-1.1457	0.2424	-1.2127	0.1607
Rv0409	<i>ackA</i>	-0.8016	0.1047	-1.0259	0.0362	-0.5057	0.4112	-0.0018	0.5149
Rv0428c		-0.4260	0.4551	-0.0575	0.4993	-1.2051	0.0049	-0.7587	0.1934
Rv0437c	<i>psd</i>	-0.5941	0.5005	-2.4763	0.0395	-2.0388	0.1075	-2.3372	0.1138
Rv0438c	<i>moeA2</i>	-0.4382	0.3761	-0.8712	0.0423	-0.4179	0.3886	-0.3684	0.4052
Rv0449c		0.0148	0.5005	-0.1158	0.4911	-0.5963	0.0133	0.2396	0.3334
Rv0450c	<i>mmpL4</i>	-1.7418	0.0002	-2.0418	0.0002	-2.5859	0.0002	-1.8402	0.0001
Rv0451c	<i>mmpS4</i>	-1.6533	0.0047	-1.1921	0.0736	-2.5835	0.0002	-1.2555	0.0611
Rv0454Ac		-0.8053	0.0443	-0.5652	0.2977	-0.3593	0.4399	0.1978	0.4676
Rv0464c		-0.5841	0.1223	-0.8574	0.0256	-0.1294	0.4949	-0.3415	0.4001
Rv0465c		-2.7154	0.0002	-4.5124	0.0002	-3.6451	0.0002	-3.4956	0.0001
Rv0470c	<i>pcaA</i>	-2.2275	0.0002	-2.0277	0.0002	-2.8250	0.0002	-2.7303	0.0012
Rv0472c		-3.8007	0.0002	-4.4982	0.0002	-4.9549	0.0002	-5.3569	0.0001
Rv0476		-0.3094	0.3934	-0.1831	0.4795	-0.7533	0.0163	-0.0998	0.4725
Rv0485		-2.1144	0.0002	-3.7243	0.0002	-4.7219	0.0002	-5.7242	0.0001
Rv0487		-1.1078	0.0130	-0.9409	0.0469	-0.6357	0.2344	-0.9565	0.0896
Rv0490	<i>senX3</i>	-0.8693	0.0142	-1.3631	0.0002	-1.8172	0.0002	-2.1472	0.0001
Rv0491	<i>regX3</i>	-0.8534	0.0760	-1.5485	0.0002	-1.2761	0.0143	-2.4995	0.0001
Rv0497		-0.6616	0.4514	-3.9136	0.0002	-1.7419	0.0441	-1.6842	0.0863
Rv0503c	<i>cmaA2</i>	0.4162	0.1047	0.5814	0.0395	0.7585	0.0124	0.4449	0.1246
Rv0505c	<i>serB1</i>	1.4280	0.3249	0.1280	0.4993	-1.0522	0.4104	-3.0378	0.0235
Rv0508		-1.3914	0.0342	-0.4596	0.4758	-0.7326	0.3776	-1.3979	0.0873
Rv0513		-1.4371	0.0372	-1.7696	0.0125	-1.2991	0.1090	-2.1406	0.0132
Rv0544c		-1.1154	0.1376	-2.1009	0.0052	-0.8144	0.3724	-1.0617	0.1953
Rv0545c	<i>pitA</i>	-2.6036	0.0002	-3.7489	0.0002	-5.2221	0.0002	-3.1559	0.0001
Rv0546c		-0.5827	0.4997	-0.7725	0.3173	-0.8558	0.2813	-1.6434	0.0338
Rv0554	<i>bpoC</i>	-1.0957	0.0209	-0.7246	0.1753	-1.3907	0.0038	-0.8248	0.1302

Rv0561c		-1.4845	0.0002	-1.3721	0.0028	-0.3608	0.4291	0.4152	0.4052
Rv0588	<i>yrbE2B</i>	0.6227	0.3299	0.8609	0.4314	-0.2214	0.4941	1.1050	0.0461
Rv0590A		-0.1980	0.5005	-0.4374	0.4521	-0.5491	0.4236	-1.9469	0.0202
Rv0619	<i>galTb</i>	-0.4342	0.5005	-2.5255	0.0040	-0.2216	0.4949	-0.1524	0.4916
Rv0634A		-1.2557	0.0327	-0.2797	0.4952	-1.1304	0.1080	-0.4271	0.4268
Rv0642c	<i>mmaA4</i>	-3.9825	0.0002	-4.8938	0.0002	-1.6500	0.1341	-2.8390	0.0035
Rv0645c	<i>mmaA3</i>	0.1032	0.5005	0.6881	0.0166	0.5801	0.0853	-0.0980	0.4721
Rv0655	<i>mkl</i>	-2.3229	0.0002	-2.9360	0.0002	-2.2613	0.0002	-1.7829	0.0066
Rv0692		-0.5551	0.4717	-0.5122	0.4186	-1.8675	0.0002	-2.7774	0.0024
Rv0712		-0.5745	0.3386	-0.6192	0.3390	-1.3122	0.0274	-0.8848	0.1548
Rv0744c		-0.1713	0.5005	1.0152	0.4768	-0.0338	0.5097	-1.8333	0.0374
Rv0747		-0.2825	0.5005	0.4108	0.4149	-0.7615	0.0464	-0.3976	0.3067
Rv0750		-0.3144	0.4986	-1.2777	0.0002	-0.0092	0.5008	-0.5875	0.2986
Rv0757	<i>phoP</i>	-4.2528	0.0002	-4.3726	0.0002	-5.3214	0.0002	-4.2970	0.0001
Rv0758	<i>phoR</i>	-3.1384	0.0002	-3.1344	0.0002	-3.3451	0.0002	-2.4968	0.0001
Rv0761c	<i>adhB</i>	-0.4117	0.3872	-0.5378	0.2750	-0.8691	0.0528	-1.1598	0.0211
Rv0767c		-0.1823	0.5005	-0.8776	0.0499	-0.4304	0.4144	0.2052	0.4496
Rv0784		-1.8352	0.0342	0.9160	0.4993	0.2422	0.4949	-0.4001	0.4916
Rv0805		0.0998	0.5005	-1.1795	0.0175	-0.2546	0.4949	-0.1776	0.4635
Rv0806c	<i>cpsY</i>	-0.4315	0.1691	-1.9803	0.0002	-0.4310	0.2397	-1.0248	0.0001
Rv0808	<i>purF</i>	-4.1282	0.0002	-1.4605	0.4560	-0.6995	0.4907	0.4427	0.4694
Rv0813c		-0.6439	0.0514	-0.8023	0.0084	-0.2109	0.4907	-0.3063	0.4115
Rv0815c	<i>cysA2</i>	-0.7802	0.0002	-0.4696	0.1517	-0.6468	0.0301	-0.5716	0.0720
Rv0820	<i>phoT</i>	-0.2721	0.5005	0.2993	0.4993	-2.0120	0.2812	-4.3314	0.0001
Rv0827c	<i>kmtR</i>	-1.8120	0.0017	0.4435	0.4646	-0.1162	0.4949	0.5023	0.4266
Rv0847	<i>lpqS</i>	-0.0328	0.5005	0.8270	0.3245	0.1294	0.4949	-1.6056	0.0076
Rv0859	<i>fadA</i>	-1.4199	0.1274	-1.4119	0.1821	-1.4331	0.0835	-1.8575	0.0411
Rv0860	<i>fadB</i>	-0.9708	0.2616	-2.1523	0.0028	-1.3588	0.0865	-1.1045	0.2071
Rv0877		-1.6467	0.0002	-0.9004	0.1220	-1.5046	0.0002	-2.2455	0.0001
Rv0889c	<i>citA</i>	-0.4612	0.3971	-0.9268	0.0241	-0.4070	0.3953	0.0039	0.5003
Rv0910		-0.6091	0.4775	-0.9769	0.0790	-1.3551	0.0115	-0.6467	0.2363
Rv0924c	<i>mntH</i>	1.0450	0.0233	1.0457	0.0907	1.2391	0.0792	-0.7165	0.2320
Rv0928	<i>pstS3</i>	-0.9505	0.2420	1.2712	0.4803	-0.3009	0.4948	-3.2892	0.0001
Rv0929	<i>pstC2</i>	-1.6621	0.1157	1.0701	0.4952	-3.4995	0.0002	-2.9881	0.0001
Rv0930	<i>pstA1</i>	0.2449	0.5005	-2.4529	0.0063	-0.4126	0.4948	-5.8258	0.0001
Rv0954		-0.6048	0.3111	-0.7956	0.2129	-1.2247	0.0172	-1.0425	0.0504
Rv0981	<i>mprA</i>	-0.2452	0.5005	-0.8889	0.0146	-0.5913	0.1203	-0.0328	0.4940
Rv0983	<i>pepD</i>	-1.3342	0.0017	-2.2337	0.0002	-1.9674	0.0002	-0.0456	0.5449
Rv0987		0.1073	0.5005	0.1139	0.4993	-0.0184	0.4972	0.8641	0.0448

Rv0989c	<i>grcC2</i>	3.0675	0.0002	3.5393	0.0015	2.6511	0.0796	-0.3428	0.4987
Rv0994	<i>moeA1</i>	-3.1923	0.0002	-3.2959	0.0002	-3.4041	0.0002	-6.0973	0.0001
Rv0998		-3.0680	0.0002	-4.6591	0.0002	-2.7475	0.0061	-3.8274	0.0001
Rv0999		-1.0595	0.0002	-1.1973	0.0028	0.0540	0.4949	-0.9119	0.0667
Rv1003		-0.3442	0.5005	-1.6698	0.0028	-0.4196	0.4907	-3.4073	0.0001
Rv1008	<i>tatD</i>	-0.2021	0.5005	-1.1033	0.0028	-0.2573	0.4731	0.1507	0.4651
Rv1009	<i>rpfB</i>	0.6295	0.4986	0.9673	0.4409	0.7360	0.4648	-1.4358	0.0482
Rv1013	<i>pks16</i>	-0.3869	0.4997	-0.6149	0.3413	-2.1369	0.0002	-1.8732	0.0001
Rv1019		-0.6382	0.1888	-0.7036	0.1350	-1.3434	0.0002	-0.4241	0.3579
Rv1051c		-0.1340	0.5005	-2.3695	0.0232	0.7844	0.4907	0.2503	0.4772
Rv1065		-0.5783	0.1197	-0.4595	0.2588	-0.8724	0.0201	-0.8982	0.0202
Rv1069c		-0.4354	0.1095	-0.7877	0.0015	-0.6598	0.0133	-0.3675	0.2630
Rv1070c	<i>echA8</i>	-1.2398	0.0002	-1.0526	0.0263	-1.4381	0.0002	-1.1065	0.0228
Rv1071c	<i>echA9</i>	-0.4149	0.2936	-0.6284	0.0790	-1.3368	0.0002	-1.0363	0.0066
Rv1072		-2.7664	0.4623	-2.9777	0.3902	-2.4162	0.4542	-5.4004	0.0001
Rv1082	<i>mca</i>	-0.3418	0.4775	-0.9048	0.0232	-0.6485	0.1463	-0.5771	0.3728
Rv1085c		-0.4304	0.3914	-0.3460	0.4646	-0.7974	0.0702	-1.0885	0.0123
Rv1086		-2.8297	0.0047	-6.0054	0.0002	-6.0448	0.0002	-4.3832	0.0001
Rv1096		-2.0521	0.0002	-2.0560	0.0002	-1.7529	0.0002	-1.9198	0.0012
Rv1099c	<i>glpX</i>	-2.4151	0.0017	-5.8436	0.0002	-1.9419	0.0792	-5.6931	0.0001
Rv1100		-2.1938	0.0002	-2.0690	0.0002	-1.5281	0.0133	-1.0495	0.1626
Rv1111c		-0.5638	0.3110	-0.9418	0.0272	-1.0676	0.0038	-0.6211	0.2446
Rv1126c		-3.8591	0.0062	-0.0278	0.5260	0.5360	0.4953	-3.9322	0.0317
Rv1127c	<i>ppdK</i>	-1.3217	0.0164	-2.6382	0.0002	-0.9280	0.4529	-4.6803	0.0001
Rv1128c		0.1880	0.5005	-0.1449	0.4993	0.0933	0.4949	-2.6697	0.0001
Rv1130	<i>prpD</i>	-0.8155	0.0155	-0.5530	0.2355	-1.3119	0.0002	-0.3381	0.4016
Rv1131	<i>prpC</i>	-0.6396	0.5005	-2.8861	0.0002	-0.7555	0.4731	0.0466	0.4988
Rv1135A		-0.3403	0.5005	0.0262	0.4993	-1.2472	0.0094	0.1207	0.4805
Rv1151c		-0.5052	0.1740	-1.0126	0.0015	-0.8604	0.0143	-0.4226	0.2875
Rv1157c		-0.3412	0.5005	-3.0815	0.0084	-3.6962	0.0014	-2.3841	0.0749
Rv1161	<i>narG</i>	-0.1446	0.5005	-0.3172	0.1737	-0.5131	0.0084	-0.3130	0.1930
Rv1167c		-0.2430	0.5005	-1.9988	0.0040	-0.6243	0.4731	-0.3774	0.4439
Rv1174c		-0.2222	0.5005	-0.6714	0.1305	-0.9250	0.0230	-0.6067	0.2188
Rv1178		-1.4552	0.0002	-1.0464	0.0213	-2.5078	0.0002	-1.6736	0.0001
Rv1183	<i>mmpL10</i>	-0.2642	0.4340	-0.2110	0.4462	-0.7217	0.0094	-1.4700	0.0001
Rv1193	<i>fadD36</i>	-5.0810	0.0002	-6.4199	0.0002	-5.9588	0.0002	-6.3590	0.0001
Rv1194c		0.8474	0.0334	0.3227	0.4460	0.7060	0.1676	0.9905	0.1087
Rv1196	<i>ppe18</i>	0.8270	0.0185	0.5589	0.3318	0.4620	0.3308	0.5305	0.3243
Rv1205		-1.9818	0.0002	-0.9615	0.2983	-1.8831	0.0115	-2.9220	0.0001

Rv1206	<i>fadD6</i>	-1.6018	0.0002	-1.6631	0.0002	-1.5042	0.0002	-0.9362	0.0001
Rv1219c		-0.1138	0.5005	-1.1301	0.0837	-0.4565	0.4499	-2.5241	0.0001
Rv1220c		-0.4685	0.4986	-0.6522	0.2977	-1.3264	0.0115	-1.3315	0.0405
Rv1234		-0.6742	0.4601	-0.5462	0.4505	-0.9484	0.3223	-2.6089	0.0159
Rv1235	<i>lpqY</i>	-1.1869	0.0002	-2.2816	0.0002	-2.5994	0.0002	-2.7015	0.0001
Rv1236	<i>sugA</i>	-1.3505	0.0047	-2.4421	0.0002	-1.6417	0.0026	-3.5776	0.0001
Rv1237	<i>sugB</i>	-1.7169	0.0047	-5.1169	0.0002	-7.2495	0.0002	-1.1531	0.1162
Rv1238	<i>sugC</i>	-1.2542	0.0002	-1.4993	0.0002	-2.3173	0.0002	-2.9359	0.0001
Rv1244	<i>lpqZ</i>	-0.9246	0.1047	-0.5213	0.4114	-1.0115	0.1591	-1.8263	0.0086
Rv1272c		-1.6153	0.0002	-1.6974	0.0002	-2.7416	0.0002	-0.4829	0.4718
Rv1273c		-1.3745	0.0017	-1.8273	0.0002	-2.8706	0.0002	-2.2600	0.0001
Rv1277		-0.1798	0.5005	-0.2732	0.4617	-0.8654	0.0417	-0.2956	0.4328
Rv1280c	<i>oppA</i>	-0.5114	0.1166	-0.4413	0.3092	-0.6829	0.0404	-0.5155	0.1209
Rv1287		-1.8235	0.0002	-0.8510	0.1483	-0.8477	0.1850	-1.7169	0.0001
Rv1290A		0.0041	0.5008	-0.5336	0.4646	-1.3211	0.1455	-2.0256	0.0401
Rv1314c		-0.9099	0.0185	-1.4189	0.0015	-1.1449	0.0115	-0.9169	0.1098
Rv1323	<i>fadA4</i>	-0.5406	0.0453	-1.3166	0.0002	-0.7729	0.0115	-0.5126	0.1610
Rv1331		-0.2227	0.5005	-1.0415	0.0185	-0.4864	0.3993	-0.9523	0.0393
Rv1332		-0.4383	0.5005	-2.1758	0.0002	-0.7876	0.4158	-3.4950	0.0001
Rv1333		0.1211	0.5005	0.5860	0.3869	-0.3260	0.4907	-1.0848	0.0177
Rv1336	<i>cysM</i>	-0.7195	0.1095	-0.3609	0.4535	-0.5281	0.3206	-1.3541	0.0035
Rv1337		-0.7075	0.1012	-0.8522	0.2641	-1.5412	0.0002	-2.1683	0.0001
Rv1339		-4.4603	0.0002	-4.1147	0.0052	-2.0582	0.1214	-3.4687	0.0252
Rv1345	<i>mbtM</i>	-2.6609	0.0002	-2.9079	0.0002	-3.6583	0.0002	-2.4051	0.0001
Rv1347c	<i>mbtK</i>	-4.9791	0.0017	-5.0452	0.0028	-5.1065	0.0002	-4.4110	0.0001
Rv1348	<i>irtA</i>	-1.7241	0.0033	-3.6347	0.0002	-4.5783	0.0002	-5.1430	0.0001
Rv1349	<i>irtB</i>	-3.5275	0.0002	-4.5665	0.0002	-4.8295	0.0002	-5.0782	0.0001
Rv1364c		-0.2798	0.4997	-0.8829	0.0249	0.2530	0.4949	-0.4781	0.3862
Rv1388	<i>mihF</i>	-1.8056	0.1247	-4.2857	0.0040	-4.3189	0.0002	-0.7815	0.4283
Rv1401		0.6786	0.5005	0.9544	0.4993	-3.5235	0.0133	-1.5118	0.2306
Rv1404		0.3574	0.5032	-2.6024	0.0116	-3.2822	0.0002	-5.5823	0.0001
Rv1405c		-2.0594	0.0002	-2.0629	0.0002	-2.7816	0.0002	-3.4065	0.0001
Rv1411c	<i>lprG</i>	-4.9395	0.0002	-4.5809	0.0002	-4.6283	0.0002	-3.9316	0.0001
Rv1421		0.4939	0.5005	-1.5222	0.2806	-1.6199	0.1795	-3.7062	0.0001
Rv1422		-0.3872	0.5005	-1.4107	0.1552	-2.0524	0.0319	-4.7647	0.0001
Rv1432		-4.0208	0.0074	-3.7968	0.0040	-2.6972	0.0397	-2.2619	0.1138
Rv1433		0.0953	0.5005	-0.0581	0.4993	-0.1240	0.4949	-0.9840	0.0035
Rv1473		-0.5872	0.1579	-1.4569	0.0015	-1.7160	0.0002	-1.4757	0.0001
Rv1475c	<i>can</i>	-1.7991	0.3110	-2.7360	0.0521	-3.8725	0.0002	-3.1881	0.1289

Rv1493	<i>mutB</i>	-0.7266	0.0251	-0.5944	0.1989	-1.1171	0.0014	-0.9419	0.0168
Rv1513		0.3623	0.5005	-1.6694	0.0063	-0.3450	0.4907	-0.4940	0.4336
Rv1538c	<i>ansA</i>	-1.9600	0.0002	-2.2412	0.0002	-2.7089	0.0002	-1.9346	0.0001
Rv1565c		-2.4668	0.0033	-2.8108	0.0015	-3.4036	0.0002	-0.5299	0.4461
Rv1566c		-0.4613	0.5005	-0.6088	0.4280	-1.6194	0.0084	-0.4565	0.4336
Rv1568	<i>bioA</i>	-5.9978	0.0002	-6.3505	0.0002	-8.0330	0.0002	-9.5664	0.0001
Rv1569	<i>bioF1</i>	-5.3565	0.0002	-5.9184	0.0002	-7.7267	0.0002	-8.1090	0.0001
Rv1589	<i>bioB</i>	-6.6021	0.0002	-8.0065	0.0002	-8.7320	0.0002	-9.3914	0.0001
Rv1591		-0.0991	0.5005	-0.6771	0.0833	-0.5122	0.2721	-1.5161	0.0001
Rv1592c		-2.2688	0.0002	-2.7983	0.0002	-2.8665	0.0002	-1.8388	0.0001
Rv1598c		-0.2566	0.5005	-1.6662	0.0002	0.1058	0.4949	0.2644	0.4527
Rv1626		-2.9885	0.0002	-3.3412	0.0002	-4.3105	0.0002	-4.0000	0.0001
Rv1627c		-0.4578	0.4717	-0.4799	0.4149	-0.7230	0.3068	-1.3604	0.0482
Rv1633	<i>uvrB</i>	-0.5892	0.3795	-1.5284	0.0002	-1.3802	0.0038	-1.8125	0.0001
Rv1638	<i>uvrA</i>	-0.5005	0.4585	-1.2534	0.0015	-1.7732	0.0002	-2.1475	0.0001
Rv1640c	<i>lysX</i>	-1.3278	0.0017	-1.0570	0.0205	-1.1123	0.0094	-2.1173	0.0001
Rv1679	<i>fadE16</i>	-1.2336	0.2999	-0.0861	0.4993	-4.9007	0.0002	-0.2996	0.4765
Rv1683		-0.0543	0.5005	0.4413	0.4837	0.4932	0.4670	-1.5305	0.0300
Rv1692		-0.0180	0.5005	-1.4037	0.0040	-1.5562	0.0038	0.2714	0.4428
Rv1698	<i>mctB</i>	-1.2093	0.1166	-2.3811	0.0002	-0.7850	0.3068	1.9804	0.4709
Rv1700		0.8988	0.5032	0.3842	0.4993	-1.1493	0.3644	-4.4684	0.0012
Rv1701		-1.8649	0.1223	-4.7386	0.0002	-3.7203	0.0014	-4.0898	0.0001
Rv1740	<i>vapB34</i>	0.3454	0.5005	-1.9117	0.0256	0.6941	0.4858	-0.2798	0.4698
Rv1747		-0.1214	0.5005	-0.1465	0.4928	-0.3337	0.3724	-0.8929	0.0094
Rv1759c	<i>wag22</i>	-0.9080	0.0273	-0.3862	0.4342	-0.4077	0.4158	0.1014	0.4772
Rv1769		-0.7891	0.0262	-0.7459	0.0499	-0.0870	0.4949	-0.4622	0.3097
Rv1771		-0.2453	0.4717	-0.5895	0.0389	0.2411	0.4650	-0.0946	0.4699
Rv1780		-0.5075	0.1557	-1.2518	0.0002	-0.4645	0.2897	-0.1215	0.4784
Rv1785c	<i>cyp143</i>	-0.2140	0.5005	-0.9520	0.0538	-0.2871	0.4907	-2.8602	0.0001
Rv1790	<i>ppe27</i>	-0.8564	0.0283	-1.0821	0.0074	-0.9470	0.0154	-1.0583	0.0352
Rv1791	<i>pe19</i>	-6.1418	0.0002	-6.9401	0.0002	-5.9168	0.0002	-6.2831	0.0001
Rv1793	<i>esxN</i>	-2.4577	0.0002	-3.1710	0.0002	-6.5435	0.0002	-5.0796	0.0001
Rv1798	<i>eccA5</i>	-5.4898	0.0002	-5.4462	0.0002	-6.1998	0.0002	-7.0075	0.0001
Rv1805c		-0.8684	0.4601	-2.8996	0.0002	0.1484	0.4949	3.6503	0.4255
Rv1810		-0.1640	0.5005	-0.8009	0.0445	-1.1392	0.0061	-0.5730	0.2799
Rv1819c	<i>bacA</i>	-0.3191	0.2418	-0.4964	0.0263	-0.7210	0.0014	-0.3692	0.2022
Rv1820	<i>ilvG</i>	-0.8527	0.0062	-0.5724	0.0947	-0.9062	0.0061	-1.1244	0.0001
Rv1821	<i>secA2</i>	-0.4400	0.5005	-1.4174	0.0175	-0.3729	0.4907	-1.5055	0.0324
Rv1823		-0.6323	0.2713	-0.7779	0.1818	-1.0536	0.0433	-1.3087	0.0202

Rv1825		-0.4521	0.4304	-0.9147	0.0729	-1.3793	0.0026	-0.6887	0.2134
Rv1829		-1.6691	0.0062	-2.5701	0.0002	-3.3129	0.0002	-7.0382	0.0001
Rv1831		-0.2324	0.5005	0.1386	0.4993	-0.0440	0.5003	-2.1965	0.0276
Rv1836c		-1.0682	0.5005	-1.0208	0.4162	-1.6825	0.1455	-4.4000	0.0001
Rv1853	<i>ureD</i>	-0.4057	0.5005	-0.6867	0.3902	-1.6975	0.0201	-1.8939	0.0123
Rv1860	<i>apa</i>	0.1275	0.5005	-1.3046	0.0074	-0.7730	0.0671	-1.5924	0.0001
Rv1906c		-0.7430	0.2355	-1.5282	0.0084	-1.0922	0.0523	-1.1874	0.0899
Rv1925	<i>fadD31</i>	-0.4796	0.3914	-0.4537	0.3870	-1.0150	0.0274	-0.7288	0.2236
Rv1932	<i>tpx</i>	-1.6554	0.0047	-0.8808	0.2082	-2.0578	0.0014	-1.1605	0.1840
Rv1957		-1.7927	0.0471	-1.5471	0.1137	-1.8208	0.0449	-1.5659	0.1442
Rv1963c	<i>mce3R</i>	-1.6612	0.0002	-1.1686	0.0249	-1.9745	0.0002	-0.8604	0.2380
Rv1964	<i>yrbE3A</i>	-0.4328	0.3049	-0.8072	0.0125	-0.6489	0.1508	0.0541	0.4825
Rv1965	<i>yrbE3B</i>	-0.1896	0.5005	-0.0373	0.4993	-1.0480	0.0002	-0.0029	0.5071
Rv1968	<i>mce3C</i>	0.0641	0.5005	0.1809	0.4993	0.1784	0.4949	-1.7465	0.0024
Rv1970	<i>lprM</i>	-0.9878	0.2028	-1.4871	0.0290	-0.8309	0.3359	0.2652	0.4663
Rv1975		0.0986	0.5005	-0.1783	0.4914	-0.0368	0.4949	0.7840	0.0405
Rv1984c	<i>cfp21</i>	-0.0238	0.5005	-0.4820	0.1800	-0.0880	0.4949	0.7862	0.0368
Rv2014		-1.0916	0.0002	-0.0722	0.4993	-0.2145	0.4949	-0.2695	0.4662
Rv2018		-0.0932	0.5005	-0.3704	0.4993	-0.9508	0.4140	-2.6583	0.0066
Rv2030c		-0.5432	0.0334	-0.3054	0.3640	-0.0594	0.4949	0.2455	0.4124
Rv2039c		-0.0986	0.5005	-0.0778	0.4993	-0.7358	0.2602	-1.3898	0.0228
Rv2043c	<i>pncA</i>	2.5078	0.0002	2.5088	0.0002	2.3324	0.0002	5.1232	0.0001
Rv2044c		-0.0133	0.5005	0.3179	0.4879	0.0544	0.4949	1.5943	0.0228
Rv2047c		-1.5905	0.0002	-1.5454	0.0002	-1.7637	0.0002	-2.4084	0.0001
Rv2048c	<i>pks12</i>	-1.1017	0.0002	-1.8614	0.0002	-1.7407	0.0002	-1.9336	0.0001
Rv2051c	<i>ppm1</i>	-0.8315	0.0731	-0.1337	0.4993	-1.8179	0.0002	0.4356	0.4541
Rv2052c		-0.7059	0.0017	-0.5646	0.0232	-0.2494	0.4512	-0.1130	0.4613
Rv2069	<i>sigC</i>	-1.4401	0.0185	-2.9547	0.0002	-3.0863	0.0002	-5.8746	0.0001
Rv2091c		-3.0597	0.0002	-4.2093	0.0002	-2.9999	0.0002	-3.2115	0.0001
Rv2097c	<i>paFA</i>	-3.3495	0.0002	-3.8744	0.0002	-3.9166	0.0002	-2.5265	0.0292
Rv2098c		-1.3813	0.0185	-0.7495	0.2874	-1.1303	0.0888	0.6908	0.3067
Rv2106		0.3516	0.1885	0.4729	0.0723	0.4647	0.0639	0.5312	0.0374
Rv2115c	<i>mpa</i>	-2.5436	0.0283	-3.3039	0.0002	-2.8731	0.0094	-1.2562	0.2305
Rv2124c	<i>methH</i>	-0.1181	0.5005	-0.2874	0.3902	-0.3471	0.2957	-0.9115	0.0046
Rv2127	<i>ansP1</i>	-0.8958	0.0002	-0.7031	0.0290	-0.7309	0.0230	-0.8680	0.0086
Rv2140c		-3.6968	0.0002	-5.7156	0.0002	-4.4221	0.0002	-7.6009	0.0001
Rv2160A		0.2141	0.5005	0.3236	0.4952	0.6625	0.4824	-2.6829	0.0076
Rv2170		-0.5364	0.3707	-0.2164	0.4993	-0.7111	0.2687	-1.2285	0.0393
Rv2184c		0.0042	0.5005	-0.2406	0.4696	0.2730	0.4650	1.1339	0.0177

Rv2206		-0.9579	0.4601	-0.2924	0.4993	-2.2203	0.0345	-2.1854	0.0872
Rv2214c	<i>ephD</i>	-0.2371	0.4725	-0.6200	0.0371	-0.2902	0.3886	0.5498	0.1146
Rv2221c	<i>glnE</i>	-3.9545	0.0316	-2.2701	0.1681	-4.0668	0.0410	-3.3851	0.0001
Rv2222c	<i>glnA2</i>	-2.2724	0.0002	-1.6994	0.0002	-2.4081	0.0002	-3.1445	0.0001
Rv2224c	<i>caeA</i>	-1.4818	0.0002	-1.4234	0.0015	-2.7183	0.0002	-3.2993	0.0001
Rv2230c		-0.6245	0.5005	-1.9739	0.0074	-3.7613	0.0002	0.2525	0.4801
Rv2239c		-2.1958	0.0047	-2.6590	0.0015	-3.3379	0.0014	-4.2274	0.0001
Rv2241	<i>aceE</i>	-2.5235	0.0002	-2.1964	0.0002	-4.1822	0.0002	-4.1288	0.0001
Rv2249c	<i>glpD1</i>	-1.7600	0.0002	-2.2122	0.0002	-2.0672	0.0002	-1.8022	0.0001
Rv2253		-0.0997	0.5005	-0.2883	0.4993	-1.6186	0.0238	-0.1022	0.4846
Rv2258c		-0.2977	0.4725	-0.4506	0.3542	-0.1931	0.4907	-0.9981	0.0345
Rv2272		-1.2928	0.1579	-0.4950	0.4952	-2.9723	0.0002	-4.9530	0.0001
Rv2289	<i>cdh</i>	-0.0174	0.5005	0.2570	0.4185	1.0952	0.0328	0.2093	0.4283
Rv2344c	<i>dgt</i>	-0.6606	0.0233	-1.3957	0.0002	-1.9149	0.0002	-0.3517	0.4772
Rv2345		-0.0210	0.5005	-0.2707	0.3077	-0.1720	0.4629	-0.4961	0.0389
Rv2358	<i>smtB</i>	-1.2393	0.3562	-1.9747	0.1354	-3.0983	0.0410	-2.4995	0.1103
Rv2374c	<i>hrcA</i>	-3.3674	0.0002	-2.8593	0.0063	-2.3523	0.1288	-5.0488	0.0001
Rv2378c	<i>mbtG</i>	-4.1813	0.0002	-4.4552	0.0002	-5.5566	0.0002	-5.5278	0.0001
Rv2379c	<i>mbtF</i>	-4.2011	0.0002	-5.1290	0.0002	-4.8274	0.0002	-6.1962	0.0001
Rv2380c	<i>mbtE</i>	-6.4114	0.0002	-6.3445	0.0002	-6.8061	0.0002	-7.8800	0.0001
Rv2381c	<i>mbtD</i>	-4.7324	0.0002	-4.9188	0.0002	-3.7941	0.0002	-4.8801	0.0001
Rv2382c	<i>mbtC</i>	-4.9356	0.0002	-5.4328	0.0002	-4.5045	0.0014	-4.7969	0.0001
Rv2383c	<i>mbtB</i>	-5.1678	0.0002	-5.5583	0.0002	-6.4761	0.0002	-5.9313	0.0001
Rv2384	<i>mbtA</i>	-3.7888	0.0002	-5.1644	0.0002	-4.3154	0.0002	-5.7823	0.0001
Rv2386c	<i>mbtI</i>	-4.3602	0.0002	-5.8438	0.0002	-4.7597	0.0002	-4.1321	0.0001
Rv2387		-0.4085	0.1047	-0.7462	0.0015	-0.3363	0.3679	-1.2261	0.0001
Rv2404c	<i>lepA</i>	-0.8862	0.0089	-0.9363	0.0095	-1.3114	0.0002	-0.2387	0.4439
Rv2427c	<i>proA</i>	-1.3652	0.0185	-1.6040	0.0040	-1.0019	0.2496	-2.3308	0.0001
Rv2428	<i>ahpC</i>	0.3116	0.5005	0.7889	0.4803	-1.8074	0.0293	-0.3684	0.4669
Rv2437		-1.3442	0.0351	-0.3439	0.4940	-0.7391	0.3308	-1.7712	0.0159
Rv2451		-1.9585	0.0164	-2.2010	0.0445	-0.2305	0.4949	-1.2088	0.3551
Rv2462c	<i>tig</i>	-0.3445	0.4997	-0.2149	0.4993	-0.2042	0.4949	-1.8537	0.0001
Rv2467	<i>pepN</i>	-0.6282	0.0565	-1.1517	0.0002	-0.5202	0.1565	-0.3777	0.3190
Rv2474c		-1.8784	0.0164	-2.0530	0.0063	-2.5070	0.0002	-1.6017	0.0504
Rv2475c		-1.5857	0.0142	-2.2953	0.0002	-1.9505	0.0014	-1.1701	0.1214
Rv2476c	<i>gdh</i>	-0.5436	0.0402	-1.1509	0.0002	-1.3255	0.0002	-1.0761	0.0001
Rv2481c		0.1363	0.5005	-0.0447	0.4993	-1.4642	0.0049	-0.3755	0.4433
Rv2498c	<i>citE</i>	-2.6051	0.0002	-2.1374	0.0166	-3.5149	0.0002	-3.3569	0.0001
Rv2506		-2.3496	0.0002	-2.8141	0.0002	-3.2859	0.0002	-2.0806	0.0001

Rv2525c		-0.3323	0.3678	-0.5816	0.1237	-0.9436	0.0038	-0.5155	0.1588
Rv2535c	<i>pepQ</i>	-3.3605	0.0351	-1.2575	0.3902	0.1706	0.4949	-2.8090	0.1228
Rv2549c	<i>vapC20</i>	-0.3616	0.4320	-0.5566	0.2983	-0.1523	0.4939	-0.7024	0.0381
Rv2563		-1.0743	0.1104	-1.8205	0.0095	-1.6739	0.0221	-0.5595	0.3862
Rv2564	<i>glnQ</i>	-1.6602	0.0002	-1.2228	0.0074	-1.2882	0.0014	-1.0038	0.0405
Rv2566		-0.0276	0.5005	-0.5421	0.0439	-0.2751	0.3534	0.3464	0.2660
Rv2567		-0.9809	0.0461	-0.6854	0.2038	-1.2622	0.0143	-2.0588	0.0001
Rv2569c		-0.8627	0.2108	-2.7267	0.0002	-1.4189	0.0038	-2.7118	0.0001
Rv2583c	<i>relA</i>	-2.3969	0.0002	-3.3728	0.0002	-3.4822	0.0002	-3.1439	0.0001
Rv2584c	<i>apt</i>	0.2479	0.5005	0.6563	0.2377	-0.1603	0.4907	-0.8348	0.0442
Rv2589	<i>gabT</i>	-0.3505	0.3594	-0.4975	0.1717	-0.5573	0.0809	-0.9290	0.0012
Rv2604c	<i>snoP</i>	-2.6342	0.0074	-6.3528	0.0002	-7.3879	0.0002	-6.6923	0.0001
Rv2605c	<i>tesB2</i>	-1.7948	0.0074	-1.9553	0.0040	-2.4865	0.0014	-2.2041	0.0123
Rv2606c	<i>snzP</i>	-6.6609	0.0002	-7.7229	0.0002	-7.5974	0.0002	-8.1542	0.0001
Rv2609c		-1.2302	0.0142	-1.2379	0.0116	-1.5104	0.0002	-3.2920	0.0001
Rv2633c		-0.8116	0.0412	-0.5524	0.2408	-0.8170	0.0625	-0.4037	0.3715
Rv2635		-0.3067	0.5005	0.1287	0.4993	-1.7020	0.0172	-2.1537	0.0001
Rv2640c		-3.2954	0.0002	-0.9460	0.2641	-3.3312	0.0002	-4.2575	0.0001
Rv2642		-0.0896	0.5005	-1.0661	0.0263	-0.7851	0.2084	0.1257	0.4743
Rv2657c		0.2994	0.5005	0.5604	0.4326	0.2177	0.4949	-1.3967	0.0202
Rv2672		-0.4688	0.2728	-0.7090	0.1107	-0.5151	0.2606	-1.2450	0.0094
Rv2680		-2.4419	0.0002	-0.7338	0.3902	-0.5670	0.4907	-0.9514	0.2189
Rv2681		-0.8187	0.0185	-1.0675	0.0028	-0.9364	0.0026	0.4077	0.2822
Rv2683		-1.3413	0.0017	-2.5066	0.0002	-1.1819	0.0528	-1.4292	0.0103
Rv2684	<i>arsA</i>	-2.1937	0.0002	-1.8258	0.0002	-2.2065	0.0002	-2.3585	0.0001
Rv2685	<i>arsB1</i>	-0.4488	0.4986	-1.4698	0.0028	-0.9212	0.1423	-1.2233	0.0569
Rv2689c		-0.8247	0.0074	0.2178	0.4916	-0.3126	0.3930	-0.1127	0.4698
Rv2700		-1.5770	0.2328	-3.1901	0.0136	-4.3041	0.0002	-4.2187	0.0001
Rv2702	<i>ppgK</i>	-0.3214	0.5005	0.5532	0.4505	-0.6604	0.4212	-1.4846	0.0360
Rv2707		-1.7442	0.0002	-1.5500	0.0002	-1.8598	0.0002	-1.9711	0.0001
Rv2714		-1.0628	0.0017	-1.2195	0.0028	-0.3496	0.4609	-1.5993	0.0001
Rv2716		-0.5274	0.4320	-0.7720	0.1950	-1.4298	0.0073	0.3350	0.4699
Rv2733c		-1.3610	0.0002	-1.3606	0.0002	-0.1984	0.4939	-1.4442	0.0001
Rv2736c	<i>recX</i>	0.6071	0.5005	1.5914	0.4185	-2.9943	0.0002	1.9529	0.3745
Rv2772c		-1.2197	0.0334	-0.8763	0.1800	-1.8002	0.0014	-1.4172	0.0338
Rv2778c		-0.3004	0.5005	0.6698	0.3926	0.2532	0.4949	-1.9377	0.0276
Rv2788	<i>sirR</i>	-1.0232	0.0696	-1.8448	0.0002	-1.4072	0.0115	-0.9996	0.1416
Rv2793c	<i>truB</i>	-1.5344	0.3249	-4.2019	0.0015	-1.0705	0.4664	-3.1829	0.0159
Rv2799		-0.6399	0.0155	-0.4424	0.4326	-1.0853	0.0002	-1.2584	0.0001

Rv2826c		0.3922	0.4601	-0.0697	0.5014	0.5433	0.3724	1.2457	0.0427
Rv2829c	<i>vapC22</i>	-0.3249	0.5005	-0.6033	0.4085	0.2442	0.4907	-2.4670	0.0001
Rv2861c	<i>mapB</i>	-2.1400	0.3756	-2.8632	0.0002	-1.9227	0.3499	-2.2243	0.3083
Rv2864c		-0.1587	0.5005	-1.0249	0.0175	-1.0885	0.0094	-1.1890	0.0103
Rv2869c	<i>rip</i>	-2.2093	0.2206	-3.5198	0.0002	-3.5710	0.0002	-2.8839	0.2436
Rv2887		-1.0007	0.3579	-3.8151	0.0002	-0.7289	0.4907	-2.3255	0.0202
Rv2896c		-0.0608	0.5005	-0.9457	0.0195	0.0594	0.4949	0.2797	0.4188
Rv2901c		-0.7111	0.1104	-0.5561	0.3125	-1.4973	0.0014	-1.3355	0.0046
Rv2912c		-0.7049	0.4130	-1.0765	0.0195	-0.2659	0.4949	-2.1282	0.0001
Rv2914c	<i>pknI</i>	0.2152	0.4978	0.1178	0.4952	0.3354	0.3953	0.6161	0.0332
Rv2923c		-0.3229	0.5005	-0.9100	0.2887	-0.6023	0.4542	-1.8807	0.0252
Rv2933	<i>ppsC</i>	0.1550	0.5005	-0.0266	0.4993	-0.1885	0.4629	0.6571	0.0024
Rv2936	<i>drrA</i>	-0.6553	0.1274	-1.2734	0.0002	-1.2011	0.0014	-1.1105	0.0103
Rv2937	<i>drrB</i>	-0.7754	0.0704	-0.8947	0.0326	-0.7611	0.1522	-1.6545	0.0001
Rv2938	<i>drrC</i>	-1.0227	0.0002	-0.5008	0.2078	-1.3520	0.0002	-1.3238	0.0001
Rv2940c	<i>mas</i>	0.1600	0.5005	0.1041	0.4968	-0.0801	0.4949	0.6069	0.0066
Rv2942	<i>mmpL7</i>	-0.7150	0.0017	-0.6819	0.0166	-1.5984	0.0002	-1.2363	0.0001
Rv2945c	<i>lppX</i>	-1.2565	0.0033	-0.2470	0.4993	-1.2952	0.0124	-1.2965	0.0066
Rv2950c	<i>fadD29</i>	-0.5107	0.0342	-0.5531	0.0249	-0.5244	0.0572	-0.1202	0.4612
Rv2966c		-0.7322	0.4764	-1.6591	0.0760	-1.1488	0.3061	-3.1409	0.0046
Rv2967c	<i>pca</i>	-4.1993	0.0002	-4.5153	0.0002	-4.4449	0.0002	-2.2048	0.0001
Rv2985	<i>mutT1</i>	0.1186	0.5005	-1.6208	0.0052	-0.5827	0.3351	-2.9503	0.0001
Rv2989		-2.8539	0.0002	-3.4568	0.0002	-3.9179	0.0002	-2.7412	0.0001
Rv2997		0.1016	0.5005	-0.0479	0.4993	-0.8228	0.0336	-0.3617	0.3540
Rv3005c		-1.5994	0.0002	-1.9212	0.0002	-2.0395	0.0002	-0.8704	0.0300
Rv3010c	<i>pfkA</i>	-1.2631	0.0062	-0.4941	0.4272	-1.4617	0.0014	-0.4020	0.4237
Rv3016	<i>lpqA</i>	0.1701	0.5005	0.3000	0.4728	-1.0009	0.0026	0.0820	0.4794
Rv3036c		-0.1670	0.5005	-0.2831	0.4875	0.1138	0.4949	-1.8300	0.0001
Rv3041c		0.1733	0.5005	-0.3832	0.4755	-0.7212	0.2084	-1.1112	0.0482
Rv3050c		-0.3020	0.5005	-3.4190	0.0002	-0.8129	0.4549	0.9134	0.4552
Rv3057c		-1.3053	0.0002	-1.3973	0.0002	-1.2240	0.0002	-1.3634	0.0001
Rv3058c		-0.9069	0.0185	-1.9430	0.0002	-1.8481	0.0002	-1.8391	0.0001
Rv3077		-0.2830	0.3403	-0.6148	0.0157	-0.2807	0.3688	-0.5133	0.0814
Rv3106	<i>fprA</i>	-0.2059	0.5005	-0.2696	0.4621	-0.1115	0.4949	-1.1088	0.0086
Rv3117	<i>cysA3</i>	-0.7535	0.0002	-0.4809	0.1107	-0.5415	0.0829	-0.4485	0.1568
Rv3120		-0.2890	0.4986	-0.4634	0.3765	-0.3686	0.4212	-0.8789	0.0285
Rv3131		-0.5631	0.3006	-1.6888	0.0002	-0.9074	0.0859	-1.0175	0.0252
Rv3132c	<i>devS</i>	-1.2175	0.0002	-1.3782	0.0002	-0.4580	0.4209	-0.5743	0.3083
Rv3135	<i>ppe50</i>	-1.1921	0.0002	-0.7732	0.0116	-0.6647	0.0397	-0.9227	0.0057

Rv3136	<i>ppe51</i>	-0.9306	0.0002	-1.0512	0.0002	-1.7017	0.0002	-1.8782	0.0001
Rv3136Ac		-1.0155	0.0047	-0.9865	0.0040	-0.7827	0.0371	-0.2014	0.4461
Rv3139	<i>fadE24</i>	-0.7348	0.0893	-1.0480	0.0074	-1.7019	0.0002	0.3578	0.4115
Rv3140	<i>fadE23</i>	-0.8647	0.0461	-1.1633	0.0063	-1.5248	0.0014	-0.0731	0.4951
Rv3147	<i>nuoC</i>	-0.5837	0.3779	-0.3611	0.4862	-0.6805	0.3517	-1.3815	0.0235
Rv3149	<i>nuoE</i>	-1.2559	0.0164	-0.0638	0.4993	-0.8817	0.3060	-0.6186	0.3596
Rv3155	<i>nuoK</i>	0.4925	0.5005	-1.3306	0.1787	0.7707	0.4748	-3.2183	0.0001
Rv3160c		-5.1069	0.0002	-5.6280	0.0002	-5.8176	0.0002	-5.9697	0.0001
Rv3178A		0.0601	0.5005	0.4148	0.4774	-1.5172	0.0014	-0.5866	0.3272
Rv3193c		-3.0544	0.0002	-4.8477	0.0002	-4.8918	0.0002	-2.9883	0.0001
Rv3194c		-0.3057	0.4994	-0.2390	0.4952	-1.6649	0.0002	-1.4455	0.0001
Rv3195		-0.1717	0.5005	-0.7682	0.0272	-0.4501	0.2602	-0.4965	0.2240
Rv3197		-0.9908	0.0033	-1.6737	0.0002	-1.1572	0.0014	-0.9595	0.0338
Rv3199c	<i>nudC</i>	0.0953	0.5005	-1.1566	0.0256	-0.0492	0.4949	-0.5580	0.3529
Rv3207c		0.2366	0.5005	-0.5667	0.3774	-0.5224	0.4864	-1.5532	0.0094
Rv3208A		-0.3020	0.5005	-1.3316	0.0136	-1.7654	0.0002	-2.4655	0.0001
Rv3210c		-5.1573	0.0002	-3.4386	0.0002	0.8382	0.4824	-4.1441	0.0012
Rv3220c		-3.4496	0.0002	-3.7027	0.0002	-4.2283	0.0002	-4.2332	0.0001
Rv3226c		-0.0278	0.5005	-0.9705	0.0084	-0.0840	0.4949	-0.2255	0.4435
Rv3228		-1.3594	0.3796	-0.3187	0.4993	-2.3451	0.0002	-1.6586	0.0001
Rv3229c	<i>desA3</i>	-0.5304	0.0900	-0.6248	0.0904	-0.6322	0.1011	-1.6643	0.0001
Rv3230c		-0.0028	0.5020	-0.3507	0.4079	-1.1924	0.0014	-1.1239	0.0035
Rv3249c		-0.6956	0.3468	-0.2732	0.4952	0.3977	0.4805	-2.1354	0.0076
Rv3253c		-0.4985	0.1274	-0.2822	0.4185	-0.6345	0.0516	-0.8783	0.0066
Rv3261	<i>fbiA</i>	2.3681	0.0731	0.8829	0.4709	1.7016	0.4644	2.7687	0.0292
Rv3262	<i>fbiB</i>	3.3359	0.0002	2.3555	0.0002	2.1227	0.3430	4.1120	0.0001
Rv3263		-0.3433	0.3779	0.1848	0.4928	-0.1998	0.4824	-0.9410	0.0086
Rv3267		-2.0368	0.0295	-1.3232	0.3640	0.5358	0.4954	-3.7031	0.0001
Rv3270	<i>ctpC</i>	1.6242	0.4588	0.7511	0.4928	-1.1755	0.4349	-1.7791	0.0001
Rv3283	<i>sseA</i>	-0.6116	0.2208	-1.4188	0.0002	-0.5156	0.2397	0.5892	0.1349
Rv3291c	<i>lrpA</i>	-0.9984	0.3090	-2.2062	0.0028	-0.8828	0.3877	0.2244	0.4726
Rv3311		-2.5497	0.0002	-2.8067	0.0002	-2.3129	0.0002	-4.5124	0.0001
Rv3316	<i>sdhC</i>	-2.1135	0.0033	-3.1682	0.0002	-3.5877	0.0002	-3.2114	0.0001
Rv3317	<i>sdhD</i>	-2.5036	0.0002	-1.3953	0.0084	-3.0063	0.0002	-2.9301	0.0001
Rv3318	<i>sdhA</i>	-0.1626	0.5005	-1.0684	0.0116	-0.6211	0.2603	-0.7666	0.1083
Rv3319	<i>sdhB</i>	-1.3605	0.0262	-1.3801	0.0263	-1.8047	0.0049	-1.1682	0.1442
Rv3335c		-0.2944	0.5005	-1.3951	0.0063	-0.3056	0.4907	-0.3873	0.4283
Rv3340	<i>metC</i>	-0.7093	0.5005	-2.4759	0.0116	-1.4002	0.2344	-0.9858	0.3492
Rv3342		-0.8511	0.2083	-0.7834	0.3236	-1.5229	0.0336	-2.1733	0.0012

Rv3343c	<i>ppe54</i>	0.1682	0.4521	0.2086	0.3343	0.1075	0.4832	0.4420	0.0324
Rv3377c		0.2514	0.5005	0.4105	0.3240	0.3823	0.3824	0.8437	0.0159
Rv3400		-2.8866	0.0002	-5.2777	0.0002	-4.3978	0.0002	-3.3621	0.0001
Rv3412		-1.3717	0.0033	-1.2782	0.0125	-1.0563	0.0404	-1.7182	0.0001
Rv3413c		-0.7273	0.0985	-1.6072	0.0002	-1.1513	0.0084	-0.7558	0.1487
Rv3416	<i>whiB3</i>	-0.2642	0.5005	-1.4883	0.0445	-1.7428	0.0433	-1.5261	0.1386
Rv3420c	<i>rimI</i>	-0.8489	0.3111	-1.1874	0.1776	-3.1701	0.0002	-1.8987	0.0259
Rv3433c		-1.1853	0.1975	-0.9374	0.2733	-2.2856	0.0002	-3.0852	0.0012
Rv3434c		-0.1307	0.5005	-0.8802	0.0213	-0.1409	0.4949	-0.0066	0.5013
Rv3449	<i>mycP4</i>	0.0716	0.5005	-0.8132	0.0308	-0.2015	0.4907	-0.0375	0.4959
Rv3483c		0.2214	0.5005	-0.3193	0.4436	0.2018	0.4907	-0.8111	0.0381
Rv3484	<i>cpsA</i>	-5.0188	0.0002	-6.2611	0.0002	-8.9658	0.0002	10.9337	0.0001
Rv3492c		-1.7958	0.0002	-1.5401	0.0002	-0.8182	0.3060	-2.6582	0.0001
Rv3493c		-1.0918	0.0316	-1.2338	0.0499	-1.9270	0.0002	-4.2693	0.0001
Rv3494c	<i>mce4F</i>	-1.3386	0.0002	-1.5603	0.0002	-1.8568	0.0002	-2.6439	0.0001
Rv3495c	<i>lprN</i>	-0.9653	0.0176	-0.9687	0.0345	-1.6443	0.0002	-1.6533	0.0001
Rv3496c	<i>mce4D</i>	-1.3805	0.0002	-1.2580	0.0002	-2.1654	0.0002	-1.8397	0.0001
Rv3497c	<i>mce4C</i>	-1.2493	0.0002	-1.0926	0.0002	-1.5014	0.0002	-1.7012	0.0001
Rv3498c	<i>mce4B</i>	-0.7119	0.1975	-1.3182	0.0084	-1.4692	0.0002	-1.8245	0.0012
Rv3499c	<i>mce4A</i>	-0.8640	0.0002	-0.7010	0.0980	-1.2866	0.0002	-2.4138	0.0001
Rv3500c	<i>yrbE4B</i>	-1.3221	0.0002	-1.4297	0.0002	-1.6668	0.0002	-1.7209	0.0001
Rv3501c	<i>yrbE4A</i>	-1.1581	0.0176	-2.0780	0.0002	-1.1698	0.0362	-1.7263	0.0057
Rv3502c		-3.7660	0.0002	-3.4590	0.0002	-5.5212	0.0002	-4.5282	0.0001
Rv3526	<i>kshA</i>	-0.3081	0.5005	-0.3862	0.4202	-0.3979	0.4516	-1.0156	0.0455
Rv3534c	<i>hsaF</i>	-0.6865	0.1604	-1.4211	0.0015	-1.6224	0.0014	-1.6862	0.0012
Rv3535c	<i>hsaG</i>	-1.2357	0.0002	-1.1847	0.0002	-1.9180	0.0002	-2.2344	0.0001
Rv3536c	<i>hsaE</i>	-0.8593	0.2083	-0.3182	0.4952	-1.1819	0.0651	-2.0939	0.0057
Rv3537	<i>kstD</i>	-0.8078	0.1345	-0.9540	0.1120	-1.5334	0.0094	-0.5461	0.3932
Rv3538		-1.5887	0.0392	-0.8561	0.2977	-0.4345	0.4907	-1.4677	0.1709
Rv3540c	<i>ltp2</i>	-3.9207	0.0002	-7.6074	0.0002	-7.8171	0.0002	-7.5925	0.0001
Rv3542c		-3.9008	0.0002	-5.1856	0.0002	-4.7792	0.0002	-8.2790	0.0001
Rv3543c	<i>fadE29</i>	-2.3784	0.0116	-6.1170	0.0002	-2.9340	0.0002	-5.4349	0.0001
Rv3544c	<i>fadE28</i>	-4.3733	0.0002	-6.3029	0.0002	-8.5038	0.0002	-5.0990	0.0001
Rv3545c	<i>cyp125</i>	-1.3414	0.0002	-1.7315	0.0002	-1.0047	0.0038	-1.8834	0.0001
Rv3546	<i>fadA5</i>	-1.6871	0.0074	-1.5652	0.0619	-2.7189	0.0026	-3.9688	0.0001
Rv3548c		-0.8036	0.0855	-0.5766	0.2563	-0.6250	0.2196	-1.2270	0.0259
Rv3549c		-1.2528	0.0251	-2.1004	0.0015	-1.8365	0.0038	-2.9842	0.0001
Rv3550	<i>echA20</i>	-5.5091	0.0002	-5.9283	0.0002	-6.4657	0.0002	-5.7729	0.0001
Rv3551		-5.2372	0.0002	-8.1869	0.0002	-9.2955	0.0002	-9.2714	0.0001

Rv3552		-7.6192	0.0002	-5.5501	0.0002	-6.7970	0.0002	-6.5918	0.0001
Rv3553		-3.9610	0.0002	-2.5190	0.0002	-5.1074	0.0002	-3.1633	0.0001
Rv3556c	<i>fadA6</i>	-3.5007	0.0002	-2.7480	0.0002	-3.5618	0.0002	-7.6579	0.0001
Rv3557c		-0.8088	0.0663	-1.4723	0.0002	-1.2923	0.0026	-0.6799	0.2375
Rv3559c		-4.6268	0.0002	-1.6855	0.0676	-7.0904	0.0002	-6.8750	0.0001
Rv3560c	<i>fadE30</i>	-1.4048	0.0102	-2.5529	0.0002	-4.0735	0.0002	-3.9364	0.0001
Rv3562	<i>fadE31</i>	-1.8481	0.0164	-0.6205	0.4641	-1.3005	0.2084	-3.8749	0.0001
Rv3563	<i>fadE32</i>	-2.1000	0.0002	-1.8327	0.0002	-2.3748	0.0002	-2.7289	0.0001
Rv3564	<i>fadE33</i>	-3.3294	0.0002	-1.8784	0.0362	-7.8339	0.0002	-5.6001	0.0001
Rv3568c	<i>hsaC</i>	-1.4442	0.0074	-1.1350	0.0461	-0.3117	0.4949	-2.2780	0.0012
Rv3569c	<i>hsaD</i>	-3.4797	0.0002	-6.1882	0.0002	-3.7490	0.0002	-2.5706	0.0001
Rv3570c	<i>hsaA</i>	-0.8546	0.2168	-1.7264	0.0002	-1.2860	0.0500	-0.7644	0.3048
Rv3574	<i>kstR</i>	-2.7274	0.0002	-2.9688	0.0002	-2.4126	0.0014	0.1045	0.4916
Rv3575c		-0.5405	0.1197	-0.6045	0.1027	-0.4782	0.3206	-1.0194	0.0141
Rv3614c	<i>espD</i>	-4.4361	0.0002	-4.5172	0.0002	-4.1978	0.0002	-2.9828	0.0012
Rv3615c	<i>espC</i>	-4.0009	0.0002	-4.5043	0.0002	-3.6649	0.0002	-4.2500	0.0001
Rv3616c	<i>espA</i>	-3.5901	0.0002	-3.9552	0.0002	-4.2429	0.0002	-6.3459	0.0001
Rv3620c	<i>esxW</i>	0.3215	0.5005	-0.3833	0.4154	-0.8983	0.0274	0.3963	0.4028
Rv3631		-1.1252	0.1040	-0.9995	0.1978	-2.2218	0.0002	-4.5187	0.0001
Rv3632		-1.1634	0.0221	-0.9739	0.0755	-2.3245	0.0002	-1.8714	0.0001
Rv3656c		0.4446	0.5005	-0.2467	0.4993	-0.0239	0.4997	-2.5383	0.0076
Rv3679		0.7384	0.5005	2.6604	0.4916	0.2906	0.4949	-4.2101	0.0001
Rv3682	<i>ponA2</i>	-1.1003	0.0243	-1.9552	0.0002	-0.8078	0.1676	-1.8438	0.0001
Rv3683		-1.2083	0.0565	-1.3998	0.0612	-0.3434	0.4907	-2.8907	0.0001
Rv3687c	<i>rsfB</i>	0.1206	0.5005	-1.6175	0.0431	1.6990	0.2528	0.6037	0.4430
Rv3689		0.0273	0.5005	0.1437	0.4993	0.2286	0.4664	-0.8121	0.0132
Rv3692	<i>moxR2</i>	-0.4339	0.4997	-0.0437	0.4993	-0.0176	0.4997	-1.2202	0.0046
Rv3696c	<i>glpK</i>	-1.5989	0.0002	-1.0831	0.0002	-2.1531	0.0002	-1.1299	0.0001
Rv3704c	<i>gshA</i>	-0.0324	0.5005	-0.5017	0.3092	-0.6581	0.1542	-0.9535	0.0393
Rv3716c		-1.4847	0.0392	-1.6854	0.0213	-1.1850	0.1160	-1.2735	0.1216
Rv3717		-1.6557	0.0002	-4.5008	0.0002	-4.9351	0.0002	-1.9783	0.0001
Rv3719		-0.4878	0.1609	-0.6466	0.0723	-0.9693	0.0002	-0.0948	0.4784
Rv3720		-1.0608	0.0002	-1.2871	0.0002	-0.3566	0.4612	-1.1890	0.0001
Rv3722c		0.5629	0.5005	-0.5410	0.4993	-2.5928	0.0362	-5.2164	0.0012
Rv3723		-2.3892	0.0002	-2.4201	0.0002	-3.2366	0.0002	-1.8959	0.0001
Rv3746c	<i>pe34</i>	-0.6735	0.3131	-1.4052	0.0612	-1.6935	0.0238	-1.6086	0.0564
Rv3749c		-0.0505	0.5005	0.3153	0.4947	-0.0122	0.5039	-1.3738	0.0066
Rv3755c		-1.7567	0.0002	-2.0650	0.0002	-1.5452	0.0002	-1.8266	0.0012
Rv3763	<i>lpqH</i>	-0.0662	0.5005	-0.3486	0.4837	0.1141	0.4953	-1.6345	0.0405

Rv3779		-1.3583	0.0002	-1.3434	0.0002	-2.2002	0.0002	-3.1611	0.0001
Rv3788		-0.0199	0.5005	-0.7022	0.0499	-0.1710	0.4907	-0.1241	0.4699
Rv3794	<i>embA</i>	0.5797	0.5005	-3.8555	0.0028	-2.6728	0.0472	1.2698	0.4726
Rv3811		-0.0168	0.5005	-0.7100	0.0002	-0.2653	0.3971	-0.3328	0.2898
Rv3816c		-1.1421	0.0209	-0.4919	0.4768	-1.1351	0.0410	-1.7040	0.0001
Rv3818		-0.0724	0.5005	-0.9712	0.1521	-0.6971	0.3706	-3.5417	0.0001
Rv3823c	<i>mmpL8</i>	-1.1150	0.0002	-0.5298	0.2481	-1.0544	0.0002	-1.5136	0.0001
Rv3825c	<i>pks2</i>	-0.3698	0.0002	-0.1841	0.2377	-0.3205	0.0163	0.0389	0.4721
Rv3830c		-1.0891	0.3959	-0.9297	0.4290	-1.5292	0.1491	-1.7837	0.0393
Rv3848		-3.9860	0.0002	-5.8509	0.0002	-4.6037	0.0002	-6.3981	0.0001
Rv3849	<i>espR</i>	-3.3955	0.0002	-6.2137	0.0002	-4.9030	0.0002	-5.5679	0.0001
Rv3855	<i>ethR</i>	-0.1825	0.5005	-2.4312	0.0002	-1.9426	0.0002	-2.0892	0.0001
Rv3866	<i>espG1</i>	-0.8364	0.0102	-0.7911	0.0643	-0.2323	0.4907	-0.7293	0.1138
Rv3867	<i>espH</i>	-1.0071	0.1023	-0.9482	0.2137	-2.6310	0.0002	-2.6007	0.0001
Rv3868	<i>eccA1</i>	-2.4600	0.0002	-2.8111	0.0002	-2.3753	0.0002	-5.3535	0.0001
Rv3869	<i>eccB1</i>	-4.6175	0.0002	-4.7485	0.0002	-3.8557	0.0002	-5.9158	0.0001
Rv3870	<i>eccCa1</i>	-3.9342	0.0002	-3.8212	0.0002	-4.1914	0.0002	-5.6461	0.0001
Rv3871	<i>eccCb1</i>	-4.4373	0.0002	-4.7247	0.0002	-5.1717	0.0002	-6.8352	0.0001
Rv3873	<i>ppe68</i>	-2.6932	0.0002	-2.6952	0.0002	-3.6131	0.0002	-3.4535	0.0001
Rv3874	<i>esxB</i>	-4.7553	0.0002	-6.5924	0.0002	-3.9850	0.0002	-2.9788	0.0046
Rv3876	<i>espl</i>	-2.1905	0.0002	-2.0876	0.0002	-2.5518	0.0002	-2.3376	0.0001
Rv3877	<i>eccD1</i>	-4.0758	0.0002	-3.5948	0.0002	-4.8600	0.0002	-4.1390	0.0001
Rv3881c	<i>espB</i>	-1.5131	0.0002	-1.0485	0.0002	-1.4068	0.0002	-1.3242	0.0001
Rv3882c	<i>eccE1</i>	-4.3062	0.0002	-4.1300	0.0002	-3.9600	0.0002	-4.8039	0.0001
Rv3883c	<i>mycP1</i>	-3.9018	0.0002	-4.0789	0.0002	-4.1048	0.0002	-7.2250	0.0001
Rv3910		-1.7009	0.0002	-1.7469	0.0002	-1.6552	0.0002	-2.3040	0.0001

LFC = log₂ fold change. Q-value = significance adjusting for multiple tests. Red = LFC ≥ -1.5. Bold = Q-value < 0.05 at indicated time point.

Table A3.2 | Significantly underrepresented genes post INH treatment compared to pretreatment

ID	gene	INH 1wk		INH 2.5wks		INH 5wks	
		LFC	Q-value	LFC	Q-value	LFC	Q-value
Rv0180c		-0.4245	0.5160	-0.4788	0.5108	-0.3517	0.0008
Rv0353	<i>hspR</i>	0.0363	0.5160	-1.6864	0.5108	-4.9729	0.0008
Rv0465c		-2.0776	0.0017	-1.9177	0.0016	1.0625	0.2814
Rv0505c	<i>serB1</i>	-2.7861	0.5160	-1.4604	0.5108	-5.3713	0.0008
Rv0767c		-3.2152	0.0297	-3.4108	0.0016	-3.7853	0.0008
Rv0806c	<i>cpsY</i>	-0.9997	0.5032	-0.7100	0.5108	-1.9326	0.0069
Rv0859	<i>fadA</i>	-2.0809	0.0017	0.7065	0.5108	-1.9603	0.0008
Rv1157c		-0.5784	0.5160	-3.3411	0.5108	-3.1888	0.0008
Rv1183	<i>mmpL10</i>	-1.2585	0.1321	-2.1866	0.0016	-1.6719	0.0069
Rv1193	<i>fadD36</i>	-2.0882	0.0017	-2.1222	0.5108	2.0427	0.1907
Rv1235	<i>lpqY</i>	-0.7984	0.5160	-0.7006	0.5108	-2.4641	0.0169
Rv1328	<i>glgP</i>	-1.1282	0.5160	-2.2561	0.0016	-2.4369	0.0008
Rv1349	<i>irtB</i>	-1.1596	0.0017	-1.1713	0.5108	1.4939	0.4666
Rv1356c		0.1122	0.5160	0.4618	0.5108	-2.5156	0.0169
Rv1445c	<i>devB</i>	-1.2658	0.5201	-2.8609	0.5143	-4.0876	0.0008
Rv1543		-1.9942	0.3837	-3.4910	0.0016	-1.5454	0.2779
Rv1747		-1.1588	0.2418	-1.4045	0.0390	-1.3753	0.0491
Rv1823		-1.2228	0.5160	-1.2871	0.5108	-3.8516	0.0119
Rv1901	<i>cinA</i>	-3.8215	0.0017	-4.5596	0.0016	-4.9181	0.0008
Rv2048c	<i>pks12</i>	-1.7110	0.0017	-1.2722	0.0346	-1.0930	0.0667
Rv2061c		-0.0619	0.5366	-0.1116	0.5206	-4.2577	0.0361
Rv2140c		-1.9829	0.5160	-2.4595	0.5108	-3.4176	0.0008
Rv2183c		0.4148	0.5160	-4.8028	0.0016	-4.6649	0.0008
Rv2344c	<i>dgt</i>	-0.4860	0.5160	-1.4186	0.2908	-2.3388	0.0119
Rv2378c	<i>mbtG</i>	-0.9324	0.5160	-0.9637	0.0016	-0.8251	0.0008
Rv2381c	<i>mbtD</i>	1.5035	0.5160	0.6038	0.5108	-0.3678	0.0008
Rv2563		-4.1301	0.0017	-4.3760	0.0016	-1.8044	0.3272
Rv2564	<i>glnQ</i>	-3.8129	0.0164	-3.2652	0.0125	-3.4993	0.0119
Rv2931	<i>ppsA</i>	-0.4164	0.5160	-1.5311	0.0125	1.5334	0.0008
Rv2932	<i>ppsB</i>	-0.4673	0.5160	-1.7432	0.0346	1.2914	0.0119
Rv2933	<i>ppsC</i>	-0.5407	0.5160	-1.6448	0.0016	1.3916	0.0008
Rv2934	<i>ppsD</i>	-0.5570	0.5160	-1.7214	0.0125	1.3795	0.0008
Rv2935	<i>ppsE</i>	-0.9301	0.5160	-1.6253	0.0390	1.2650	0.0169
Rv2940c	<i>mas</i>	-0.4319	0.5160	-1.2111	0.0390	1.1273	0.0008

Rv2942	<i>mmpL7</i>	-0.7282	0.5160	-1.4662	0.0125	-1.0005	0.2708
Rv3036c		-1.3248	0.5160	-1.2481	0.5108	-3.4137	0.0326
Rv3131		-1.8787	0.5160	-3.8044	0.0125	-2.7985	0.0933
Rv3211	<i>rhIE</i>	-3.9017	0.5160	-2.4049	0.5108	-4.7662	0.0008
Rv3232c	<i>ppk2</i>	-0.0928	0.5160	-0.3110	0.5108	-1.1719	0.0406
Rv3262	<i>fbiB</i>	-1.9417	0.0017	-1.9815	0.5108	-1.8464	0.4793
Rv3267		0.5915	0.5160	-1.4269	0.5108	-3.2811	0.0008
Rv3283	<i>sseA</i>	-3.5296	0.0017	-2.5805	0.0125	-0.8332	0.4519
Rv3539	<i>ppe63</i>	-0.0677	0.5160	-0.3359	0.5108	-1.7706	0.0361
Rv3586		-1.0116	0.5160	-0.6509	0.5108	-3.2116	0.0008
Rv3848		-2.7843	0.0017	-0.6724	0.5108	0.7922	0.4809
Rv3849	<i>espR</i>	-1.7815	0.5160	-1.8059	0.0016	-1.6599	0.0008
Rv3868	<i>eccA1</i>	0.5562	0.5160	-0.1770	0.5108	-5.1671	0.0008

LFC = log₂ fold change. Q-value = significance adjusting for multiple tests. Red = LFC ≥ -1.5. Bold = Q-value < 0.05 at indicated time point.

Table A3.3 | Significantly overrepresented genes post INH treatment compared to pretreatment

ID	gene	INH 1wk		INH 2.5wks		INH 5wks	
		LFC	Q-value	LFC	Q-value	LFC	Q-value
Rv0096	<i>ppe1</i>	0.7757	0.5160	1.7328	0.0016	3.0402	0.0008
Rv0097		1.5404	0.1562	1.9138	0.0390	2.9111	0.0008
Rv0098	<i>fcoT</i>	1.6116	0.5032	2.1722	0.1722	3.0989	0.0008
Rv0099	<i>fadD10</i>	1.4461	0.5160	1.7136	0.3895	2.9776	0.0008
Rv0101	<i>nrp</i>	0.7704	0.0950	1.5810	0.0016	2.3902	0.0008
Rv0249c		0.2312	0.5160	0.3342	0.5108	2.4865	0.0119
Rv0485		-0.0257	0.5185	0.5654	0.5108	2.3416	0.0008
Rv0554	<i>bpoC</i>	2.1364	0.0017	1.2209	0.3370	2.0217	0.0069
Rv0877		1.0426	0.0950	1.2351	0.0472	1.7533	0.0008
Rv1345	<i>mbtM</i>	2.9315	0.0017	1.4722	0.0016	2.7578	0.0008
Rv1798	<i>eccA5</i>	1.8892	0.1301	2.3901	0.0390	1.5407	0.4155
Rv2069	<i>sigC</i>	0.4126	0.5160	1.5369	0.5108	3.2615	0.0119
Rv2210c	<i>ilvE</i>	1.2221	NA	1.2043	NA	3.6786	0.0449
Rv2380c	<i>mbtE</i>	3.1817	0.0017	0.9327	0.5108	2.1159	0.3095
Rv2383c	<i>mbtB</i>	2.4169	0.0017	0.8960	0.5108	-0.8922	0.4028
Rv2930	<i>fadD26</i>	-0.0434	0.5185	-0.8710	0.5108	1.8078	0.0008
Rv2931	<i>ppsA</i>	-0.4164	0.5160	-1.5311	0.0125	1.5334	0.0008
Rv2932	<i>ppsB</i>	-0.4673	0.5160	-1.7432	0.0346	1.2914	0.0119
Rv2933	<i>ppsC</i>	-0.5407	0.5160	-1.6448	0.0016	1.3916	0.0008
Rv2934	<i>ppsD</i>	-0.5570	0.5160	-1.7214	0.0125	1.3795	0.0008
Rv2935	<i>ppsE</i>	-0.9301	0.5160	-1.6253	0.0390	1.2650	0.0169
Rv2940c	<i>mas</i>	-0.4319	0.5160	-1.2111	0.0390	1.1273	0.0008
Rv3135	<i>ppe50</i>	0.6124	0.5160	0.2440	0.5108	1.2726	0.0361
Rv3220c		1.5534	0.0297	0.1202	0.5108	1.4038	0.0276
Rv3331	<i>sugI</i>	0.8609	0.5160	0.4698	0.5108	1.5490	0.0069
Rv3575c		0.4505	0.5160	1.2116	0.1375	1.7785	0.0119
Rv3696c	<i>glpK</i>	3.7527	0.0017	2.5745	0.0016	4.9956	0.0008

LFC = log₂ fold change. Q-value = significance adjusting for multiple tests. Green = LFC ≥ 1.5. Bold = Q-value < 0.05 at indicated time point.

Table A3.4 | Significantly underrepresented genes post EMB treatment compared to pretreatment

ID	gene	EMB 1wk		EMB 2.5wks		EMB 5wks	
		LFC	Q-value	LFC	Q-value	LFC	Q-value
Rv0101	<i>nrp</i>	-0.2629	0.5212	-0.3874	0.5284	-1.1784	0.0078
Rv0111		-0.7440	0.5212	-0.9993	0.5284	-1.5728	0.0254
Rv0216		-1.3175	0.5212	-1.3104	0.5284	-6.5361	0.0009
Rv0296c		-0.7958	0.5212	-0.9035	0.5284	-1.8499	0.0078
Rv0450c	<i>mmpL4</i>	-0.3227	0.5212	-1.1094	0.1927	-2.2812	0.0009
Rv0503c	<i>cmaA2</i>	-0.5661	0.5212	-0.8557	0.2497	-1.1361	0.0199
Rv0757	<i>phoP</i>	-0.7731	0.5212	-0.6818	0.5284	-5.4654	0.0009
Rv0806c	<i>cpsY</i>	-0.9239	0.5212	-1.3422	0.1927	-2.3371	0.0009
Rv0998		-1.8514	0.5212	-1.8759	0.0017	-1.7428	0.5091
Rv1006		-0.3518	0.5212	-0.5826	0.5284	-2.0760	0.0142
Rv1183	<i>mmpL10</i>	-0.9184	0.5212	-1.0910	0.2477	-1.5218	0.0009
Rv1235	<i>lpqY</i>	-0.9297	0.5212	-1.3086	0.5284	-2.7902	0.0009
Rv1364c		-1.0143	0.5212	-0.6277	0.5284	-2.5027	0.0427
Rv1589	<i>bioB</i>	-1.3148	0.5212	-0.8198	0.5284	-2.3669	0.0009
Rv1635c		-0.4318	0.5212	-0.5041	0.5284	-1.1494	0.0199
Rv1701		-1.8577	0.5212	0.0882	0.5284	-1.7708	0.0009
Rv2048c	<i>pkS12</i>	-0.4964	0.5212	-0.7838	0.4897	-1.6127	0.0009
Rv2224c	<i>caeA</i>	-1.7459	0.5212	-1.6524	0.5284	-4.1851	0.0254
Rv2476c	<i>gdh</i>	-0.5923	0.5212	-0.8331	0.5284	-2.7278	0.0009
Rv2894c	<i>xerC</i>	-2.6890	0.0016	0.1334	0.5284	-0.7989	0.5629
Rv2936	<i>drrA</i>	-0.9407	0.5212	-0.8495	0.5284	-1.8161	0.0479
Rv2942	<i>mmpL7</i>	-1.1307	0.2866	-0.8315	0.5284	-1.6590	0.0142
Rv3283	<i>sseA</i>	-1.3593	0.5212	-2.2187	0.0299	-1.8270	0.0655
Rv3543c	<i>fadE29</i>	-2.6011	0.5212	-3.8238	0.5284	-3.6129	0.0009
Rv3559c		-1.9140	0.5212	-0.1475	0.5474	-1.7859	0.0009
Rv3823c	<i>mmpL8</i>	0.0202	0.5212	-0.8865	0.5284	-2.8551	0.0009
Rv3849	<i>espR</i>	0.2171	0.5212	-0.2979	0.5284	-1.7056	0.0009

LFC = log₂ fold change. Q-value = significance adjusting for multiple tests. Red = LFC ≥ -1.5. Bold = Q-value < 0.05 at indicated time point.

Table A3.5 | Significantly overrepresented genes post EMB treatment compared to pretreatment

ID	gene	EMB 1wk		EMB 2.5wks		EMB 5wks	
		LFC	Q-value	LFC	Q-value	LFC	Q-value
Rv0177		0.8241	0.5212	0.3103	0.5284	1.4909	0.0078
Rv0244c	<i>fadE5</i>	2.1189	0.0149	1.2743	0.5284	4.6923	0.0009
Rv0270	<i>fadD2</i>	0.9060	0.1506	1.2120	0.0017	2.2608	0.0009
Rv0554	<i>bpoC</i>	2.0021	0.0016	2.0906	0.0017	1.4672	0.0655
Rv0818		0.1970	0.5212	0.9343	0.5284	3.4258	0.0311
Rv0877		0.8737	0.4430	1.0406	0.0017	3.5486	0.0009
Rv1151c		0.8294	0.5212	0.8062	0.5284	1.9677	0.0009
Rv1205		0.3169	0.5212	0.8461	0.5284	2.9183	0.0078
Rv1206	<i>fadD6</i>	1.4953	0.0016	1.2569	0.0017	3.4614	0.0009
Rv1345	<i>mbtM</i>	2.6354	0.0016	2.7976	0.0017	2.3265	0.0009
Rv1626		2.4395	0.0284	2.5178	0.0017	1.7911	0.2876
Rv1798	<i>eccA5</i>	2.1337	0.0016	-0.0673	0.5284	1.5386	0.5091
Rv2378c	<i>mbtG</i>	3.4335	0.0016	3.8489	0.0017	3.2231	0.1791
Rv2379c	<i>mbtF</i>	3.8625	0.0016	4.6703	0.0017	3.2054	0.0009
Rv2380c	<i>mbtE</i>	5.6454	0.0016	6.1164	0.0017	5.1205	0.0009
Rv2381c	<i>mbtD</i>	4.4276	0.0016	4.1867	0.0017	3.7573	0.0009
Rv2382c	<i>mbtC</i>	3.5541	0.0680	4.3838	0.0017	4.1548	0.0009
Rv2383c	<i>mbtB</i>	4.1328	0.0016	4.5681	0.0017	4.0021	0.0009
Rv2384	<i>mbtA</i>	3.4323	0.0016	3.6058	0.0017	2.8827	0.0199
Rv2386c	<i>mbtI</i>	4.5436	0.0016	4.7244	0.0017	3.8018	0.0142
Rv2567		1.1455	0.5212	0.7535	0.5284	2.4908	0.0078
Rv2684	<i>arsA</i>	1.1006	0.2866	1.5348	0.0157	3.0202	0.0009
Rv2689c		0.4044	0.5212	0.8126	0.5284	1.5196	0.0078
Rv3135	<i>ppe50</i>	1.2821	0.0149	0.8567	0.2785	0.9944	0.0778
Rv3220c		2.6952	0.0016	2.7328	0.0017	3.6728	0.0009
Rv3696c	<i>glpK</i>	2.8640	0.0016	2.8913	0.0017	5.6685	0.0009
Rv3842c	<i>glpQ1</i>	-0.0346	0.5246	0.1913	0.5284	2.3757	0.0142

LFC = log₂ fold change. Q-value = significance adjusting for multiple tests. Green = LFC ≥ 1.5. Bold = Q-value < 0.05 at indicated time point.

Table A3.6 | Significantly underrepresented genes post RIF treatment compared to pretreatment

ID	gene	RIF 1wk		RIF 2.5wks	
		LFC	Q-value	LFC	Q-value
Rv0436c	<i>pssA</i>	-0.5678	0.5022	-5.5344	0.0255
Rv0450c	<i>mmpL4</i>	-1.7122	0.0014	-0.8414	0.0565
Rv0805		-1.6027	0.3548	-3.0054	0.0098
Rv0820	<i>phoT</i>	-2.2146	0.3373	-4.1651	0.0322
Rv0989c	<i>grcC2</i>	-2.7020	0.0665	-2.7571	0.0374
Rv0998		-3.0483	0.0014	-3.0570	0.2339
Rv1174c		-2.1951	0.0014	-3.8456	0.0011
Rv1184c		-3.4355	0.0014	-3.5120	0.0011
Rv1244	<i>lpqZ</i>	-1.9205	0.0122	-2.6759	0.0011
Rv1272c		-1.4369	0.2360	-1.9917	0.0179
Rv1273c		-4.4242	0.0014	-4.1301	0.0011
Rv1328	<i>glgP</i>	-0.9490	0.1670	-1.7269	0.0011
Rv1492	<i>mutA</i>	-0.2269	0.5022	-1.4187	0.0428
Rv1543		-3.1632	0.0014	-3.8412	0.0011
Rv1592c		-1.7169	0.0014	-0.6144	0.4322
Rv1925	<i>fadD31</i>	-1.5265	0.0372	-1.3086	0.1615
Rv2004c		-0.9234	0.5022	-2.4414	0.0098
Rv2190c		-2.1909	0.4452	-5.0327	0.0098
Rv2224c	<i>caeA</i>	-3.0024	0.0014	-1.6165	0.3205
Rv2241	<i>aceE</i>	-3.3945	0.0372	-2.1791	0.1250
Rv2462c	<i>tig</i>	-1.7061	0.0316	-0.7692	0.4720
Rv2563		-3.4297	0.0014	-1.5044	0.2505
Rv2564	<i>glnQ</i>	-2.0061	0.0122	-0.6872	0.4689
Rv2985	<i>mutT1</i>	-0.3361	0.5022	-2.7061	0.0255
Rv3005c		-2.6197	0.0014	-1.5296	0.1191
Rv3036c		-1.6094	0.1604	-2.7727	0.0011
Rv3139	<i>fadE24</i>	-2.4794	0.0014	-0.3523	0.4972
Rv3194c		-1.3651	0.1074	-1.5973	0.0428
Rv3229c	<i>desA3</i>	-1.0095	0.0316	-0.4218	0.4768
Rv3484	<i>cpsA</i>	-2.7913	0.1207	-4.2602	0.0011
Rv3682	<i>ponA2</i>	-1.2339	0.4691	-2.7299	0.0322
Rv3717		-3.4527	0.0372	-1.0415	0.4972
Rv3779		-1.1374	0.0234	-0.6217	0.4433
Rv3822		-4.9282	0.0014	-5.3026	0.0011

Rv3867	<i>espH</i>	-5.3489	0.0014	-2.6985	0.1250
Rv3868	<i>eccA1</i>	-3.0616	0.0014	-5.5009	0.0011

LFC = log₂ fold change. Q-value = significance adjusting for multiple tests.
Red = LFC ≥ -1.5. Bold = Q-value < 0.05 at indicated time point.

Table A3.7 | Significantly overrepresented genes post RIF treatment compared to pretreatment

ID	gene	RIF 1wk		RIF 2.5wks	
		LFC	Q-value	LFC	Q-value
Rv0079		0.3208	0.5022	1.8283	0.0179
Rv0248c		1.6133	0.0372	1.7721	0.0011
Rv0249c		2.0384	0.0451	1.9250	0.0374
Rv0270	<i>fadD2</i>	0.8636	0.0122	0.7017	0.1125
Rv0485		-0.3750	0.5022	1.8146	0.0011
Rv0503c	<i>cmaA2</i>	1.1372	0.0014	2.2285	0.0011
Rv0554	<i>bpoC</i>	0.6998	0.4778	1.2884	0.0098
Rv0643c	<i>mmaA3</i>	0.7850	0.0934	1.5440	0.0011
Rv0758	<i>phoR</i>	-0.1768	0.5022	1.9234	0.0011
Rv1345	<i>mbtM</i>	1.9028	0.0014	1.6531	0.0011
Rv1538c	<i>ansA</i>	0.5687	0.5022	2.0356	0.0011
Rv2098c		1.7029	0.0316	0.2357	0.4972
Rv2214c	<i>ephD</i>	1.2531	0.0014	1.3558	0.0011
Rv2689c		1.1285	0.0122	0.5123	0.4624
Rv2930	<i>fadD26</i>	0.3658	0.5022	1.2857	0.0374
Rv2940c	<i>mas</i>	0.0273	0.5022	0.8555	0.0179
Rv2967c	<i>pca</i>	1.5891	0.3373	2.5459	0.0011
Rv3220c		1.8870	0.0014	0.9803	0.1191
Rv3535c	<i>hsaG</i>	0.3171	0.5022	1.3422	0.0489
Rv3696c	<i>glpK</i>	1.6695	0.0014	1.9889	0.0011
Rv3820c	<i>papA2</i>	0.4975	0.4928	1.0818	0.0011
Rv3824c	<i>papA1</i>	0.6877	0.1207	0.9812	0.0011
Rv3825c	<i>pks2</i>	0.5521	0.0014	0.9465	0.0011

LFC = log₂ fold change. Q-value = significance adjusting for multiple tests.
Green = LFC ≥ 1.5. Bold = Q-value < 0.05 at indicated time point.

Table A3.8 | Significantly underrepresented genes post PZA treatment compared to pretreatment

ID	gene	PZA 1wk	
		LFC	Q-value
Rv0757	<i>phoP</i>	-3.8796	0.0020
Rv1212c	<i>glgA</i>	-3.4518	0.0020
Rv1770		-1.1589	0.0330
Rv2614A		-3.4209	0.0174
Rv3135	<i>ppe50</i>	-1.5908	0.0020
Rv3136	<i>ppe51</i>	-3.6612	0.0020
Rv3262	<i>fbiB</i>	-2.7801	0.0020
Rv3277		-3.7506	0.0020
Rv3855	<i>ethR</i>	-2.4174	0.0174
Rv3868	<i>eccA1</i>	-2.9265	0.0020

LFC = log₂ fold change. Q-value = significance adjusting for multiple tests. Red = LFC ≥ -1.5. Bold = Q-value < 0.05.

Table A3.9 | Significantly overrepresented genes post PZA treatment compared to pretreatment

ID	gene	PZA 1wk	
		LFC	Q-value
Rv1206	<i>fadD6</i>	1.4982	0.0020
Rv2043c	<i>pncA</i>	3.2043	0.0020
Rv2476c	<i>gdh</i>	2.0322	0.0020
Rv2940c	<i>mas</i>	0.8895	0.0470
Rv3696c	<i>glpK</i>	3.1416	0.0020

LFC = log₂ fold change. Q-value = significance adjusting for multiple tests. Green = LFC ≥ 1.5. Bold = Q-value < 0.05.

Table A3.10 | Genes significantly associated with varimax dimension 1, INH treatment

ID		Varimax dimension 1 INH (1-, 2.5-, 5-weeks)	
		LFC	Q-value
Rv0096	<i>ppe1</i>	-2.2000	0.0000
Rv0097		-2.0000	0.0000
Rv0101	<i>nrp</i>	-1.6000	0.0000

LFC = log fold change of varimax projection. Q-value = significance adjusting for multiple tests. Red = LFC ≥ -1.5 . Bold = Q-value < 0.025 .

Table A3.11 | Genes significantly associated with varimax dimension 2, untreated

ID		Varimax dimension 2 Untreated	
		LFC	Q-value
<i>Rv2563</i>		-2.9000	0.0034

LFC = log fold change of varimax projection. Q-value = significance adjusting for multiple tests. Red = LFC ≥ -1.5 . Green = LFC ≥ 1.5 . Bold = Q-value < 0.025 .

Table A3.12 | Genes significantly associated with varimax dimension 3, PZA and HRZE treated

ID	gene	Varimax dimension 3 PZA/HRZE (1-week)	
		LFC	Q-value
Rv0805		-1.7000	0.0132
Rv1592c		-1.8000	0.0220
Rv2043c	<i>pncA</i>	-2.8000	0.0000
Rv2476c	<i>gdh</i>	-2.1000	0.0000
Rv2571c		-2.9000	0.0000
Rv2931	<i>ppsA</i>	-1.2000	0.0000
Rv2934	<i>ppsD</i>	-1.1000	0.0000
Rv2940c	<i>mas</i>	-0.8000	0.0062
Rv3136	<i>PPE51</i>	2.4000	0.0000
Rv3229c	<i>desA3</i>	1.6000	0.0132
Rv3717		-3.9000	0.0062

LFC = log fold change of varimax projection. Q-value = significance adjusting for multiple tests. Red = LFC \geq -1.5. Green = LFC \geq 1.5. Bold = Q-value < 0.025.

Table A3.13 | Genes significantly associated with varimax dimension 4, RIF treatment

ID	gene	Varimax dimension 4 RIF (1-, 2.5-, 5-weeks)	
		LFC	Q-value
Rv0248c		-2.0000	0.0062
Rv0485		-2.1000	0.0088
Rv0503c	<i>cmaA2</i>	-1.9000	0.0000
Rv0643c	<i>mmaA3</i>	-1.2000	0.0000
Rv0758	<i>phoR</i>	-1.4000	0.0000
Rv1184c		2.8000	0.0111
Rv2214c	<i>ephD</i>	-1.1000	0.0034
Rv3822		3.5000	0.0000
Rv3825c	<i>pks2</i>	-0.6000	0.0000

LFC = log fold change of varimax projection. Q-value = significance adjusting for multiple tests. Red = LFC ≥ -1.5 . Green = LFC ≥ 1.5 . Bold = Q-value < 0.025 .

Table A3.14 | Genes significantly associated with varimax dimensions 5 and 6, EMB treatment

ID	gene	Varimax dimension 5 EMB (1- and 2.5-weeks)		Varimax dimension 6 EMB (5-weeks)	
		LFC	Q-value	LFC	Q-value
		Rv0244c	<i>fadE5</i>	0.9000	0.7175
Rv0554	<i>bpoC</i>	-1.1000	0.0111	0.2000	0.8173
Rv1193	<i>fadD36</i>	-2.5000	0.0000	1.2000	0.6827
Rv1206	<i>fadD6</i>	-0.2000	0.8550	-1.8000	0.0000
Rv1345	<i>mbtM</i>	-0.9000	0.0385	-0.9000	0.0220
Rv1626		-2.0000	0.0000	0.2000	0.8895
Rv2378c	<i>mbtG</i>	-1.6000	0.2460	-2.6000	0.0154
Rv2379c	<i>mbtF</i>	-2.6000	0.0000	-0.8000	0.5546
Rv2380c	<i>mbtE</i>	-2.1000	0.0000	-2.0000	0.0000
Rv2381c	<i>mbtD</i>	-2.9000	0.0034	-0.6000	0.8288
Rv2383c	<i>mbtB</i>	-2.4000	0.0000	-1.5000	0.0000
Rv2384	<i>mbtA</i>	-3.7000	0.0000	0.3000	0.8550
Rv2684	<i>arsA</i>	-0.8000	0.3162	-1.7000	0.0000
Rv3220c		-0.7000	0.5362	-2.2000	0.0000
Rv3696c	<i>glpK</i>	0.2000	0.8979	-1.6000	0.0088
Rv3855	<i>ethR</i>	-1.9000	0.0000	1.4000	0.4194

LFC = log fold change of varimax projection. Q-value = significance adjusting for multiple tests. Red = LFC \geq -1.5. Green = LFC \geq 1.5. Bold = Q-value < 0.025.

REFERENCES

1. Sakula A. 1982. Robert Koch: centenary of the discovery of the tubercle bacillus, 1882. *Thorax* 37:246-251.
2. Comas I, Coscolla M, Luo T, Borrell S, Holt KE, Kato-Maeda M, Parkhill J, Malla B, Berg S, Thwaites G, Yeboah-Manu D, Bothamley G, Mei J, Wei L, Bentley S, Harris SR, Niemann S, Diel R, Aseffa A, Gao Q, Young D, Gagneux S. 2013. Out-of-Africa migration and Neolithic coexpansion of *Mycobacterium tuberculosis* with modern humans. *Nat Genet* 45:1176-82.
3. Gagneux S, DeRiemer K, Van T, Kato-Maeda M, de Jong BC, Narayanan S, Nicol M, Niemann S, Kremer K, Gutierrez MC, Hilty M, Hopewell PC, Small PM. 2006. Variable host-pathogen compatibility in *Mycobacterium tuberculosis*. *Proc Natl Acad Sci U S A* 103:2869-73.
4. Boritsch EC, Supply P, Honore N, Seemann T, Stinear TP, Brosch R. 2014. A glimpse into the past and predictions for the future: the molecular evolution of the tuberculosis agent. *Mol Microbiol* 93:835-52.
5. World Health Organization. 2019. Global Tuberculosis Report 2019. World Health Organization, Geneva, Switzerland.
6. Tiemersma EW, van der Werf MJ, Borgdorff MW, Williams BG, Nagelkerke NJ. 2011. Natural history of tuberculosis: duration and fatality of untreated pulmonary tuberculosis in HIV negative patients: a systematic review. *PLoS One* 6:e17601.
7. Council MR. 1948. Streptomycin treatment of pulmonary tuberculosis. *British Medical Journal*:769-782.
8. Crofton J, Mitchison DA. 1948. Streptomycin resistance in pulmonary tuberculosis. *British Medical Journal* 2:1009-1015.
9. Council MR. 1950. Treatment of pulmonary tuberculosis with streptomycin and *para*-amino-salicylic acid. *British Medical Journal* 2:1073-1085.
10. Medical Research Council Tuberculosis Chemotherapy Trials Committee. 1952. The treatment of pulmonary tuberculosis with isoniazid. *British Medical Journal*:735-746.
11. Medical Research Council Tuberculosis Chemotherapy Trials Committee. 1953. Isoniazid in the treatment of pulmonary tuberculosis. *British Medical Journal*:521-536.
12. Medical Research Council Tuberculosis Chemotherapy Trials Committee. 1953. Isoniazid in combination with streptomycin or with P.A.S. in the treatment of pulmonary tuberculosis. *British Medical Journal*:1005-1014.
13. Crofton J. 1959. Chemotherapy of pulmonary tuberculosis. *British Medical Journal*:1610-1614.
14. Fox W, Ellard GA, Mitchison DA. 1999. Studies on the treatment of tuberculosis undertaken by the British Medical Research Council Tuberculosis Units, 1946-

- 1986, with relevant subsequent publications. *International Journal of Tuberculosis and Lung Disease* 3:S231-S279.
15. World Health Organization. 2010. Treatment of tuberculosis guidelines, fourth edition. World Health Organization, Geneva, Switzerland.
 16. Winder FG, Collins PB. 1970. Inhibition by isoniazid of synthesis of mycolic acids in *Mycobacterium tuberculosis*. *Journal of General Microbiology* 63:41-48.
 17. Takayama K, Wang L, David HL. 1972. Effect of isoniazid on the *in vivo* mycolic acid synthesis, cell growth, and viability of *Mycobacterium tuberculosis*. *Antimicrob Agents Chemother* 2:29-35.
 18. Johnsson K, Schultz PG. 1994. Mechanistic studies of the oxidation of isoniazid by the catalase peroxidase from *Mycobacterium tuberculosis*. *J Am Chem Soc* 116:7425-7426.
 19. Rozwarski DA, Grant GA, Barton DHR, Jacobs WR, Jr., Sacchettini J. 1998. Modification of the NADH of the Isoniazid Target (InhA) from *Mycobacterium tuberculosis*. *Science* 279:98-102.
 20. Dessen A, Quemard A, Blanchard JS, Jacobs WR, Jr., Sacchettini J. 1995. Crystal structure and function of the isoniazid target of *Mycobacterium tuberculosis*. *Science* 267:1638-1641.
 21. Quemard A, Sacchettini J, Dessen A, Vilcheze C, Bittman R, Jacobs WR, Jr., Blanchard JS. 1995. Enzymatic characterization of the target for isoniazid in *Mycobacterium tuberculosis*. *Biochemistry* 34:8235-8241.
 22. Takayama K, Schnoes HK, Armstrong EL, Boyle RW. 1975. Site of inhibitory action of isoniazid in the synthesis of mycolic acids in *Mycobacterium tuberculosis*. *Journal of Lipid Research* 16:308-317.
 23. Wehrli W, Staehelin M. 1971. Actions of the rifamycins. *Bacteriological Reviews* 35:290-309.
 24. White RJ, Lancini GC, Silvestri LG. 1971. Mechanism of action of rifampin on *Mycobacterium smegmatis*. *J Bacteriol* 108:736-741.
 25. Konno K, Oizumi K, Arijji F, Yamaguchi J, Oka S. 1973. Mode of Action of Rifampin on Mycobacteria. I. Electron Microscopic Study of the Effect of Rifampin on *Mycobacterium tuberculosis*. *American Review of Respiratory Disease* 107:1002-1005.
 26. Konno K, Oizumi K, Oka S. 1973. Mode of Action of Rifampin on Mycobacteria. II. Biosynthetic studies on the inhibition of ribonucleic acid polymerase of *Mycobacterium bovis* BCG by rifampin and uptake of rifampin-14C by *Mycobacterium phlei*. *American Review of Respiratory Disease* 107:1006-1012.
 27. Takayama K, Kilburn JO. 1989. Inhibition of synthesis of arabinogalactan by ethambutol in *Mycobacterium smegmatis*. *Antimicrob Agents Chemother* 33:1493-1499.
 28. Mikusova K, Slayden RA, Besra GS, Brennan PJ. 1995. Biogenesis of the mycobacterial cell wall and the site of action of ethambutol. *Antimicrob Agents Chemother* 39:2484-9.

29. Goude R, Amin AG, Chatterjee D, Parish T. 2009. The arabinosyltransferase EmbC is inhibited by ethambutol in *Mycobacterium tuberculosis*. *Antimicrob Agents Chemother* 53:4138-46.
30. Konno K, Feldmann FM, McDermott W. 1967. Pyrazinamide susceptibility and amidase activity of tubercle bacilli. *American Review of Respiratory Disease* 95:461-469.
31. Scorpio A, Zhang Y. 1996. Mutations in *pncA*, a gene encoding pyrazinamidase/nicotinamidase, cause resistance to the antituberculous drug pyrazinamide in tubercle bacillus. *Nature Medicine* 2:662-667.
32. McCune RM, Tompsett R, McDermott W. 1956. The Fate of *Mycobacterium Tuberculosis* in Mouse Tissues as Determined by the Microbial Enumeration Technique: II. The conversion of tuberculous infection to the latent state by the administration of pyrazinamide and a companion drug. *The Journal of Experimental Medicine* 104:763-802.
33. Zhang Y, Scorpio A, Nikaido H, Sun Z. 1999. Role of Acid pH and Deficient Efflux of Pyrazinoic Acid in Unique Susceptibility of *Mycobacterium tuberculosis* to Pyrazinamide. *J Bacteriol* 181:2044-2049.
34. Zimhony O, Cox JS, Welch JT, Vilcheze C, Jacobs WR, Jr. 2000. Pyrazinamide inhibits the eukaryotic-like fatty acid synthetase I (FASI) of *Mycobacterium tuberculosis*. *Nature Medicine* 6:1043-1047.
35. Zhang Y, Wade MM, Scorpio A, Zhang H, Sun Z. 2003. Mode of action of pyrazinamide: disruption of *Mycobacterium tuberculosis* membrane transport and energetics by pyrazinoic acid. *J Antimicrob Chemother* 52:790-5.
36. Shi W, Zhang X, Jiang X, Lee JS, Barry CE, 3rd, Wang H, Zhang W, Zhang Y. 2011. Pyrazinamide inhibits trans-translation in *Mycobacterium tuberculosis*. *Science* 333:1630-1632.
37. Kim H, Shibayama K, Rimbara E, Mori S. 2014. Biochemical characterization of quinolinic acid phosphoribosyltransferase from *Mycobacterium tuberculosis* H37Rv and inhibition of its activity by pyrazinamide. *PLoS One* 9:e100062.
38. Njire M, Wang N, Wang B, Tan Y, Cai X, Liu Y, Mugweru J, Guo J, Hameed HMA, Tan S, Liu J, Yew WW, Nuermberger E, Lamichhane G, Liu J, Zhang T. 2017. Pyrazinoic Acid Inhibits a Bifunctional Enzyme in *Mycobacterium tuberculosis*. *Antimicrob Agents Chemother* 61.
39. Shi W, Cui P, Niu H, Zhang S, Tønjum T, Zhu B, Zhang Y. 2019. Introducing PrsA Point Mutations Δ 438A and D123A into the Chromosome of *Mycobacterium tuberculosis* Confirms their Role in Causing Resistance to Pyrazinamide. *Antimicrobial Agents and Chemotherapy* 63:e02681-18.
40. Shi W, Chen J, Feng J, Cui P, Zhang S, Weng X, Zhang W, Zhang Y. 2014. Aspartate decarboxylase (PanD) as a new target of pyrazinamide in *Mycobacterium tuberculosis*. *Emerg Microbes Infect* 3:e58.
41. Gopal P, Yee M, Sarathy J, Low JL, Sarathy JP, Kaya F, Dartois V, Gengenbacher M, Dick T. 2016. Pyrazinamide Resistance Is Caused by Two

- Distinct Mechanisms: Prevention of Coenzyme A Depletion and Loss of Virulence Factor Synthesis. *ACS Infect Dis* 2:616-626.
42. Gopal P, Narthey W, Rangunathan P, Sarathy J, Kaya F, Yee M, Setzer C, Manimekalai MSS, Dartois V, Gruber G, Dick T. 2017. Pyrazinoic Acid Inhibits Mycobacterial Coenzyme A Biosynthesis by Binding to Aspartate Decarboxylase PanD. *ACS Infect Dis* 3:807-819.
 43. Gopal P, Sarathy JP, Yee M, Rangunathan P, Shin J, Bhushan S, Zhu J, Akopian T, Kandror O, Lim TK, Gengenbacher M, Lin Q, Rubin EJ, Grüber G, Dick T. 2020. Pyrazinamide triggers degradation of its target aspartate decarboxylase. *Nature Communications* 11.
 44. Sun Q, Li X, Perez LM, Shi W, Zhang Y, Sacchettini JC. 2020. The molecular basis of pyrazinamide activity on *Mycobacterium tuberculosis* PanD. *Nat Commun* 11:339.
 45. Chopra S, Pai H, Ranganathan A. 2002. Expression, purification, and biochemical characterization of *Mycobacterium tuberculosis* aspartate decarboxylase, PanD. *Protein Expression and Purification* 25:533-540.
 46. Zierski M, Bek E. 1980. Side-Effects of Drug Regimens Used in Short-Course Chemotherapy for Pulmonary Tuberculosis. A Controlled Clinical Study. *Tubercle* 61:41-49.
 47. Yee D, Valiquette C, Pelletier M, Parisien I, Rocher I, Menzies D. 2003. Incidence of serious side effects from first-line antituberculosis drugs among patients treated for active tuberculosis. *Am J Respir Crit Care Med* 167:1472-7.
 48. Munro SA, Lewin SA, Smith HJ, Engel ME, Fretheim A, Volmink J. 2007. Patient Adherence to Tuberculosis Treatment: A Systematic Review of Qualitative Research. *PLOS Medicine* 4:1230-1245.
 49. Gillespie SH, Crook AM, McHugh TD, Mendel CM, Meredith SK, Murray SR, Pappas F, Phillips PP, Nunn AJ, REMoxTB Consortium. 2014. Four-month moxifloxacin-based regimens for drug-sensitive tuberculosis. *N Engl J Med* 371:1577-87.
 50. Jarlier V, Nikaido H. 1990. Permeability Barrier to Hydrophilic Solutes in *Mycobacterium chelonae*. *J Bacteriol* 172:1418-1423.
 51. Davidson LA, Draper P, Minnikin DE. 1982. Studies on the mycolic acids from the walls of *Mycobacterium microti*. *Journal of General Microbiology* 128:823-828.
 52. Liu J, Barry CE, 3rd, Besra GS, Nikaido H. 1996. Mycolic Acid Structure Determines the Fluidity of the Mycobacterial Cell Wall. *The Journal of Biological Chemistry* 271:29545-29551.
 53. Rodriguez-Rivera FP, Zhou X, Theriot JA, Bertozzi CR. 2017. Visualization of mycobacterial membrane dynamics in live cells. *J Am Chem Soc* 139:3488-3495.
 54. Paulsen IT, Chen J, Nelson KE, Saier Jr MH. 2001. Comparative genomics of microbial drug efflux systems. *J Mol Microbiol Biotechnol* 3:145-150.

55. Liu J, Takiff HE, Nikaido H. 1996. Active Efflux of Fluoroquinolones in *Mycobacterium smegmatis* mediated by LfrA, a multidrug efflux pump. *J Bacteriol* 178:3791-3795.
56. Ainsa JA, Blokpoel MCJ, Otal I, Young DB, De Smet KAL, Martin C. 1998. Molecular cloning and characterization of Tap, a putative multidrug efflux pump present in *Mycobacterium fortuitum* and *Mycobacterium tuberculosis*. *J Bacteriol* 180:5836-5843.
57. Balganesch M, Dinesh N, Sharma S, Kuruppath S, Nair AV, Sharma U. 2012. Efflux pumps of *Mycobacterium tuberculosis* play a significant role in antituberculosis activity of potential drug candidates. *Antimicrob Agents Chemother* 56:2643-51.
58. Dinesh N, Sharma S, Balganesch M. 2013. Involvement of efflux pumps in the resistance to peptidoglycan synthesis inhibitors in *Mycobacterium tuberculosis*. *Antimicrob Agents Chemother* 57:1941-3.
59. Ramon-Garcia S, Martin C, Thompson CJ, Ainsa JA. 2009. Role of the *Mycobacterium tuberculosis* P55 efflux pump in intrinsic drug resistance, oxidative stress responses, and growth. *Antimicrob Agents Chemother* 53:3675-82.
60. Gupta AK, Katoch VM, Chauhan DS, Sharma R, Singh M, Venkatesan K, Sharma VD. 2010. Microarray analysis of efflux pump genes in multidrug-resistant *Mycobacterium tuberculosis* during stress induced by common anti-tuberculous drugs. *Microbial Drug Resistance* 16:21-28.
61. Adams KN, Takaki K, Connolly LE, Wiedenhof H, Winglee K, Humbert O, Edelstein PH, Cosma CL, Ramakrishnan L. 2011. Drug tolerance in replicating mycobacteria mediated by a macrophage-induced efflux mechanism. *Cell* 145:39-53.
62. Garima K, Pathak R, Tandon R, Rathor N, Sinha R, Bose M, Varma-Basil M. 2015. Differential expression of efflux pump genes of *Mycobacterium tuberculosis* in response to varied subinhibitory concentrations of antituberculosis agents. *Tuberculosis (Edinb)* 95:155-61.
63. Calgin MK, Sahin F, Turegun B, Gerceker D, Atasever M, Koksall D, Karasartova D, Kiyam M. 2013. Expression analysis of efflux pump genes among drug-susceptible and multidrug-resistant *Mycobacterium tuberculosis* clinical isolates and reference strains. *Diagn Microbiol Infect Dis* 76:291-7.
64. Pule CM, Sampson SL, Warren RM, Black PA, van Helden PD, Victor TC, Louw GE. 2016. Efflux pump inhibitors: targeting mycobacterial efflux systems to enhance TB therapy. *J Antimicrob Chemother* 71:17-26.
65. Abraham EP, Gardner AD, Chain E, Heatley NG, Fletcher CM, Jennings MA. 1941. Further observations on penicillin. *The Lancet* 42:3-15.
66. Flores AR, Parsons LM, Pavelka MS, Jr. 2005. Characterization of novel *Mycobacterium tuberculosis* and *Mycobacterium smegmatis* mutants hypersusceptible to beta-lactam antibiotics. *J Bacteriol* 187:1892-900.

67. Flores AR, Parsons LM, Pavelka MS. 2005. Genetic analysis of the beta-lactamases of *Mycobacterium tuberculosis* and *Mycobacterium smegmatis* and susceptibility to beta-lactam antibiotics. *Microbiology* 151:521-532.
68. Wang F, Cassidy C, Sacchettini JC. 2006. Crystal structure and activity studies of the *Mycobacterium tuberculosis* beta-lactamase reveal its critical role in resistance to beta-lactam antibiotics. *Antimicrob Agents Chemother* 50:2762-71.
69. Hugonnet J-E, Tremblay LW, Boshoff HI, Barry CE, 3rd, Blanchard JS. 2009. Meropenem-Clavulanate is effective against extensively drug-resistant *Mycobacterium tuberculosis*. *Science* 323:1215-1217.
70. Buriankova K, Doucet-Populaire F, Dorson O, Gondran A, Ghnassia JC, Weiser J, Pernodet JL. 2004. Molecular basis of intrinsic macrolide resistance in the *Mycobacterium tuberculosis* complex. *Antimicrob Agents Chemother* 48:143-50.
71. Madsen CT, Jakobsen L, Buriankova K, Doucet-Populaire F, Pernodet JL, Douthwaite S. 2005. Methyltransferase Erm(37) slips on rRNA to confer atypical resistance in *Mycobacterium tuberculosis*. *J Biol Chem* 280:38942-7.
72. Tsai MC, Chakravarty S, Zhu G, Xu J, Tanaka K, Koch C, Tufariello J, Flynn J, Chan J. 2006. Characterization of the tuberculous granuloma in murine and human lungs: cellular composition and relative tissue oxygen tension. *Cell Microbiol* 8:218-32.
73. Davis JM, Ramakrishnan L. 2009. The role of the granuloma in expansion and dissemination of early tuberculous infection. *Cell* 136:37-49.
74. Prideaux B, Via LE, Zimmerman MD, Eum S, Sarathy J, O'Brien P, Chen C, Kaya F, Weiner DM, Chen PY, Song T, Lee M, Shim TS, Cho JS, Kim W, Cho SN, Olivier KN, Barry CE, 3rd, Dartois V. 2015. The association between sterilizing activity and drug distribution into tuberculosis lesions. *Nat Med* 21:1223-7.
75. Cicchese JM, Dartois V, Kirschner DE, Linderman JJ. 2020. Both Pharmacokinetic Variability and Granuloma Heterogeneity Impact the Ability of the First-Line Antibiotics to Sterilize Tuberculosis Granulomas. *Front Pharmacol* 11:333.
76. Zhang Y, Heym B, Allen B, Young D, Cole S. 1992. The catalase-peroxidase gene and isoniazid resistance of *Mycobacterium tuberculosis*. *Nature* 358:591-593.
77. Zhang Y, Garbe T, Young D. 1993. Transformation with *katG* restores isoniazid-sensitivity in *Mycobacterium tuberculosis* isolates resistant to a range of drug concentrations. *Mol Microbiol* 8:521-524.
78. Altamirano M, Marostenmaki J, Wong A, FitzGerald M, Black WA, Smith JA. 1994. Mutations in the catalase-peroxidase gene from isoniazid-resistant *Mycobacterium tuberculosis* isolates. *The Journal of Infectious Diseases* 169:1162-1165.
79. Cockerill III FR, Uhl JR, Temesgen Z, Zhang Y, Stockman L, Roberts GD, Williams DL, Kline BC. 1995. Rapid identification of a point mutation of the

- Mycobacterium tuberculosis* catalase-peroxidase (*katG*) gene associated with isoniazid resistance. The Journal of Infectious Diseases 171:240-245.
80. Heym B, Alzari PM, Honore N, Cole ST. 1995. Missense mutations in the catalase-peroxidase gene, *katG*, are associated with isoniazid resistance in *Mycobacterium tuberculosis*. Mol Microbiol 15:235-245.
 81. Hazbon MH, Brimacombe M, Bobadilla del Valle M, Cavatore M, Guerrero MI, Varma-Basil M, Billman-Jacobe H, Lavender C, Fyfe J, Garcia-Garcia L, Leon CI, Bose M, Chaves F, Murray M, Eisenach KD, Sifuentes-Osornio J, Cave MD, Ponce de Leon A, Alland D. 2006. Population genetics study of isoniazid resistance mutations and evolution of multidrug-resistant *Mycobacterium tuberculosis*. Antimicrob Agents Chemother 50:2640-9.
 82. Pym AS, Saint-Joanis B, Cole ST. 2002. Effect of *katG* mutations on the virulence of *Mycobacterium tuberculosis* and the implication for transmission in humans. Infect Immun 70:4955-60.
 83. Vilcheze C, Wang F, Arai M, Hazbon MH, Colangeli R, Kremer L, Weisbrod TR, Alland D, Sacchettini JC, Jacobs WR, Jr. 2006. Transfer of a point mutation in *Mycobacterium tuberculosis* *inhA* resolves the target of isoniazid. Nat Med 12:1027-9.
 84. Basso LA, Zheng R, Musser JM, Jacobs WR, Jr., Blanchard JS. 1998. Mechanisms of isoniazid resistance in *Mycobacterium tuberculosis*: enzymatic characterization of enoyl reductase mutants identified in isoniazid-resistant clinical isolates. The Journal of Infectious Diseases 178:769-775.
 85. Lee AS, Teo AS, Wong SY. 2001. Novel mutations in *ndh* in isoniazid-resistant *Mycobacterium tuberculosis* isolates. Antimicrob Agents Chemother 45:2157-9.
 86. Vilcheze C, Weisbrod TR, Chen B, Kremer L, Hazbon MH, Wang F, Alland D, Sacchettini JC, Jacobs WR, Jr. 2005. Altered NADH/NAD⁺ ratio mediates coresistance to isoniazid and ethionamide in mycobacteria. Antimicrob Agents Chemother 49:708-20.
 87. Vilcheze C, Jacobs WR, Jr. 2007. The mechanism of isoniazid killing: clarity through the scope of genetics. Annu Rev Microbiol 61:35-50.
 88. Ramaswamy SV, Amin AG, Goksel S, Stager CE, Dou S-J, El Sahly H, Moghazeh SL, Kreiswirth BN, Musser JM. 2000. Molecular Genetic Analysis of Nucleotide Polymorphisms Associated with Ethambutol Resistance in Human Isolates of *Mycobacterium tuberculosis*. Antimicrob Agents Chemother 44:326-336.
 89. Sreevatsan S, Stockbauer KE, Pan X, Kreiswirth BN, Moghazeh SL, Jacobs WR, Jr., Telenti A, Musser JM. 1997. Ethambutol resistance in *Mycobacterium tuberculosis*: critical role of *embB* mutations. Antimicrob Agents Chemother 41:1677-1681.
 90. Telenti A, Philipp WJ, Sreevatsan S, Bernasconi C, Stockbauer KE, Wieles B, Musser JM, Jacobs WR, Jr. 1997. The *emb* operon, a gene cluster of

- Mycobacterium tuberculosis* involved in resistance to ethambutol. *Nature Medicine* 3:567-570.
91. Hazbon MH, Bobadilla del Valle M, Guerrero MI, Varma-Basil M, Filliol I, Cavatore M, Colangeli R, Safi H, Billman-Jacobe H, Lavender C, Fyfe J, Garcia-Garcia L, Davidow A, Brimacombe M, Leon CI, Porras T, Bose M, Chaves F, Eisenach KD, Sifuentes-Osornio J, Ponce de Leon A, Cave MD, Alland D. 2005. Role of embB codon 306 mutations in *Mycobacterium tuberculosis* revisited: a novel association with broad drug resistance and IS6110 clustering rather than ethambutol resistance. *Antimicrob Agents Chemother* 49:3794-802.
 92. Safi H, Sayers B, Hazbon MH, Alland D. 2008. Transfer of embB codon 306 mutations into clinical *Mycobacterium tuberculosis* strains alters susceptibility to ethambutol, isoniazid, and rifampin. *Antimicrob Agents Chemother* 52:2027-34.
 93. Telenti A, Imboden P, Marchesi F, Lowrie D, Cole S, Colston MJ, Matter L, Schopfer K, Bodmer T. 1993. Detection of rifampicin-resistance mutations in *Mycobacterium tuberculosis*. *The Lancet* 341:647-650.
 94. Telenti A, Imboden P, Marchesi F, Schmidheini T, Bodmer T. 1993. Direct, Automated detection of rifampin-resistant *Mycobacterium tuberculosis* by polymerase chain reaction and single-strand conformation polymorphism analysis. *Antimicrob Agents Chemother* 37:2054-2058.
 95. Gagneux S, Long CD, Small PM, Van T, Schoolnik GK, Bohannan BJM. 2006. The Competitive Cost of Antibiotic Resistance in *Mycobacterium tuberculosis*. *Science* 312:1944-1946.
 96. Comas I, Borrell S, Roetzer A, Rose G, Malla B, Kato-Maeda M, Galagan J, Niemann S, Gagneux S. 2011. Whole-genome sequencing of rifampicin-resistant *Mycobacterium tuberculosis* strains identifies compensatory mutations in RNA polymerase genes. *Nat Genet* 44:106-10.
 97. Scorpio A, Lindholm-Levy P, Heifets L, Gilman R, Siddiqi S, Cynamon M, Zhang Y. 1997. Characterization of *pncA* mutations in pyrazinamide-resistant *Mycobacterium tuberculosis*. *Antimicrob Agents Chemother* 41:540-543.
 98. Jureen P, Werngren J, Toro JC, Hoffner S. 2008. Pyrazinamide resistance and *pncA* gene mutations in *Mycobacterium tuberculosis*. *Antimicrob Agents Chemother* 52:1852-4.
 99. Lemaitre N, Sougakoff W, Truffot-Pernot C, Jarlier V. 1999. Characterization of new mutations in pyrazinamide-resistant strains of *Mycobacterium tuberculosis* and identification of conserved regions important for the catalytic activity of the pyrazinamidase PncA. *Antimicrob Agents Chemother* 43:1761-1763.
 100. Du X, Wang W, Kim R, Yakota H, Nguyen H, Kim S-H. 2001. Crystal structure and mechanism of catalysis of a pyrazinamidase from *Pyrococcus horikoshii*. *Biochemistry* 40:14166-14172.
 101. Alexander DC, Ma JH, Guthrie JL, Blair J, Chedore P, Jamieson FB. 2012. Gene sequencing for routine verification of pyrazinamide resistance in *Mycobacterium tuberculosis*: a role for *pncA* but not *rpsA*. *J Clin Microbiol* 50:3726-8.

102. Zhang S, Chen J, Shi W, Liu W, Zhang W, Zhang Y. 2013. Mutations in panD encoding aspartate decarboxylase are associated with pyrazinamide resistance in *Mycobacterium tuberculosis*. *Emerg Microbes Infect* 2:e34.
103. Tan Y, Hu Z, Zhang T, Cai X, Kuang H, Liu Y, Chen J, Yang F, Zhang K, Tan S, Zhao Y. 2014. Role of pncA and rpsA gene sequencing in detection of pyrazinamide resistance in *Mycobacterium tuberculosis* isolates from southern China. *J Clin Microbiol* 52:291-7.
104. Zhang Y, Permar S, Sun Z. 2002. Conditions that may affect the results of susceptibility testing of *Mycobacterium tuberculosis* to pyrazinamide. *J Med Microbiol* 51:42-49.
105. Cui Z, Wang J, Lu J, Huang X, Zheng R, Hu Z. 2013. Evaluation of methods for testing the susceptibility of clinical *Mycobacterium tuberculosis* isolates to pyrazinamide. *J Clin Microbiol* 51:1374-80.
106. Tuomanen E, Durack DT, Tomasz A. 1986. Antibiotic tolerance among clinical isolates of bacteria. *Antimicrob Agents Chemother* 30:521-527.
107. Brauner A, Fridman O, Gefen O, Balaban NQ. 2016. Distinguishing between resistance, tolerance and persistence to antibiotic treatment. *Nat Rev Microbiol* 14:320-30.
108. Tomasz A, Albino A, Zanati E. 1970. Multiple antibiotic resistance in a bacterium with suppressed autolytic system. *Nature* 227:138-140.
109. Kim KS, Anthony BF. 1981. Importance of bacterial growth phase in determining minimal bactericidal concentrations of penicillin and methicillin. *Antimicrob Agents Chemother* 19.
110. Tuomanen E, Cozens R, Tosch W, Zak O, Tomasz A. 1986. The rate of killing of *Escherichia coli* by B-lactam antibiotics is strictly proportional to the rate of bacterial growth. *Journal of General Microbiology* 132:1297-1304.
111. Eng RHK, Padberg FT, Smith SM, Tan EN, Cherubin CE. 1991. Bactericidal effects of antibiotics on slowly growing and nongrowing bacteria. *Antimicrob Agents Chemother* 35:1824-1828.
112. van der Woude MW, Baumberg AJ. 2004. Phase and antigenic variation in bacteria. *Clin Microbiol Rev* 17:581-611, table of contents.
113. Wallis RS, Patil S, Cheon S-H, Edmonds K, Phillips M, Perkins MD, Joloba M, Namale A, Johnson JL, Teixeira L, Dietze R, Siddiqi S, Mugerwa RD, Eisenach K, Ellner JJ. 1999. Drug Tolerance in *Mycobacterium tuberculosis*. *Antimicrob Agents Chemother* 43:2600-2606.
114. Hobby GL, Lenert TF. 1957. The *in vitro* action of antituberculous agents against multiplying and non-multiplying microbial cells. *American Review of Tuberculosis and Pulmonary Diseases* 76:1031-1048.
115. Herbert D, Paramasivan CN, Venkatesan P, Kubendiran G, Prabhakar R, Mitchison DA. 1996. Bactericidal Action of Ofloxacin, Sulbactam-Ampicillin, Rifampin, and Isoniazid on Logarithmic- and Stationary-Phase Cultures of *Mycobacterium tuberculosis*. *Antimicrob Agents Chemother* 40:2296-2299.

116. Munoz-Elias EJ, Timm J, Botha T, Chan WT, Gomez JE, McKinney JD. 2005. Replication dynamics of *Mycobacterium tuberculosis* in chronically infected mice. *Infect Immun* 73:546-51.
117. Gill WP, Harik NS, Whiddon MR, Liao RP, Mittler JE, Sherman DR. 2009. A replication clock for *Mycobacterium tuberculosis*. *Nat Med* 15:211-4.
118. Aldridge BB, Fernandez-Suarez M, Heller D, Ambravaneswaran V, Irimia D, Toner M, Fortune SM. 2012. Asymmetry and aging of Mycobacterial cells lead to variable growth and antibiotic susceptibility. *Science* 335:100-104.
119. Wakamoto Y, Dhar N, Chait R, Schneider K, Signorino-Gelo F, Leibler S, McKinney JD. 2013. Dynamic persistence of antibiotic-stressed Mycobacteria. *Science* 339:91-95.
120. Loebel RO, Shorr E, Richardson HB. 1933. The influence of adverse conditions upon the respiratory metabolism and growth of human tubercle bacilli. *J Bacteriol* 26:167-200.
121. Wayne LG. 1976. Dynamics of submerged growth of *Mycobacterium tuberculosis* under aerobic and microaerophilic conditions. *American Review of Respiratory Disease* 114:807-811.
122. Wayne LG, Hayes LG. 1996. An in vitro model for sequential study of shutdown of *Mycobacterium tuberculosis* through two stages of nonreplicating persistence. *Infect Immun* 64:2062-2069.
123. Betts JC, Lukey PT, Robb LC, McAdam RA, Duncan K. 2002. Evaluation of a nutrient starvation model of *Mycobacterium tuberculosis* persistence by gene and protein expression profiling. *Mol Microbiol* 43:717-731.
124. Rao SP, Alonso S, Rand L, Dick T, Pethe K. 2008. The protonmotive force is required for maintaining ATP homeostasis and viability of hypoxic, nonreplicating *Mycobacterium tuberculosis*. *Proc Natl Acad Sci U S A* 105:11945-50.
125. Gengenbacher M, Rao SP, Pethe K, Dick T. 2010. Nutrient-starved, non-replicating *Mycobacterium tuberculosis* requires respiration, ATP synthase and isocitrate lyase for maintenance of ATP homeostasis and viability. *Microbiology* 156:81-7.
126. Cunningham AF, Spreadbury CL. 1998. Mycobacterial stationary phase induced by low oxygen tension: cell wall thickening and localization of the 16-kilodalton α -crystallin homolog. *J Bacteriol* 180:801-808.
127. Lavollay M, Arthur M, Fourgeaud M, Dubost L, Marie A, Veziris N, Blanot D, Gutmann L, Mainardi JL. 2008. The peptidoglycan of stationary-phase *Mycobacterium tuberculosis* predominantly contains cross-links generated by L,D-transpeptidation. *J Bacteriol* 190:4360-6.
128. Sarathy J, Dartois V, Dick T, Gengenbacher M. 2013. Reduced drug uptake in phenotypically resistant nutrient-starved nonreplicating *Mycobacterium tuberculosis*. *Antimicrob Agents Chemother* 57:1648-53.

129. de Carvalho LP, Fischer SM, Marrero J, Nathan C, Ehrt S, Rhee KY. 2010. Metabolomics of *Mycobacterium tuberculosis* reveals compartmentalized co-catabolism of carbon substrates. *Chem Biol* 17:1122-31.
130. Cole ST, Parkhill J, Garnier T, Churcher DH, Gordon SV, Eiglmeier K, Gas S, Barry CE, 3rd, Tekaia F, Badcock K, Basham D, Brown D, Chillingworth T, Connor R, Davies R, Devlin K, Feltwell T, Gentles S, Hamlin N, Holroyd S, Hornsby T, Jagels K, Krogh A, McLean J, Moule S, Murphy L, Oliver K, Osborne J, Quail MA, Rajandream M-A, Rogers J, Rutter S, Seeger K, Skelton J, Squares R, Squares S, Sulston JE, Taylor K, Whitehead S, Barrell BG. 1998. Deciphering the biology of *Mycobacterium tuberculosis* from the complete genome sequence. *Nature* 393:537-544.
131. Sassetti CM, Boyd DH, Rubin EJ. 2001. Comprehensive identification of conditionally essential genes in mycobacteria. *Proc Natl Acad Sci U S A* 98:12712-7.
132. Schnappinger D, Ehrt S, Voskuil MI, Liu Y, Mangan JA, Monahan IM, Dolganov G, Efron B, Butcher PD, Nathan C, Schoolnik GK. 2003. Transcriptional Adaptation of *Mycobacterium tuberculosis* within Macrophages: Insights into the Phagosomal Environment. *J Exp Med* 198:693-704.
133. Timm J, Post FA, Bekker LG, Walther GB, Wainwright HC, Manganelli R, Chan WT, Tsenova L, Gold B, Smith I, Kaplan G, McKinney JD. 2003. Differential expression of iron-, carbon-, and oxygen-responsive mycobacterial genes in the lungs of chronically infected mice and tuberculosis patients. *Proc Natl Acad Sci U S A* 100:14321-6.
134. Beste DJ, Hooper T, Stewart G, Bonde B, Avignone-Rossa C, Bushell ME, Wheeler P, Klamt S, Kierzek AM, McFadden J. 2007. GSMN-TB: a web-based genome-scale network model of *Mycobacterium tuberculosis* metabolism. *Genome Biol* 8:R89.
135. Shi L, Sohaskey CD, Pheiffer C, Datta P, Parks M, McFadden J, North RJ, Gennaro ML. 2010. Carbon flux rerouting during *Mycobacterium tuberculosis* growth arrest. *Mol Microbiol* 78:1199-215.
136. Griffin JE, Gawronski JD, Dejesus MA, Ioerger TR, Akerley BJ, Sassetti CM. 2011. High-resolution phenotypic profiling defines genes essential for mycobacterial growth and cholesterol catabolism. *PLoS Pathog* 7:e1002251.
137. Segal W, Bloch H. 1956. Biochemical differentiation of *Mycobacterium tuberculosis* grown *in vivo* and *in vitro*. *J Bacteriol* 72:132-141.
138. McKinney JD, Honer zu Bentrup K, Munoz-Elias EJ, Miczak A, Chen B, Chan WT, Swenson D, Sacchettini JC, Jacobs WR, Jr., Russell DG. 2000. Persistence of *Mycobacterium tuberculosis* in macrophages and mice requires the glyoxylate shunt enzyme isocitrate lyase. *Nature* 406:735-8.
139. Shi S, Ehrt S. 2006. Dihydrolipoamide acyltransferase is critical for *Mycobacterium tuberculosis* pathogenesis. *Infect Immun* 74:56-63.

140. Puckett S, Trujillo C, Wang Z, Eoh H, Ioerger TR, Krieger I, Sacchettini J, Schnappinger D, Rhee KY, Ehrt S. 2017. Glyoxylate detoxification is an essential function of malate synthase required for carbon assimilation in *Mycobacterium tuberculosis*. *Proc Natl Acad Sci U S A* 114:E2225-E2232.
141. Daniel J, Deb C, Dubey VS, Sirakova TD, Abomoelak B, Morbidoni HR, Kolattukudy PE. 2004. Induction of a novel class of diacylglycerol acyltransferases and triacylglycerol accumulation in *Mycobacterium tuberculosis* as it goes into a dormancy-like state in culture. *J Bacteriol* 186:5017-30.
142. Deb C, Daniel J, Sirakova TD, Abomoelak B, Dubey VS, Kolattukudy PE. 2006. A novel lipase belonging to the hormone-sensitive lipase family induced under starvation to utilize stored triacylglycerol in *Mycobacterium tuberculosis*. *J Biol Chem* 281:3866-75.
143. Baek SH, Li AH, Sasseti CM. 2011. Metabolic regulation of mycobacterial growth and antibiotic sensitivity. *PLoS Biol* 9:e1001065.
144. Rittershaus ESC, Baek SH, Krieger IV, Nelson SJ, Cheng YS, Nambi S, Baker RE, Leszyk JD, Shaffer SA, Sacchettini JC, Sasseti CM. 2018. A Lysine Acetyltransferase Contributes to the Metabolic Adaptation to Hypoxia in *Mycobacterium tuberculosis*. *Cell Chem Biol* 25:1495-1505 e3.
145. Hicks ND, Yang J, Zhang X, Zhao B, Grad YH, Liu L, Ou X, Chang Z, Xia H, Zhou Y, Wang S, Dong J, Sun L, Zhu Y, Zhao Y, Jin Q, Fortune SM. 2018. Clinically prevalent mutations in *Mycobacterium tuberculosis* alter propionate metabolism and mediate multidrug tolerance. *Nat Microbiol* 3:1032-1042.
146. Lysnyansky I, Rosengarten R, Yogev D. 1996. Phenotypic switching of variable surface lipoproteins in *Mycoplasma bovis* involves high-frequency chromosomal rearrangements. *J Bacteriol* 178:5395-5401.
147. Pawlik A, Garnier G, Orgeur M, Tong P, Lohan A, Le Chevalier F, Sapriel G, Roux AL, Conlon K, Honore N, Dillies MA, Ma L, Bouchier C, Coppee JY, Gaillard JL, Gordon SV, Loftus B, Brosch R, Herrmann JL. 2013. Identification and characterization of the genetic changes responsible for the characteristic smooth-to-rough morphotype alterations of clinically persistent *Mycobacterium abscessus*. *Mol Microbiol* 90:612-29.
148. Zhang H, Li D, Zhao L, Fleming J, Lin N, Wang T, Liu Z, Li C, Galwey N, Deng J, Zhou Y, Zhu Y, Gao Y, Wang T, Wang S, Huang Y, Wang M, Zhong Q, Zhou L, Chen T, Zhou J, Yang R, Zhu G, Hang H, Zhang J, Li F, Wan K, Wang J, Zhang XE, Bi L. 2013. Genome sequencing of 161 *Mycobacterium tuberculosis* isolates from China identifies genes and intergenic regions associated with drug resistance. *Nat Genet* 45:1255-60.
149. Coll F, Phelan J, Hill-Cawthorne GA, Nair MB, Mallard K, Ali S, Abdallah AM, Alghamdi S, Alsomali M, Ahmed AO, Portelli S, Oppong Y, Alves A, Bessa TB, Campino S, Caws M, Chatterjee A, Crampin AC, Dheda K, Furnham N, Glynn JR, Grandjean L, Minh Ha D, Hasan R, Hasan Z, Hibberd ML, Joloba M, Jones-Lopez EC, Matsumoto T, Miranda A, Moore DJ, Mocillo N, Panaiotov S, Parkhill

- J, Penha C, Perdigao J, Portugal I, Rchiad Z, Robledo J, Sheen P, Shesha NT, Sirgel FA, Sola C, Oliveira Sousa E, Streicher EM, Helden PV, Viveiros M, Warren RM, McNerney R, Pain A, et al. 2018. Genome-wide analysis of multi- and extensively drug-resistant *Mycobacterium tuberculosis*. *Nat Genet* 50:307-316.
150. Farhat MR, Freschi L, Calderon R, Ioerger T, Snyder M, Meehan CJ, de Jong B, Rigouts L, Sloutsky A, Kaur D, Sunyaev S, van Soolingen D, Shendure J, Sacchettini J, Murray M. 2019. GWAS for quantitative resistance phenotypes in *Mycobacterium tuberculosis* reveals resistance genes and regulatory regions. *Nat Commun* 10:2128.
 151. Zhang Y, Shi W, Zhang W, Mitchison D. 2014. Mechanisms of Pyrazinamide Action and Resistance. *Microbiology Spectrum* 2.
 152. Liu Y, Tan S, Huang L, Abramovitch RB, Rohde KH, Zimmerman MD, Chen C, Dartois V, VanderVen BC, Russell DG. 2016. Immune activation of the host cell induces drug tolerance in *Mycobacterium tuberculosis* both *in vitro* and *in vivo*. *J Exp Med* 213:809-25.
 153. Long JE, DeJesus M, Ward D, Baker RE, Ioerger T, Sassetti CM. 2015. Identifying essential genes in *Mycobacterium tuberculosis* by global phenotypic profiling. *Methods Mol Biol* 1279:79-95.
 154. Barkan D, Liu Z, Sacchettini JC, Glickman MS. 2009. Mycolic acid cyclopropanation is essential for viability, drug resistance, and cell wall integrity of *Mycobacterium tuberculosis*. *Chem Biol* 16:499-509.
 155. Bosserman RE, Champion PA. 2017. Esx Systems and the Mycobacterial Cell Envelope: What's the Connection? *J Bacteriol* 199:e00131-17.
 156. Pandey AK, Sassetti CM. 2008. Mycobacterial persistence requires the utilization of host cholesterol. *Proc Natl Acad Sci U S A* 105:4376-80.
 157. Hafner M, Niepel M, Chung M, Sorger PK. 2016. Growth rate inhibition metrics correct for confounders in measuring sensitivity to cancer drugs. *Nature Methods* 13:521-531.
 158. Pethe K, Sequeira PC, Agarwalla S, Rhee K, Kuhen K, Phong WY, Patel V, Beer D, Walker JR, Duraiswamy J, Jiricek J, Keller TH, Chatterjee A, Tan MP, Ujjini M, Rao SP, Camacho L, Bifani P, Mak PA, Ma I, Barnes SW, Chen Z, Plouffe D, Thayalan P, Ng SH, Au M, Lee BH, Tan BH, Ravindran S, Nanjundappa M, Lin X, Goh A, Lakshminarayana SB, Shoen C, Cynamon M, Kreiswirth B, Dartois V, Peters EC, Glynn R, Brenner S, Dick T. 2010. A chemical genetic screen in *Mycobacterium tuberculosis* identifies carbon-source-dependent growth inhibitors devoid of *in vivo* efficacy. *Nat Commun* 1:57.
 159. Kang HY, Wada T, Iwamoto T, Maeda S, Murase Y, Kato S, Kim HJ, Park YK. 2010. Phylogeographical particularity of the *Mycobacterium tuberculosis* Beijing family in South Korea based on international comparison with surrounding countries. *J Med Microbiol* 59:1191-7.

160. Keating LA, Wheeler PR, Mansoor H, Inwald JK, Dale J, Hewinson RG, Gordon SV. 2005. The pyruvate requirement of some members of the *Mycobacterium tuberculosis* complex is due to an inactive pyruvate kinase: implications for in vivo growth. *Mol Microbiol* 56:163-74.
161. Gomez JE, McKinney JD. 2004. *M. tuberculosis* persistence, latency, and drug tolerance. *Tuberculosis (Edinb)* 84:29-44.
162. Richardson AR, Stojiljkovic I. 2001. Mismatch repair and the regulation of phase variation in *Neisseria meningitidis*. *Mol Microbiol* 40:645-655.
163. Lyons DM, O'Brien PJ. 2010. Human base excision repair creates a bias toward -1 frameshift mutations. *J Biol Chem* 285:25203-12.
164. Torrey HL, Keren I, Via LE, Lee JS, Lewis K. 2016. High Persister Mutants in *Mycobacterium tuberculosis*. *PLoS One* 11:e0155127.
165. Wanner RM, Guthlein C, Springer B, Bottger EC, Ackermann M. 2008. Stabilization of the genome of the mismatch repair deficient *Mycobacterium tuberculosis* by context-dependent codon choice. *BMC Genomics* 9:249.
166. Fox W, Mitchison DA. 1975. Short-Course Chemotherapy for Pulmonary Tuberculosis. *American Review of Respiratory Disease* 111:325-353.
167. McCune RM, Tompsett R. 1956. The Fate of *Mycobacterium tuberculosis* in Mouse Tissues as Determined by the Microbial Enumeration Technique: I. The persistence of drug-susceptible tubercle bacilli in the tissues despite prolonged antimicrobial therapy. *The Journal of Experimental Medicine* 104:737-762.
168. Kester JC, Fortune SM. 2014. Persisters and beyond: mechanisms of phenotypic drug resistance and drug tolerance in bacteria. *Crit Rev Biochem Mol Biol* 49:91-101.
169. Burian J, Ramon-Garcia S, Sweet G, Gomez-Velasco A, Av-Gay Y, Thompson CJ. 2012. The mycobacterial transcriptional regulator whiB7 gene links redox homeostasis and intrinsic antibiotic resistance. *J Biol Chem* 287:299-310.
170. Jain M, Petzold CJ, Schelle MW, Leavell MD, Mougous JD, Bertozzi CR, Leary JA, Cox JS. 2007. Lipidomics reveals control of *Mycobacterium tuberculosis* virulence lipids via metabolic coupling. *Proc Natl Acad Sci U S A* 104:5133-8.
171. Gygli SM, Borrell S, Trauner A, Gagneux S. 2017. Antimicrobial resistance in *Mycobacterium tuberculosis*: mechanistic and evolutionary perspectives. *FEMS Microbiol Rev* 41:354-373.
172. Colangeli R, Jedrey H, Kim S, Connell R, Ma S, Chippada Venkata UD, Chakravorty S, Gupta A, Sizemore EE, Diem L, Sherman DR, Okwera A, Dietze R, Boom WH, Johnson JL, Mac Kenzie WR, Alland D, Teams DTTCS. 2018. Bacterial Factors That Predict Relapse after Tuberculosis Therapy. *N Engl J Med* 379:823-833.
173. Nguyen L, Chinnapapagari S, Thompson CJ. 2005. FbpA-Dependent biosynthesis of trehalose dimycolate is required for the intrinsic multidrug resistance, cell wall structure, and colonial morphology of *Mycobacterium smegmatis*. *J Bacteriol* 187:6603-11.

174. Nandakumar M, Nathan C, Rhee KY. 2014. Isocitrate lyase mediates broad antibiotic tolerance in *Mycobacterium tuberculosis*. *Nat Commun* 5:4306.
175. Xu W, DeJesus MA, Rucker N, Engelhart CA, Wright MG, Healy C, Lin K, Wang R, Park SW, Ioerger TR, Schnappinger D, Ehrt S. 2017. Chemical Genetic Interaction Profiling Reveals Determinants of Intrinsic Antibiotic Resistance in *Mycobacterium tuberculosis*. *Antimicrob Agents Chemother* 61.
176. Sassetti CM, Rubin EJ. 2003. Genetic requirements for mycobacterial survival during infection. *Proc Natl Acad Sci U S A* 100:12989-94.
177. Lamichhane G, Tyagi S, Bishai WR. 2005. Designer arrays for defined mutant analysis to detect genes essential for survival of *Mycobacterium tuberculosis* in mouse lungs. *Infect Immun* 73:2533-40.
178. Zhang YJ, Reddy MC, Ioerger TR, Rothchild AC, Dartois V, Schuster BM, Trauner A, Wallis D, Galaviz S, Huttenhower C, Sacchettini JC, Behar SM, Rubin EJ. 2013. Tryptophan biosynthesis protects mycobacteria from CD4 T-cell-mediated killing. *Cell* 155:1296-308.
179. Mishra BB, Lovewell RR, Olive AJ, Zhang G, Wang W, Eugenin E, Smith CM, Phuah JY, Long JE, Dubuke ML, Palace SG, Goguen JD, Baker RE, Nambi S, Mishra R, Booty MG, Baer CE, Shaffer SA, Dartois V, McCormick BA, Chen X, Sassetti CM. 2017. Nitric oxide prevents a pathogen-permissive granulocytic inflammation during tuberculosis. *Nat Microbiol* 2:17072.
180. Subramaniam S, DeJesus MA, Zaveri A, Smith CM, Baker RE, Ehrt S, Schnappinger D, Sassetti CM, Ioerger TR. 2019. Statistical analysis of variability in TnSeq data across conditions using zero-inflated negative binomial regression. *BMC Bioinformatics* 20:603.
181. Woong Park S, Klotzsche M, Wilson DJ, Boshoff HI, Eoh H, Manjunatha U, Blumenthal A, Rhee K, Barry CE, 3rd, Aldrich CC, Ehrt S, Schnappinger D. 2011. Evaluating the sensitivity of *Mycobacterium tuberculosis* to biotin deprivation using regulated gene expression. *PLoS Pathog* 7:e1002264.
182. Dhar N, McKinney JD. 2010. *Mycobacterium tuberculosis* persistence mutants identified by screening in isoniazid-treated mice. *Proc Natl Acad Sci U S A* 107:12275-80.
183. Bellerose MM, Baek S-H, Huang C-C, Moss CE, Koh E-I, Proulx MK, Smith CM, Baker RE, Lee JS, Eum S, Shin SJ, Cho S-N, Murray M, Sassetti CM. 2019. Common variants in the glycerol kinase gene reduce tuberculosis drug efficacy. *mBio* 10:e00663-19.
184. Kaiser HF. 1958. The Varimax Criterion for Analytic Rotation in Factor Analysis. *Psychometrika* 23:187-200.
185. Sirakova TD, Thirumala AK, Dubey VS, Sprecher H, Kolattukudy PE. 2001. The *Mycobacterium tuberculosis* pks2 gene encodes the synthase for the hepta- and octamethyl-branched fatty acids required for sulfolipid synthesis. *J Biol Chem* 276:16833-9.

186. Takayama K, Wang C, Besra GS. 2005. Pathway to synthesis and processing of mycolic acids in *Mycobacterium tuberculosis*. *Clin Microbiol Rev* 18:81-101.
187. Dinadayala P, Kaur D, Berg S, Amin AG, Vissa VD, Chatterjee D, Brennan PJ, Crick DC. 2006. Genetic basis for the synthesis of the immunomodulatory mannose caps of lipoarabinomannan in *Mycobacterium tuberculosis*. *J Biol Chem* 281:20027-35.
188. Gonzalo Asensio J, Maia C, Ferrer NL, Barilone N, Laval F, Soto CY, Winter N, Daffe M, Gicquel B, Martin C, Jackson M. 2006. The virulence-associated two-component PhoP-PhoR system controls the biosynthesis of polyketide-derived lipids in *Mycobacterium tuberculosis*. *J Biol Chem* 281:1313-6.
189. Madacki J, Laval F, Grzegorzewicz A, Lemassu A, Zahorszka M, Arand M, McNeil M, Daffe M, Jackson M, Laneelle MA, Kordulakova J. 2018. Impact of the epoxide hydrolase EphD on the metabolism of mycolic acids in mycobacteria. *J Biol Chem* 293:5172-5184.
190. Wang Q, Boshoff HIM, Harrison JR, Ray PC, Green SR, Barry CE, 3rd. 2020. PE/PPE proteins mediate nutrient transport across the outer membrane of *Mycobacterium tuberculosis*. *Science* 367:1147-1151.
191. Wilson M, DeRisi J, Kristensen H-H, Imboden P, Rane S, Brown PO, Schoolnik GK. 1999. Exploring drug-induced alterations in gene expression in *Mycobacterium tuberculosis* by microarray hybridization. *PNAS* 96:12833-12838.
192. Murphy DJ, Brown JR. 2007. Identification of gene targets against dormant phase *Mycobacterium tuberculosis* infections. *BMC Infect Dis* 7:84.
193. Van der Geize R, Yam K, Heuser T, Wilbrink MH, Hara H, Anderton MC, Sim E, Dijkhuizen L, Davies JE, Mohn WW, Eltis LD. 2007. A gene cluster encoding cholesterol catabolism in a soil actinomycete provides insight into *Mycobacterium tuberculosis* survival in macrophages. *Proc Natl Acad Sci U S A* 104:1947-52.
194. Shah S, Briken V. 2016. Modular Organization of the ESX-5 Secretion System in *Mycobacterium tuberculosis*. *Front Cell Infect Microbiol* 6:49.
195. Holt KE, McAdam P, Thai PVK, Thuong NTT, Ha DTM, Lan NN, Lan NH, Nhu NTQ, Hai HT, Ha VTN, Thwaites G, Edwards DJ, Nath AP, Pham K, Ascher DB, Farrar J, Khor CC, Teo YY, Inouye M, Caws M, Dunstan SJ. 2018. Frequent transmission of the *Mycobacterium tuberculosis* Beijing lineage and positive selection for the EsxW Beijing variant in Vietnam. *Nat Genet* 50:849-856.
196. Brodin P, Majlessi L, Marsollier L, de Jonge MI, Bottai D, Demangel C, Hinds J, Neyrolles O, Butcher PD, Leclerc C, Cole ST, Brosch R. 2006. Dissection of ESAT-6 system 1 of *Mycobacterium tuberculosis* and impact on immunogenicity and virulence. *Infect Immun* 74:88-98.
197. Hui J, Gordon N, Kajioka R. 1977. Permeability Barrier to Rifampin in *Mycobacteria*. *AAC* 11:773-779.
198. Piddock LJV, Williams KJ, Ricci V. 2000. Accumulation of rifampicin by *Mycobacterium aurum*, *Mycobacterium smegmatis*, and *Mycobacterium tuberculosis*. *J Antimicrobial Chemotherapy* 45:159-165.

199. McNeil MB, Chettiar S, Awasthi D, Parish T. 2019. Cell wall inhibitors increase the accumulation of rifampicin in *Mycobacterium tuberculosis*. *Access Microbiology* 1.
200. Braibant M, Gilot P, Content J. 2000. The ATP binding cassette (ABC) transport systems of *Mycobacterium tuberculosis*. *FEMS Microbiol Rev* 24:449-467.
201. Spivey VL, Molle V, Whalan RH, Rodgers A, Leiba J, Stach L, Walker KB, Smerdon SJ, Buxton RS. 2011. Forkhead-associated (FHA) domain containing ABC transporter Rv1747 is positively regulated by Ser/Thr phosphorylation in *Mycobacterium tuberculosis*. *J Biol Chem* 286:26198-209.
202. Walker TM, Kohl TA, Omar SV, Hedge J, Del Ojo Elias C, Bradley P, Iqbal Z, Feuerriegel S, Niehaus KE, Wilson DJ, Clifton DA, Kapatai G, Ip CLC, Bowden R, Drobniowski FA, Allix-Béguec C, Gaudin C, Parkhill J, Diel R, Supply P, Crook DW, Smith EG, Walker AS, Ismail N, Niemann S, Peto TEA. 2015. Whole-genome sequencing for prediction of *Mycobacterium tuberculosis* drug susceptibility and resistance: a retrospective cohort study. *The Lancet Infectious Diseases* 15:1193-1202.
203. CRyPTIC Consortium and the 100000 Genomes Project. 2018. Prediction of Susceptibility to First-Line Tuberculosis Drugs by DNA Sequencing. *N Engl J Med* 379:1403-1415.
204. Waksman SA. 1964. *The Conquest of Tuberculosis*. Robert Hale Limited, London.
205. Moghazeh SL, Pan X, Arain T, Stover CK, Musser JM, Kreiswirth BN. 1996. Comparative antimycobacterial activities of Rifampin, Rifapentine, and KRM-1648 against a collection of Rifampin-Resistant *Mycobacterium tuberculosis* isolates with known *rpoB* mutations. *Antimicrob Agents Chemother* 40:2655-2657.
206. Ohno H, Koga H, Kohno S, Tashiro T, Hara K. 1996. Relationship between rifampin MICs for and *rpoB* mutations of *Mycobacterium tuberculosis* strains isolated in Japan. *Antimicrob Agents Chemother* 40:1053-1056.
207. Yang B, Koga H, Ohno H, Ogawa K, Fukuda M, Hirakata Y, Maesaki S, Tomono K, Tashiro T, Kohno S. 1998. Relationship between antimycobacterial activities of rifampicin, rifabutin, and KRM-1648 and *rpoB* mutations of *Mycobacterium tuberculosis*. *J Antimicrob Chemother* 42:621-628.
208. Rustomjee R, Lienhardt C, Kanyok T, Davies GR, Levin J, Mthiyane T, Reddy C, Sturm AW, Sirgel FA, Allen J, Coleman DJ, Fourie B, Mitchison DA, The Gatifloxacin for TB study team. 2008. A Phase II study of the sterilising activities of ofloxacin, gatifloxacin and moxifloxacin in pulmonary tuberculosis. *International Journal of Tuberculosis and Lung Disease* 12:128-138.
209. Jindani A, Harrison TS, Nunn AJ, Phillips PP, Churchyard GJ, Charalambous S, Hatherill M, Geldenhuys H, McIlleron HM, Zvada SP, Mungofa S, Shah NA, Zizhou S, Magweta L, Shepherd J, Nyirenda S, van Dijk JH, Clouting HE, Coleman D, Bateson AL, McHugh TD, Butcher PD, Mitchison DA, Team RT.

2014. High-dose rifapentine with moxifloxacin for pulmonary tuberculosis. *N Engl J Med* 371:1599-608.
210. Merle CS, Fielding K, Sow OB, Gninafon M, Lo MB, Mthiyane T, Odhiambo J, Amukoye E, Bah B, Kassa F, N'Diaye A, Rustomjee R, de Jong BC, Horton J, Perronne C, Sismanidis C, Lapujade O, Olliaro PL, Lienhardt C, Project OFGfT. 2014. A four-month gatifloxacin-containing regimen for treating tuberculosis. *N Engl J Med* 371:1588-98.
211. Jawahar MS, Banurekha VV, Paramasivan CN, Rahman F, Ramachandran R, Venkatesan P, Balasubramanian R, Selvakumar N, Ponnuraja C, Iliyas AS, Gangadevi NP, Raman B, Baskaran D, Kumar SR, Kumar MM, Mohan V, Ganapathy S, Kumar V, Shanmugam G, Charles N, Sakthivel MR, Jagannath K, Chandrasekar C, Parthasarathy RT, Narayanan PR. 2013. Randomized clinical trial of thrice-weekly 4-month moxifloxacin or gatifloxacin containing regimens in the treatment of new sputum positive pulmonary tuberculosis patients. *PLoS One* 8:e67030.
212. DeJesus MA, Ambadipudi C, Baker R, Sasseti C, Ioerger TR. 2015. TRANSIT-- A Software Tool for Himar1 TnSeq Analysis. *PLoS Comput Biol* 11:e1004401.
213. Benjamini Y, Hochberg Y. 1995. Controlling the False Discovery Rate: a Practical and Powerful Approach to Multiple Testing. *Journal of the Royal statistical Society Series B (Methodological)* 57:289-300.
214. CDC. 2009. Biosafety in Microbiological and Biomedical Laboratories. Centers for Disease Control and Prevention, Atlanta, GA.
215. Murphy KC, Nelson SJ, Nambi S, Papavinasasundaram K, Baer CE, Sasseti CM. 2018. ORBIT: a New Paradigm for Genetic Engineering of Mycobacterial Chromosomes. *mBio* 9.
216. Blumenthal A, Trujillo C, Ehrt S, Schnappinger D. 2010. Simultaneous analysis of multiple *Mycobacterium tuberculosis* knockdown mutants in vitro and in vivo. *PLoS One* 5:e15667.
217. Martin CJ, Cadena AM, Leung VW, Lin PL, Maiello P, Hicks N, Chase MR, Flynn JL, Fortune SM. 2017. Digitally Barcoding *Mycobacterium tuberculosis* Reveals *In Vivo* Infection Dynamics in the Macaque Model of Tuberculosis. *mBio* 8.
218. DePristo MA, Banks E, Poplin R, Garimella KV, Maguire JR, Hartl C, Philippakis AA, del Angel G, Rivas MA, Hanna M, McKenna A, Fennell TJ, Kernytzky AM, Sivachenko AY, Cibulskis K, Gabriel SB, Altshuler D, Daly MJ. 2011. A framework for variation discovery and genotyping using next-generation DNA sequencing data. *Nat Genet* 43:491-8.
219. Poplin R, Ruano-Rubio V, DePristo MA, Fennell TJ, Carneiro MO, Van der Auwera GA, Kling DE, Gauthier LD, Levy-Moonshine A, Roazen D, Shakir K, Thibault J, Chandran S, Whelan C, Lek M, Gabriel S, Daly MJ, Neale B, MacArthur DG, Banks E. 2017. Scaling accurate genetic variant discovery to tens of thousands of samples. *BioRxiv* doi:10.1101/201178.

220. Guindon S, Dufayard JF, Lefort V, Anisimova M, Hordijk W, Gascuel O. 2010. New algorithms and methods to estimate maximum-likelihood phylogenies: assessing the performance of PhyML 3.0. *Syst Biol* 59:307-21.
221. Letunic I, Bork P. 2016. Interactive tree of life (iTOL) v3: an online tool for the display and annotation of phylogenetic and other trees. *Nucleic Acids Res* 44:W242-5.
222. Felsenstein J. 2002. PHYLIP-phylogeny inference package (version 3.2). vol 5. *Cladistics*.
223. Yang Z. 2007. PAML 4: phylogenetic analysis by maximum likelihood. *Mol Biol Evol* 24:1586-91.
224. World Health Organization. 2012. Updated interim critical concentrations for first-line and second-line DST. Organization WH, Geneva, Switzerland.
225. Li H, Handsaker B, Wysoker A, Fennell T, Ruan J, Homer N, Marth G, Abecasis G, Durbin R, Genome Project Data Processing S. 2009. The Sequence Alignment/Map format and SAMtools. *Bioinformatics* 25:2078-9.
226. Walker BJ, Abeel T, Shea T, Priest M, Abouelliel A, Sakthikumar S, Cuomo CA, Zeng Q, Wortman J, Young SK, Earl AM. 2014. Pilon: an integrated tool for comprehensive microbial variant detection and genome assembly improvement. *PLoS One* 9:e112963.
227. Stucki D, Malla B, Hostettler S, Huna T, Feldmann J, Yeboah-Manu D, Borrell S, Fenner L, Comas I, Coscolla M, Gagneux S. 2012. Two new rapid SNP-typing methods for classifying *Mycobacterium tuberculosis* complex into the main phylogenetic lineages. *PLoS One* 7:e41253.
228. Zhou X, Stephens M. 2014. Efficient multivariate linear mixed model algorithms for genome-wide association studies. *Nat Methods* 11:407-9.